

Combining Graph Neural Networks and Mixed Integer Linear Programming for Molecular Inference under the Two-Layered Model

Jianshen Zhu^{1,5} Naveed Ahmed Azam² Kazuya Haraguchi¹
 Liang Zhao³ Tatsuya Akutsu⁴

¹Graduate of Informatics, Kyoto University, Kyoto 606-8501, Japan

²Department of Mathematics, Quaid-i-Azam University, Islamabad 45320, Pakistan

³Graduate School of Advanced Integrated Studies in Human Survivability
 (Shishu-Kan), Kyoto University, Kyoto 606-8306, Japan

⁴Bioinformatics Center, Institute for Chemical Research, Kyoto University, Uji
 611-0011, Japan

⁵Department of Information Sciences, Tokyo University of Science, Noda, Chiba
 278-8510, Japan

Abstract

Recently, a novel two-phase framework named `mol-infer` for inference of chemical compounds with prescribed abstract structures and desired property values has been proposed. The framework `mol-infer` is primarily based on using mixed integer linear programming (MILP) to simulate the computational process of machine learning methods and describe the necessary and sufficient conditions to ensure such a chemical graph exists. The existing approaches usually first convert the chemical compounds into handcrafted feature vectors to construct prediction functions, but because of the limit on the kinds of descriptors originated from the need for tractability in the MILP formulation, the learning performances on datasets of some properties are not good enough. A lack of good learning performance can greatly lower the quality of the inferred chemical graphs, and thus improving learning performance is of great importance. On the other hand, graph neural networks (GNN) offer a promising machine learning method to directly utilize the chemical graphs as the input, and many existing GNN-based approaches to the molecular property prediction problem have shown that they can enjoy better learning performances compared to the traditional approaches that are based on feature vectors. In this study, we develop a molecular inference framework based on `mol-infer`, namely `mol-infer-GNN`, that utilizes GNN as the learning method while keeping the great flexibility originated from the two-layered model on the abstract structure of the chemical graph to be inferred. We conducted computational experiments on the QM9 dataset to show that our proposed GNN model can obtain satisfying learning performances for some properties despite its simple structure, and can infer small chemical graphs comprising up to 20 non-hydrogen atoms within reasonable

computational time.

Keywords: Machine Learning, Graph Neural Networks, Integer Programming, Chemoinformatics, Molecular Design, Inverse QSAR/QSPR.

1 Introduction

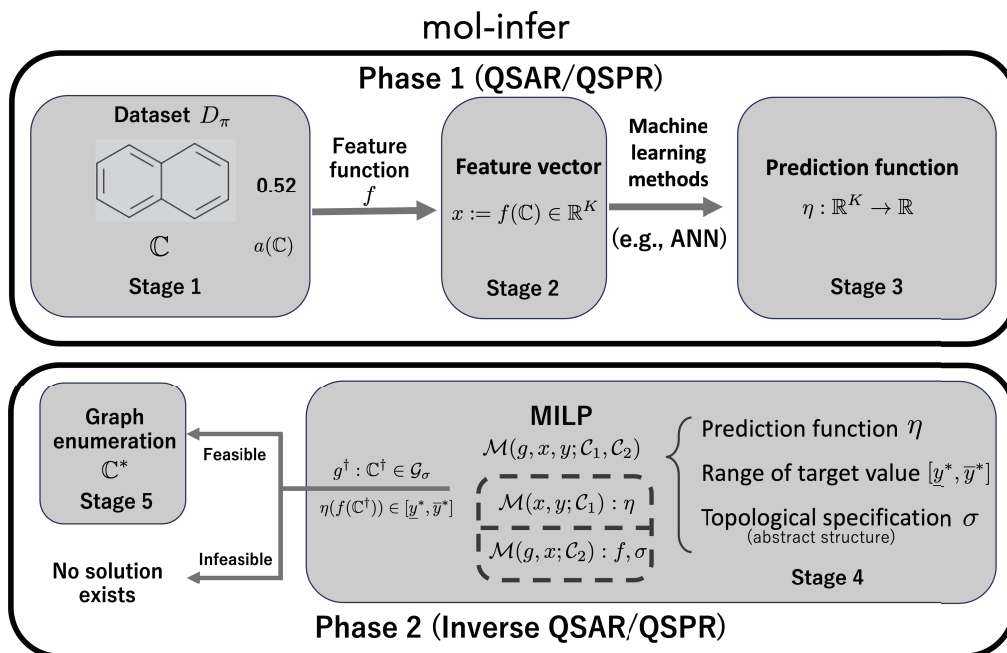
Designing novel molecules with predetermined structures and desired properties is a critical challenge across diverse research fields, including materials science [28] and drug discovery [27, 32]. In recent years, significant progress has been made in molecular design using various machine learning techniques [23, 40]. Computational molecular design, historically entrenched in chemoinformatics, has been studied under the name of *quantitative structure activity/property relationship* (QSAR/QSPR) [10, 35] and its inverse counterpart *inverse quantitative structure activity/property relationship* (inverse QSAR/QSPR) [17, 27, 30]. Analysis of the activities and properties of chemical compounds is crucial not only in chemistry but also in biology, given their pivotal roles in various metabolic pathways.

QSAR/QSPR aims to predict chemical activities from given chemical structures [10]. A prediction function is usually constructed from existing structure-activity relation data, employing machine learning-based methods, including artificial neural network (ANN)-based methods [23, 40]. On the other hand, inverse QSAR/QSPR seeks to infer chemical structures from given chemical activities [17, 27, 30]. In most classical approaches, chemical structures are typically treated as an undirected graph called *chemical graphs* and encoded as a vector of real numbers called *descriptors* or *feature vectors*. A typical approach to inverse QSAR/QSPR involves first inferring feature vectors from given chemical activities and then reconstructing chemical graphs from these feature vectors [17, 27, 30]. While these handcrafted features have been effective in many cases, the limitations become apparent when dealing with large-scale datasets [14].

Recent advancements in deep learning, especially the development of *graph neural networks* (GNNs), have provided a promising alternative to traditional feature-based methods. GNNs have demonstrated superior performance in capturing intricate relationships with chemical graphs by directly utilizing the graph structure as input, eliminating the need for manually designed descriptors [14, 21, 31]. The ability to automatically learn meaningful representations from non-Euclidean data has opened new avenues for molecular property prediction, with several GNN-based models achieving state-of-the-art results on benchmark datasets like QM9 [11, 13, 14, 31, 46]. Also, there are several GNN-based approaches to the molecular graph generation problem [41]. These methods either generate a new graph in a sequential manner [15, 22]—adding vertices and edges step by step, or in a global manner [5, 8]—outputting an entire graph at once.

However, despite the remarkable progress made with GNNs (and other deep learning-based approaches), most existing approaches focus mainly on the prediction task of QSAR/QSPR, and few studies have effectively integrated GNNs into the inverse QSAR/QSPR frameworks. A significant challenge is to ensure the following two important properties of the generated chemical structures, namely *optimality*—the quality of the solution for the inverse problem of the learning methods, and *exactness*—whether the solution admits a valid chemical graph. While many deep learning-based generative models (e.g., [6, 7, 19, 34]) aim to create chemically plausible molecules, they often fail to guarantee the optimality or the exactness of the inferred solutions mathematically, which can be problematic in practical applications [47].

To overcome these limitations, a novel framework called `mol-infer` [2, 33, 44, 49] was recently

Figure 1: An illustration of the two-phase framework **mol-infer**.

proposed for inferring chemical compounds with prescribed abstract structures and desired property values. This framework is primarily based on using the *mixed integer linear programming* (MILP) formulation to simulate the computational process of machine learning methods and also describe the necessary and sufficient conditions to ensure the existence of a valid chemical graph. As a result, **mol-infer** generates chemical graphs in a global manner and guarantees both the optimality and exactness of the inferred chemical graph. Figure 1 provides an illustration of **mol-infer**. Simply put, **mol-infer** consists of two phases. Phase 1 is the QSAR/QSPR phase aiming to construct a prediction function η between chemical compounds and their observed property values. Let \mathcal{G} denote the set of all possible chemical graphs. First, we collect a dataset $D_\pi \subseteq \mathcal{G}$ of chemical graphs consisting of chemical graphs \mathbb{C} and the observed values $a(\mathbb{C})$ (Stage 1). Then we use a feature function $f: \mathcal{G} \rightarrow \mathbb{R}^K$ (K is a positive integer) to convert chemical graphs to a K -dimensional real vectors (Stage 2). Finally, a prediction function $\eta: \mathbb{R}^K \rightarrow \mathbb{R}$ is constructed by some machine learning methods (Stage 3). Phase 2 is the inverse QSAR/QSPR phase, and the target is to infer chemical graphs with specific property values. Given a set of rules called topological specification σ that specifies the desired structure of the inferred chemical graphs, and a desired range $[y^*, \bar{y}^*]$ of the target value, Stage 4 is designed to infer chemical graphs \mathbb{C}^* that satisfy the rules σ and $\eta(f(\mathbb{C}^*)) \in [y^*, \bar{y}^*]$ by solving an MILP formulation $\mathcal{M}(g, x, y; \mathcal{C}_1, \mathcal{C}_2)$ that represents:

- (i) $\mathcal{M}(x, y; \mathcal{C}_1)$: the computation process of the prediction function η ; and
- (ii) $\mathcal{M}(g, x; \mathcal{C}_2)$: that of the feature function f and the constraints for $\mathbb{C} \in \mathcal{G}_\sigma$,

where \mathcal{G}_σ denotes the set of all chemical graphs satisfying σ . In Stage 5, dynamic programming-based graph enumeration algorithms [16] are used to generate isomers of the inferred chemical graphs \mathbb{C}^* obtained in Stage 4. This framework was originally proposed for only limited classes of chemical graphs; e.g., trees [4, 44], rank-1 graphs [18], and rank-2 graphs [52]. The *two-layered*

model (2L-model) proposed by Shi et al. [33] admits us to infer any chemical graph, where users need to design an abstract structure as a part of the input, and is now the standard model in **mol-infer**. One of the superiority of **mol-infer** is that it can suggest that \mathcal{G}_σ does not contain such a desired chemical graph when the MILP formulation $\mathcal{M}(g, x, y; \mathcal{C}_1, \mathcal{C}_2)$ is infeasible, while most existing inverse QSAR/QSPR models fail to do this. Several machine learning methods have been employed into **mol-infer**, for example, ANNs [33], linear regression [48, 49], and decision trees [39]. (We refer to the thesis [47] for a more comprehensive description of **mol-infer**.)

All of these previous approaches rely heavily on handcrafted feature vectors because of the limit on the kinds of descriptors originating from the need for tractability in the MILP formulation $\mathcal{M}(g, x; \mathcal{C}_2)$. However, the learning performances on datasets of some properties are limited. For example, the median test R^2 score for the dataset of electric dipole moment (MU) consisting of randomly selected 1000 molecules from the QM9 dataset is less than 0.7 [48, 50], and for the dataset of autoignition temperature annotated from Hazardous Substances Data Bank (HSDB) [1] on Pubchem [20] it is around 0.8 [50]. A lack of good learning performance can greatly lower the quality of chemical graphs inferred in Phase 2, and thus developing new ways to improve learning performance is of great importance. One noteworthy issue is that, more complex methods can increase the accuracy of the resultant prediction functions in Phase 1. On the other hand, it is generally hard to represent the computational process of such a method by MILP (e.g., kernel methods like support vector machine), and even in the case where it is possible, the time needed to solve the MILP formulations in Phase 2 will increase drastically as well, and thus, it is challenging to incorporate complicated learning methods into **mol-infer**.

In this paper, we introduce **mol-infer-GNN**, an advanced extension of the **mol-infer** framework that integrates GNNs as the primary learning method while retaining the rigorous MILP formulations for structure inference. By directly utilizing the chemical graph as input, the newly proposed framework overcomes the limitations of handcrafted features and enhances the predictive power of the model. The key contributions of this work are summarized as follows:

- We develop a relatively simple GNN architecture, **2L-GNN**, specifically designed for the two-layered model, ensuring efficient and effective learning from chemical graphs.
- We incorporate the **2L-GNN** model into the **mol-infer** framework, and manage to formulate the inverse problem using MILP, thereby guaranteeing both the optimality and exactness of the inferred chemical structures. While previous studies (e.g., [25, 45]) have used MILP formulations to simulate the computation process of a given GNN, these approaches have been restricted in the variety of chemical graphs they can generate. In contrast, our method benefits from the flexibility of the two-layered model, allowing for a significantly broader range of chemical structures to be inferred.
- We conduct numerical experiments on the QM9 dataset [29, 42] to evaluate the predictive accuracy and inference efficiency of our proposed approach. Specifically, we demonstrate that the inverse problem can be solved efficiently enough to infer a chemical graph comprising up to 20 non-hydrogen atoms. Additionally, we use the open-source quantum chemistry software Psi4 [36] and PySCF [37, 38] to compute the property values of the inferred molecules and compare them with the ones obtained from MILP solutions, and the experimental results demonstrate that the generated compounds are generally of good quality.

The paper is organized as follows. We introduce some basic notations on graphs, the modeling of chemical compounds, and the two-layered model in Section 2. Section 3 introduces our newly-

proposed GNN-based inverse QSAR/QSPR framework `mol-infer-GNN`. We report some results on computational experiments conducted on the QM9 dataset in Section 4. Section 5 concludes the paper. More details are available in the Appendix, including a full list of constraints in MILP formulations. All program codes and experimental results are available at <https://github.com/ku-dml/mol-infer/tree/master/2LGNN>.

2 Preliminary

In this section, we introduce some essential concepts and notations related to graph theory and the modeling of chemical compounds, which are the foundation for our proposed framework. These definitions follow mainly the work of Zhu et al. [49], with some necessary modifications tailored to our approach.

For two integers a and b such that $a \leq b$, let $[a, b]$ denote the set of integers i with $a \leq i \leq b$.

2.1 Graphs

Throughout this study, we consider a *graph* as a simple connected undirected graph. The sets of *vertices* and *edges* of G are denoted by $V(G)$ and $E(G)$, respectively. For any vertex $v \in V(G)$, the *neighborhood* of v is denoted by $N_G(v)$, and the *degree* $\deg_G(v)$ of v is defined to be $\deg_G(v) = |N_G(v)|$.

We sometimes designate a vertex in a graph G as a *root*, and call such a graph *rooted*. A *leaf-vertex* in a graph G (possibly with a root) is defined to be a non-root vertex v with degree 1. An edge uv incident to a leaf-vertex v is called a *leaf-edge*, and the sets of leaf-vertices and leaf-edges are denoted by $V_{\text{leaf}}(G)$ and $E_{\text{leaf}}(G)$, respectively. We define a sequence of graphs $G_i, i \in \mathbb{Z}_+$, for a graph G by removing the set of leaf-vertices iteratively as follows:

$$G_0 := G; \quad G_{i+1} := G_i - V_{\text{leaf}}(G_i).$$

We call a vertex v a *tree vertex* if $v \in V_{\text{leaf}}(G_i)$ for some integer $i \geq 0$, and define the *height* $\text{ht}(v)$ of v to be i . For each non-tree vertex v adjacent to a tree vertex, we define $\text{ht}(v)$ to be $\text{ht}(u) + 1$, where u is the one with the maximum $\text{ht}(u)$ among the neighbors of v . The height is left undefined for any non-tree vertex that is not adjacent to any tree vertex. The *height* $\text{ht}(T)$ of a rooted tree T is defined to be the maximum of $\text{ht}(v)$ of a vertex $v \in V(T)$.

2.2 Modeling of Chemical Compounds

To represent a chemical compound, we employ the *chemical graph* which abstracts a molecule as a graph where vertices represent atoms and edges represent bonds. We refer [49] for a more detailed description of chemical graphs.

A chemical compound \mathbb{C} is represented by a *chemical graph* which is defined to be a triplet $\mathbb{C} = (H, \alpha, \beta)$ of a graph H , $\alpha : V(H) \rightarrow \Lambda$ assigns chemical elements to vertices, and $\beta : E(H) \rightarrow [1, 3]$ assigns the bond-multiplicity to edges. Here Λ is a set of chemical elements, and we denote a chemical element \mathbf{a} with a valence i by $\mathbf{a}_{(i)}$. Such a suffix (i) is omitted for a chemical element \mathbf{a} with a unique valence. The *hydrogen-suppressed chemical graph* $\langle \mathbb{C} \rangle$ of \mathbb{C} is the graph obtained by removing all hydrogen atoms.

Two chemical graphs (H_1, α_1, β_1) and (H_2, α_2, β_2) are *isomorphic* if a bijection $\phi : V(H_1) \rightarrow V(H_2)$ exists such that chemical and structural information are preserved under ϕ ; i.e., $uv \in$

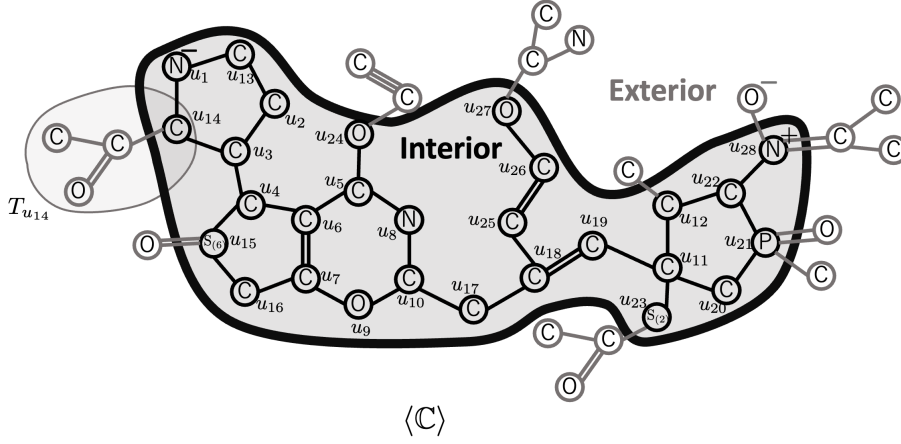


Figure 2: An illustration of the 2L-model for a chemical graph \mathbb{C} . Here $\langle \mathbb{C} \rangle$ is the hydrogen-suppressed chemical graphs of \mathbb{C} . The interior is represented by the shaded area enclosed by thick black lines, while the remaining parts form the exterior. Vertices $u_i, i \in [1, 28]$ are the interior-vertices, and $T_{u_{14}}$ is the chemical tree rooted at vertex u_{14} , outlined by a thin gray line.

$E(H_1), \alpha_1(u) = \mathbf{a}, \alpha_1(v) = \mathbf{b}, \beta_1(uv) = m$ if and only if $\phi(u)\phi(v) \in E(H_2), \alpha_2(\phi(u)) = \mathbf{a}, \alpha_2(\phi(v)) = \mathbf{b}, \beta_2(\phi(u)\phi(v)) = m$.

2.3 Two-layered Model

This subsection reviews the *two-layered model* (2L-model) proposed by Shi et al. [33] and further refined by Zhu et al. [49], which divides the hydrogen-suppressed chemical graph $\langle \mathbb{C} \rangle$ into two parts: the *interior* and the *exterior*.

Let $\rho \geq 1$ be an integer, which we call a *branch-parameter* and $\rho = 2$ is the standard value. For a chemical graph $\mathbb{C} = (H, \alpha, \beta)$, we categorize each vertex $v \in V(\langle \mathbb{C} \rangle)$ in the hydrogen-suppressed chemical graph as follows; *exterior-vertex* if $\text{ht}(v) < \rho$ for the height defined on $\langle \mathbb{C} \rangle$, and *interior-vertex* otherwise. An edge $e \in E(\langle \mathbb{C} \rangle)$ is called an *exterior-edge* if e is incident to an exterior-vertex, and *interior-edge* otherwise. We denote the sets of exterior-vertices, exterior-edges, interior-vertices and interior-edges of \mathbb{C} by $V^{\text{ex}}(\mathbb{C})$, $E^{\text{ex}}(\mathbb{C})$, $V^{\text{int}}(\mathbb{C})$ and $E^{\text{int}}(\mathbb{C})$, respectively. The *interior* of \mathbb{C} is defined to be the subgraph $\mathbb{C}^{\text{int}} := (V^{\text{int}}(\mathbb{C}), E^{\text{int}}(\mathbb{C}))$ of $\langle \mathbb{C} \rangle$. Notice that the set $E^{\text{ex}}(\mathbb{C})$ of exterior-edges consists of a collection of connected graphs, each of which can be viewed as a rooted tree T rooted at an interior-vertex $v \in V(T)$. We denote the set of these chemical rooted trees in $\langle \mathbb{C} \rangle$ as $\mathcal{T}^{\text{ex}}(\langle \mathbb{C} \rangle)$. For each interior-vertex $u \in V^{\text{int}}(\mathbb{C})$, let $T_u \in \mathcal{T}^{\text{ex}}(\langle \mathbb{C} \rangle)$ denote the chemical tree rooted at u (where T_u may consist of only one vertex u). See Figure 2 for an illustration of these concepts.

The ρ -*fringe-tree* $\mathbb{C}[u]$ is defined to be the chemical rooted tree obtained from T_u by putting back the hydrogens originally attached with T_u in \mathbb{C} . We denote the set of ρ -fringe-trees in \mathbb{C} as $\mathcal{T}(\mathbb{C})$. Figure 3 illustrates the set $\mathcal{T}(\mathbb{C}) = \{\mathbb{C}[u_i] \mid i \in [1, 28]\}$ of the 2-fringe-trees of the example \mathbb{C} with $\langle \mathbb{C} \rangle$ in Figure 2.

In order to describe the abstract structure of the chemical graph to be inferred, a set of rules called *topological specification* was introduced by Tanaka et al. [39] and later updated by Zhu et al. [49]. It consists of the following three parts:

- (i) A *seed graph* $G_{\mathbb{C}}$ that provides an abstract structure of a target chemical graph \mathbb{C} ;

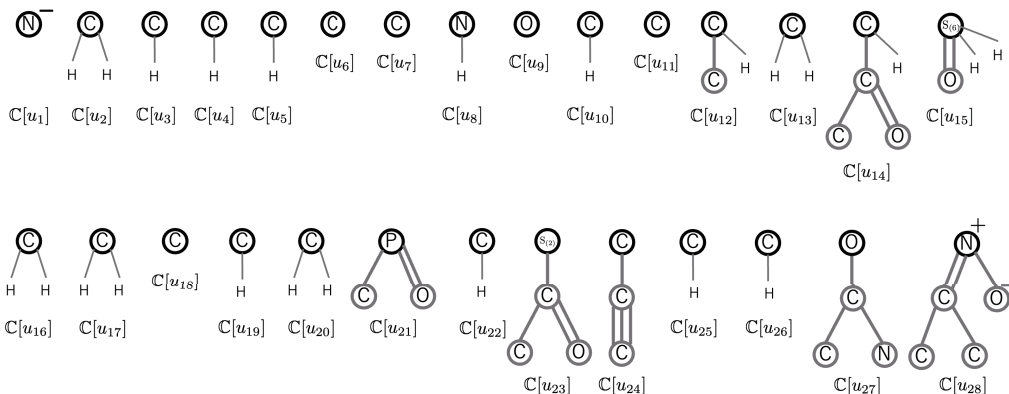


Figure 3: An illustration of 2-fringe-trees $\mathbb{C}[u_i]$, $u \in [1, 28]$ of the example \mathbb{C} depicted in Figure 2. We depict the root of each 2-fringe-tree with a black circle and omit the hydrogens attached to non-root vertices.

- (ii) A set \mathcal{F} of chemical rooted trees as candidates for the ρ -fringe-tree $\mathbb{C}[u]$ rooted at each interior-vertex u in \mathbb{C} ; and
- (iii) Lower and upper bounds on the number of components in a target chemical graph such as chemical elements, double/triple bonds and the interior-vertices in \mathbb{C} .

We refer Appendix A and [49] for a detailed description of topological specification and how the MILP in Stage 4 expands the seed graph to get a complete chemical graph.

3 mol-infer-GNN: A GNN-based Inverse QSAR/QSPR Framework

In this section, we describe our proposed molecular inference framework, **mol-infer-GNN**, which uses GNN as the learning method so that chemical graphs are directly used as the input. As a variant of **mol-infer**, **mol-infer-GNN** inherits the most important feature that the optimality and exactness of the obtained solution are guaranteed by solving MILP formulations.

The framework consists of two phases, and the basic idea of each phase remains the same as **mol-infer**. We illustrate the framework in Figure 4.

3.1 Phase 1: QSAR/QSPR Phase

Given a property π and a dataset consisting of chemical graphs \mathbb{C} and their observed values $a(\mathbb{C}) \in \mathbb{R}$, the target of Phase 1 is to construct a prediction function $\eta : \mathcal{G} \rightarrow \mathbb{R}$ between a chemical graph $\mathbb{C} = (H, \alpha, \beta)$ and its observed property value $a(\mathbb{C})$.

Graph Neural Networks Graph neural networks (GNNs) [14, 21, 26] are a specialized class of neural network models designed to process graph-structured data. Unlike traditional neural networks, which require fixed-sized vectors as inputs, GNNs can handle the irregular, non-Euclidean nature of graphs, making them ideal for tasks involving relational data, such as molecular graphs, social networks, and so on [41]. We will use the term *node* interchangeably with vertex in the context of graph neural networks.

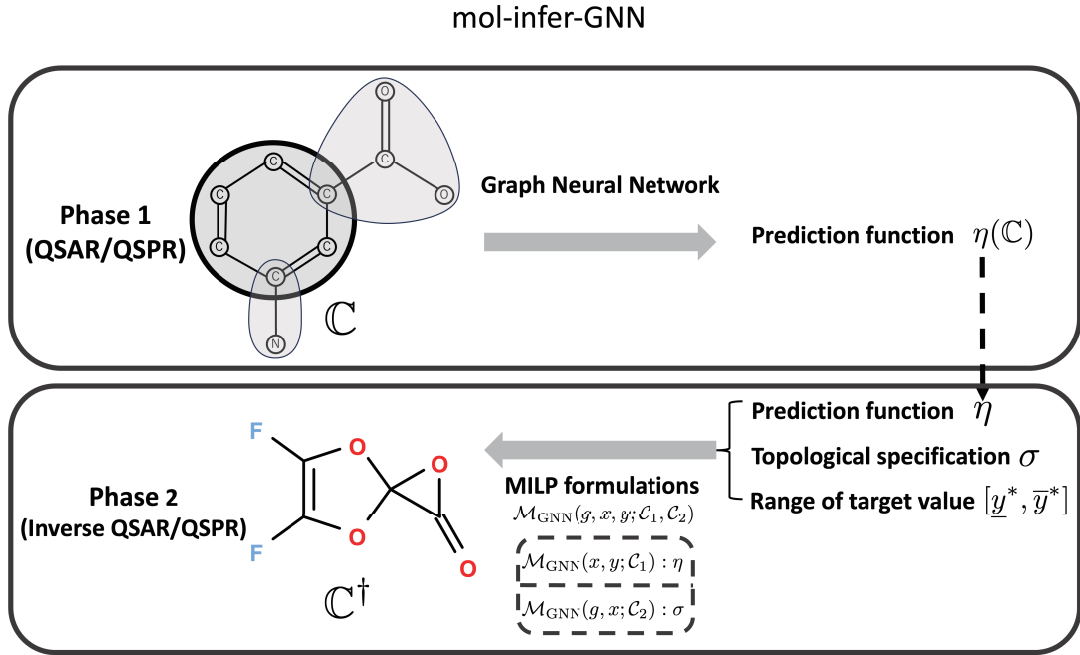


Figure 4: An illustration of the two-phase GNN-based molecular inference framework **mol-infer-GNN**.

A fundamental concept behind GNNs is *message passing*, a mechanism that enables each node in a graph to iteratively update its feature representation by aggregating information from its neighbors. This iterative exchange allows GNNs to capture both local structures (i.e., relationships between adjacent nodes) and global structures (i.e., long-range dependencies within the graph). This gives GNNs the capacity to learn highly expressive representations that encode both topological and attribute-based information, making them powerful tools for graph-based learning tasks. One of the key advantages of GNNs over traditional machine learning methods is the ability to generalize across varying graph sizes and structures, eliminating the need for handcrafted feature engineering, which greatly limits the learning performance on some datasets.

Formally, for a GNN with L layers, given a graph $G = (V, E)$ with initial node feature vectors $\theta_v^{(0)}$ for each node $v \in V$, the feature update process at the ℓ -th ($\ell \in [1, L]$) layer can be described as:

$$\begin{aligned} a_v^{(\ell)} &\leftarrow \text{AGGREGATE}^{(\ell)}(\{\theta_u^{(\ell-1)} \mid u \in N_G(v)\}), \\ \theta_v^{(\ell)} &\leftarrow \text{COMBINE}^{(\ell)}(\theta_v^{(\ell-1)}, a_v^{(\ell)}), \end{aligned}$$

where $\text{AGGREGATE}^{(\ell)}(\cdot)$ is a learnable function that collects features from neighboring nodes, and $\text{COMBINE}^{(\ell)}(\cdot)$ is a learnable function that merges the aggregated features with the current node's features.

After L layers of message passing, the node features $\theta_v^{(L)}$ will capture the structural information from the L -hop neighborhood of each node [43]. A graph-level representation vector θ_G can then be derived by a readout function, typically an aggregation like mean pooling, max pooling, or some more complex function based on attention mechanisms:

$$\theta_G \leftarrow \text{READOUT}(\{\theta_v^{(L)} \mid v \in V\}).$$

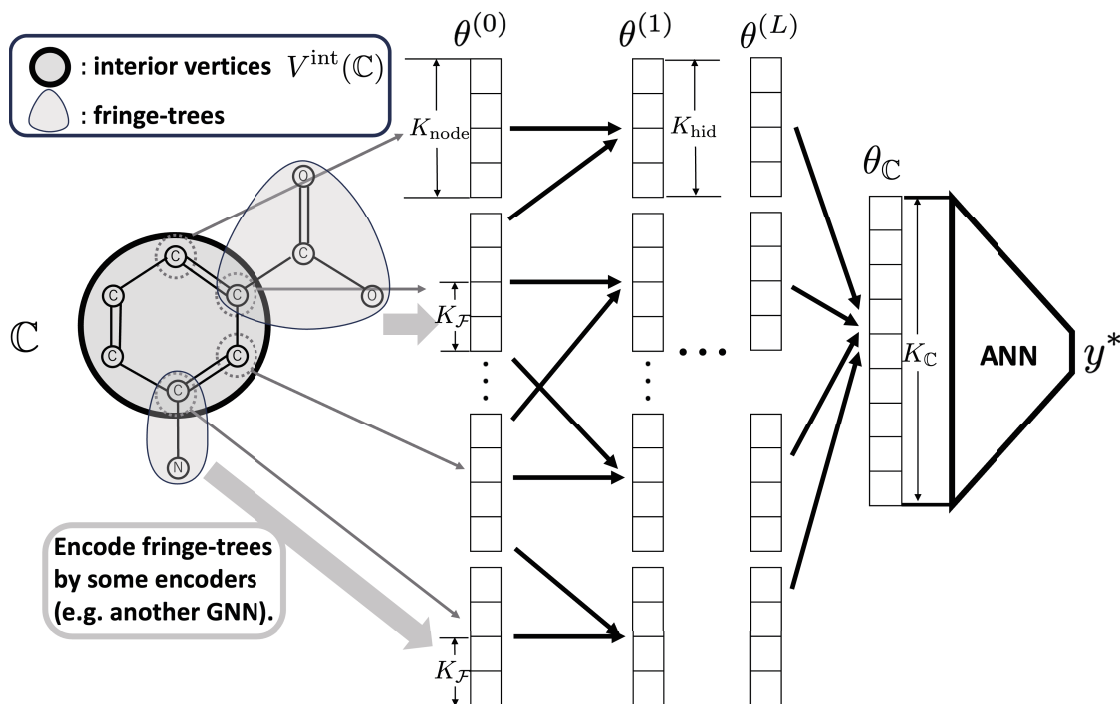


Figure 5: An illustration of the graph neural network 2L-GNN that is used in mol-infer-GNN to construct a prediction function η .

GNNs have shown remarkable success in various applications, especially in molecular property prediction, where they outperform traditional feature-based models by directly leveraging the graph structure of molecules.

2L-GNN While GNNs have demonstrated their superior performance in QSAR/QSPR tasks, integrating GNNs into inverse QSAR/QSPR frameworks faces significant challenges. Typical GNN-based methods often focus on predicting properties from molecular graphs, and they do not guarantee the optimality or exactness of the inferred structures when applied to the inverse problem. Additionally, many models rely on 3D structural information (e.g., bond angles and interatomic distances), which can be computationally expensive to obtain and process [14].

To overcome these limitations, here we propose a novel GNN architecture, 2L-GNN, which is designed specifically to enhance learning performance and maintain the flexibility of the 2L-model of chemical graphs introduced in Section 2.3. Unlike most of the existing approaches that process all nodes (including the hydrogen atoms), 2L-GNN uses only on the interior-vertices $V^{\text{int}}(\mathbb{C})$ as the nodes in GNN architecture. This selective processing reduces computational overhead while preserving essential information. An illustration of 2L-GNN is shown in Figure 5.

Let $L, K_{\text{node}}, K_{\mathcal{F}}, K_{\text{hid}}, K_{\mathbb{C}} \in \mathbb{Z}_+$ be five positive integers, where L denotes the number of layers in 2L-GNN, K_{node} denotes the length of an initial node feature vector, $K_{\mathcal{F}}$ denotes the length of the encoded feature vector that represents the local structure, K_{hid} denotes the length of a node feature vector at the other layers (hidden layers), and $K_{\mathbb{C}}$ denotes the length of the representation vector of a chemical graph \mathbb{C} . The initial feature vector $\theta_v^{(0)} \in \mathbb{R}^{K_{\text{node}}}$ for each interior vertex $v \in V^{\text{int}}(\mathbb{C})$ consists of the following components:

- Atom type: One-hot encoding of the atom type of $\alpha(v)$ (\mathbb{C} , \mathbb{O} , \mathbb{N} or not);
- Degree: The degree $\deg_{\mathbb{C}}(v)$ of the vertex in the chemical graph;
- Valence: The valence of the atom $\alpha(v)$;
- Hydrogen count: The number of hydrogens attached to the vertex v ;
- Ion-valence: The ion-valence of the atom;
- Fringe-tree encoding: A feature vector $\theta_v \in \mathbb{R}^{K_{\mathcal{F}}}$ representing the local structure (ρ -fringe-tree $\mathcal{T}_v \in \mathcal{T}(\mathbb{C})$) rooted at v , obtained via a secondary GNN model.

Notice that we include only 2D information about a molecule since the spatial information like bond angles or interatomic distances is hard to tract in our MILP formulations of Phase 2.

Because of the need to simulate the computational process by MILP formulations in Phase 2, our choice of the functions $\text{AGGREGATE}^{(\ell)}(\cdot)$ and $\text{COMBINE}^{(\ell)}(\cdot)$ are rather simple. The features of each interior vertex are updated through L layers using a straightforward yet effective message-passing scheme. At each layer $\ell, \ell \in [1, L]$, the update rule for the node feature vector $\theta_v^\ell \in \mathbb{R}^{K_{\text{hid}}}$ is given by:

$$\theta_v^{(\ell)} \leftarrow \text{LReLU}\left(\sum_{u \in N_{\text{cint}}(v) \cup \{v\}} W^\ell \theta_u^{(\ell-1)} + B^{(\ell)}\right),$$

where $W^{(\ell)} \in \mathbb{R}^{K_{\text{hid}} \times K_{\text{hid}}}$ ($W^{(1)} \in \mathbb{R}^{K_{\text{node}} \times K_{\text{hid}}}$) and $B^{(\ell)} \in \mathbb{R}^{K_{\text{hid}}}$ are learnable weight matrices and biases and the LReLU (Leaky ReLU) activation $\text{LReLU}(x) := \max(\alpha x, x)$ is used with a slope parameter of $\alpha = 0.1$ to avoid vanishing gradients.

The graph-level representation vector $\theta_{\mathbb{C}} \in \mathbb{R}^{K_{\mathbb{C}}}$ is computed by aggregating the final layer features of all interior vertices:

$$\theta_{\mathbb{C}} \leftarrow \text{LReLU}\left(\sum_{v \in V^{\text{int}}(\mathbb{C})} \theta_v^{(L)}\right).$$

The representation vector $\theta_{\mathbb{C}}$ is then fed into a fully connected artificial neural network with ReLU activation function $\text{ReLU}(x) := \max(0, x)$ (except the final layer) to output the predicted property value $y^* := \eta(\mathbb{C})$ of the chemical graph \mathbb{C} .

3.2 Phase 2: Inverse QSAR/QSPR Phase

Phase 2 is designed to address the core task of inferring a chemical graph that satisfies property and structural requirements. The challenge of ensuring both the optimality and exactness of the inferred chemical graph is achieved by formulating the problem as an MILP problem, which we denote as $\mathcal{M}_{\text{GNN}}(g, x, y; \mathcal{C}_1, \mathcal{C}_2)$.

Formally, the primary goal of Phase 2 is to infer a chemical graph \mathbb{C}^\dagger given:

- the prediction function η learned in Phase 1;
- a topological specification σ , which defines the desired abstract structure of the chemical graph to be inferred; and
- a target property range $[\underline{y}^*, \overline{y}^*]$, indicating the desired range of the predicted property value.

The objective is to find a chemical graph \mathbb{C}^\dagger that belongs to the set of all chemical graphs satisfying the specification σ and whose predicted property value lies within the specified range, i.e.:

$$\mathbb{C}^\dagger \in \mathcal{G}_\sigma, \text{ and } \eta(\mathbb{C}^\dagger) \in [\underline{y}^*, \overline{y}^*],$$

where \mathcal{G}_σ denotes the set of all chemical graphs satisfying σ .

For this, we design an MILP formulation $\mathcal{M}_{\text{GNN}}(g, x, y; \mathcal{C}_1, \mathcal{C}_2)$ consisting of two parts:

- (i) $\mathcal{M}_{\text{GNN}}(x, y; \mathcal{C}_1)$: the part that simulates the computation process of the prediction function η , i.e., the graph neural network 2L-GNN from Phase 1; and
- (ii) $\mathcal{M}_{\text{GNN}}(g, x; \mathcal{C}_2)$: the part of encoding the structural and chemical constraints of the target graph to ensure it adheres the topological specification σ , and the constraints to compute the initial node feature vectors $\theta_v^{(0)}$.

The basic idea of this formulation remains similar to `mol-infer`. In particular, the part $\mathcal{M}_{\text{GNN}}(g, x; \mathcal{C}_2)$ will be somehow similar to the one used in `mol-infer`, but the other one $\mathcal{M}_{\text{GNN}}(x, y; \mathcal{C}_1)$ that simulates the computation process of a GNN is a challenging task, and the extremely flexible rules of the topological specification make it even harder. Here, we manage to realize the computation process of 2L-GNN that is proposed in Section 3.1 under the context of the two-layered model by paying special attention to the situation that a vertex/edge may be not selected in the resultant chemical graph. We list the complete set of constraints for $\mathcal{M}_{\text{GNN}}(g, x, y; \mathcal{C}_1, \mathcal{C}_2)$ in Appendix C, especially the ones for $\mathcal{M}_{\text{GNN}}(x, y; \mathcal{C}_1)$ in Appendix C.8, since it is quite lengthy.

We acknowledge that several studies have already been done on utilizing MILP formulations to represent the computation process of a GNN under the context of molecular optimization, e.g., [25, 45]. However, our MILP formulation for the inverse problem differs significantly from these previous works, in several key aspects:

- Unlike methods that focus on optimizing the property value, our approach aims to solve a feasibility problem, find any valid chemical graph that satisfies the specified property range.
- The use of the 2L-model and topological specification provides greater flexibility in defining the abstract structure of the target chemical graph, while previous approaches like [25, 45] often rely on simple or predetermined graph structures (e.g., fixed presence of one benzene ring, at least one sulfur atom, etc.), greatly limiting the class of chemical graphs that can be inferred.

4 Experimental Results

We implemented our proposed GNN-based molecular inference framework `mol-infer-GNN` and conducted numerical experiments to evaluate its computational effectiveness. The model 2L-GNN was implemented using the library PyTorch Geometric 2.7 [12]. All the experiments were executed on a workstation with a Core i9-9900K processor (3.6 GHz; 5.0 GHz at the maximum), 128 GB DDR4 RAM memory, and an NVIDIA Quadro RTX 5000 GPU.

4.1 Results of QSAR/QSPR Phase

To assess the learning capabilities of our proposed 2L-GNN model for predicting chemical properties, we used the publicly available benchmark QM9 dataset [29, 42]. QM9 dataset comprises molecules

Table 1: Results in Phase 1 on QM9 dataset with performance comparison to LLR in `mol-infer` [49], SchNet [31], MGCN [24], DimeNet++ [13] and PAMNet [46]. The results of SchNet, MGCN, DimeNet++ and PAMNet are adapted from [46].

| π | 2L-GNN ₁₆ | 2L-GNN ₃₂ | <code>mol-infer</code> (LLR) [49] | SchNet [31] | MGCN [24] | DimeNet++ [13] | PAMNet [46] |
|-----------------------|----------------------|----------------------|-----------------------------------|-------------|-----------|----------------|-------------|
| Metric | MAE; R^2 | MAE; R^2 | MAE; R^2 | MAE | MAE | MAE | MAE |
| MU | 588.930; 0.694 | 550.239; 0.733 | 759.067; 0.538 | 21 | 56 | 29.7 | 10.8 |
| ALPHA | 2.156; 0.850 | 1.799; 0.911 | 0.898; 0.975 | 0.124 | 0.030 | 0.0435 | 0.0447 |
| HOMO | 185.550; 0.828 | 158.878; 0.870 | 222.917; 0.774 | 47 | 42.1 | 24.6 | 22.8 |
| LUMO | 205.654; 0.952 | 171.943; 0.967 | 364.419; 0.873 | 39 | 57.4 | 19.5 | 19.2 |
| GAP | 277.472; 0.916 | 232.903; 0.940 | 432.729; 0.820 | 74 | 64.2 | 32.6 | 31.0 |
| $\langle R^2 \rangle$ | 90.020; 0.796 | 79.073; 0.847 | 75.571; 0.849 | 0.158 | 0.11 | 0.331 | 0.093 |
| ZPVE | 110.482; 0.970 | 79.067; 0.984 | 16.743; 0.999 | 1.616 | 1.12 | 1.21 | 1.17 |
| Cv | 0.9188; 0.896 | 0.7947; 0.934 | 0.4610; 0.977 | 0.034 | 0.038 | 0.0230 | 0.0231 |

composed of Hydrogen (H), Carbon (C), Oxygen (O), Nitrogen (N), and Fluorine (F) atoms, with each molecule containing up to 9 heavy (non-hydrogen) atoms. In total, this dataset encompasses 133,885 drug-like organic molecules, representing a diverse array of chemistry. For each molecule in the QM9 dataset, *density functional theory* (B3LYP/6-31G(2df,p) based DFT) is employed to determine a reasonable low-energy structure, and thereby providing access to atom positions, enable a set of intriguing and fundamental chemical properties to be computed [42].

Although a larger size of network will obtain a better learning performance in general, the network size, and the time needed to solve the MILP formulation for the inverse problem in Phase 2 will be increased drastically as well. After some trials of preliminary experiments, we selected the following two variants of our proposed GNN model for the sake of balancing the learning performance and the time effectiveness of solving MILP formulations:

- 2L-GNN₁₆: a compact architecture with $L = 3$, $K_{\text{hid}} = 16$, $K_{\text{C}} = 32$; and
- 2L-GNN₃₂: a larger architecture with $L = 3$, $K_{\text{hid}} = 32$, $K_{\text{C}} = 32$.

Both models were trained and tested on the following chemical properties from the QM9 dataset:

- MU: electric dipole moment (mD);
- ALPHA: isotropic polarizability (a_0^3);
- HOMO: energy of highest occupied molecular orbital (meV);
- LUMO: energy of lowest occupied molecular orbital (meV);
- GAP: the energy difference between HOMO and LUMO (meV);
- $\langle R^2 \rangle$: electronic spatial extent (a_0^2);
- ZPVE: zero point vibrational energy (meV);
- Cv: heat capacity at 298.15K (cal/molK).

To be consistent with previous works, we first remove 3,054 molecules that fail a geometric consistency check or are difficult to converge. We use 110,000 molecules for training, 10,000 for validation, and the remaining 20,831 molecules are used for testing. We evaluate the *mean absolute error* (MAE) and the *coefficient of determination* (R^2) of each property.

Table 2: Comparison of R^2 scores on the test set for 2L-GNN₁₆ and 2L-GNN₃₂ with other approaches in the **mol-infer** framework. The results for LLR, ANN, ALR, and R-MLR are adapted from [48], and for HPS are adapted from [50]. “-” means the corresponding result is not available in the literature.

| π | 2L-GNN ₁₆ | 2L-GNN ₃₂ | LLR | ANN | ALR | R-MLR | HPS |
|-------|----------------------|----------------------|-------|-------|-------|-------|-------|
| MU | 0.694 | 0.733 | 0.367 | 0.409 | 0.403 | 0.645 | 0.708 |
| ALPHA | 0.850 | 0.911 | 0.961 | 0.888 | 0.953 | 0.980 | - |
| HOMO | 0.828 | 0.870 | 0.841 | 0.689 | 0.689 | 0.804 | 0.847 |
| LUMO | 0.952 | 0.967 | 0.841 | 0.860 | 0.833 | 0.920 | 0.948 |
| GAP | 0.916 | 0.940 | 0.784 | 0.795 | 0.755 | 0.876 | 0.907 |
| Cv | 0.896 | 0.934 | 0.970 | 0.911 | 0.966 | 0.978 | - |

Table 1 presents a comparative analysis of 2L-GNN₁₆ and 2L-GNN₃₂ against the traditional LLR (Lasso linear regression)-based **mol-infer** approach and several existing state-of-the-art GNN-based models, including SchNet [31], MGCN [24], DimeNet++ [13], and PAMNet [46]. Unlike previous **mol-infer** approaches, the LLR experiments in Table 1 were conducted on the whole QM9 dataset for a better comparison with 2L-GNN. A key distinction of our approach to other GNN-based models is that 2L-GNN does not utilize 3D coordinate information such as bond angles and interatomic distances, which are commonly leveraged by other models, including the four mentioned models. In addition, these models typically employ deeper architectures with more than 10 hidden layers. Our model makes use of only 2D graphical information and 3 hidden layers, and thus generally underperforms compared to them with no surprise. Nevertheless, our model can still obtain a commendable result with R^2 exceeding 0.9 for the properties such as ALPHA, LUMO, GAP, ZPVE, and Cv.

We also compared our new GNN-based approaches to other machine learning methods (LLR [49], ANN [3], ALR [51], R-MLR [48], and HPS [50]) within the **mol-infer** framework, as shown in Table 2. Although a direct comparison is not entirely fair due to the differences in the dataset (the baseline models were trained on a randomly selected subset of 1000 molecules from the whole QM9 dataset), our results demonstrate that 2L-GNN significantly improves the learning performance for the properties such as MU, HOMO, LUMO and GAP—properties for which **mol-infer** approaches struggled to achieve good learning performance. These improvements highlight the limitations of handcrafted features used in previous models and showcase the advantage of GNNs in learning directly from molecular graph structures. While the performance of 2L-GNN on certain properties like ALPHA and Cv was slightly worse than the traditional LLR-based **mol-infer** approach, it still achieved strong predictive performance—exceeding an R^2 score of 0.9 with the 2L-GNN₃₂ model. This suggests that for some properties, carefully crafted features may still be critical and capture key physicochemical characteristics more effectively than GNNs trained solely on 2D structures. A hybrid approach like [7], combining GNN-based learning with selected handcrafted descriptors, may improve predictive accuracy. This is left as our future work.

4.2 Results of Inverse QSAR/QSPR Phase

In Phase 2, we formulated and solved MILP formulations to infer chemical graphs with desired property values and pre-described abstract structures. For the experiments, we use a set of four

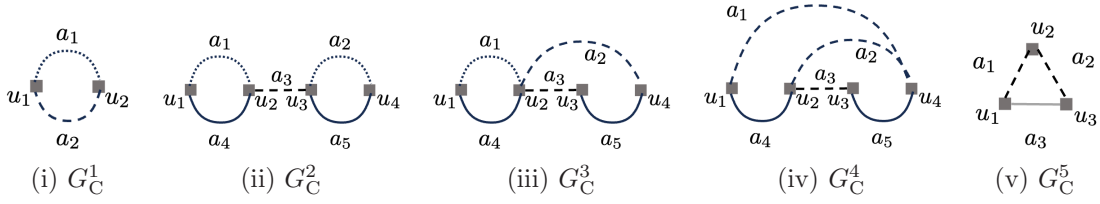


Figure 6: Illustrations of the seed graph G_C^i of instance I_i , $i \in [1, 5]$, respectively. The edges in $E_{(\geq 2)}$ are depicted with dotted lines, the edges in $E_{(\geq 1)}$ are depicted with dashed lines, the edges in $E_{(0/1)}$ are depicted in gray bold lines and the edges in $E_{(=1)}$ are depicted with black solid lines. See Appendix A for the description of the seed graphs and the sets $E_{(\geq 2)}$, $E_{(\geq 1)}$, $E_{(0/1)}$ and $E_{(=1)}$.

Table 3: Number of inverse problems that are determined as feasible/infeasible/timeout among those having 10 different target ranges (2L-GNN₁₆): The time limit is set to 1 hour.

| π | I_1 | I_2 | I_3 | I_4 | I_5 |
|-------|-------|--------|--------|-------|-------|
| HOMO | 3/0/7 | 1/0/9 | 2/0/8 | 3/0/7 | 4/0/6 |
| LUMO | 7/0/3 | 0/0/10 | 1/0/9 | 4/0/6 | 5/0/5 |
| GAP | 4/0/6 | 1/0/9 | 0/0/10 | 1/0/9 | 7/0/3 |

instances originally prepared by Zhu et al. [49], namely $I_i, i \in [1, 4]$, with slight modifications for this research, and one new instance I_5 . Instance I_1 is designed to infer chemical graphs with cycle index one (i.e., chemical graphs with one cycle), and $I_i, i \in [2, 4]$ are designed to infer chemical graphs with cycle index two (i.e., chemical graphs with two cycles). The basic settings for $I_i, i \in [1, 4]$ are the same as in [49], except for the set \mathcal{F} of chemical rooted trees, and the lower and upper bounds on the number of components in the target chemical graph. We also prepared an instance I_5 to imitate the chemical compounds appearing in the QM9 dataset. A 0/1 edge (depicted in gray, see Appendix A for the details) is introduced in I_5 to enable the generation of both a tree-like chemical graph and a chemical graph with cycle index one. The seed graphs G_C^i of the five instances $I_i, i \in [1, 5]$ are illustrated in Figure 6. See Appendix B for a detailed description of these instances.

We selected the properties HOMO, LUMO and GAP, and utilized the prediction functions constructed by 2L-GNN₁₆ and 2L-GNN₃₂ for the numerical experiments. The three properties were selected because of the good learning performance obtained by GNN, and the fact that it is easy to compute them by free and open-source softwares. For each property and the corresponding prediction function, we formulated an MILP for each instance and ten target value ranges which were selected based on the distribution of property values in the QM9 dataset. The MILP formulations were solved using CPLEX 12.10, with a time limit of 1 hour for each formulation.

Tables 3 and 4 summarize the number of formulations that could be determined within 1 hour for each property and instance with the prediction functions constructed by 2L-GNN₁₆ and 2L-GNN₃₂, respectively. In total, 43 out of 150 (28.7%) formulations for 2L-GNN₁₆ and 20 out of 150 (13.3%) formulations for 2L-GNN₃₂ were successful in obtaining a feasible solution within the time limit, showing the hardness of the inverse problem. Basically, the more complex model 2L-GNN₃₂ needs more time to be solved, matching the intuition that while a larger model improves learning performance in Phase 1, the computational time for solving the corresponding MILP formulations

Table 4: Number of inverse problems that are determined as feasible/infeasible/timeout among those having 10 different target ranges (2L-GNN₃₂): The time limit is set to 1 hour.

| π | I_1 | I_2 | I_3 | I_4 | I_5 |
|-------|--------|--------|--------|--------|-------|
| HOMO | 0/0/10 | 0/0/10 | 0/0/10 | 0/0/10 | 4/0/6 |
| LUMO | 0/0/10 | 0/0/10 | 0/0/10 | 0/0/10 | 6/0/4 |
| GAP | 1/0/9 | 0/0/10 | 1/0/9 | 2/0/8 | 6/0/4 |

Table 5: Selected results of Phase 2 on properties HOMO, LUMO, and GAP with the model 2L-GNN₁₆.

| No. | π | inst. | $\underline{y^*}, \overline{y^*}$ (eV) | #v | #c | I-time | n | η | η_{PySCF} | η_{Psi4} |
|-----|-------|-------|--|-------|-------|---------|-----|----------|-----------------------|----------------------|
| (a) | HOMO | I_1 | -8.00, -7.50 | 10517 | 55112 | 40.644 | 19 | -7.63504 | -7.39256 | -7.71839 |
| (b) | | I_2 | -7.00, -6.50 | 10163 | 57570 | 4.134 | 10 | -6.51518 | -6.25516 | -7.31964 |
| (c) | | I_4 | -6.50, -6.00 | 10151 | 58342 | 4.123 | 10 | -6.27818 | -5.87852 | -6.38071 |
| (d) | | I_5 | -7.50, -7.00 | 7377 | 34508 | 19.008 | 9 | -7.01391 | -5.84124 | -6.36345 |
| (e) | LUMO | I_1 | -2.00, -1.50 | 10517 | 55112 | 60.889 | 19 | -1.76264 | -2.01727 | -2.15115 |
| (f) | | I_3 | -3.50, -3.00 | 10159 | 57958 | 4.013 | 11 | -3.35504 | -4.74164 | Err. |
| (g) | | I_5 | 1.00, 1.50 | 7377 | 34508 | 881.593 | 9 | 1.03216 | 1.14088 | 0.73261 |
| (h) | GAP | I_1 | 6.00, 6.50 | 10517 | 55112 | 62.145 | 20 | 6.27711 | 6.07699 | 6.28504 |
| (i) | | I_5 | 7.00, 7.50 | 7377 | 34508 | 753.747 | 9 | 7.13251 | 6.45730 | 6.48175 |

Table 6: Selected results of Phase 2 on properties HOMO, LUMO, and GAP with the model 2L-GNN₃₂.

| No. | π | inst. | $\underline{y^*}, \overline{y^*}$ (eV) | #v | #c | I-time | n | η | η_{PySCF} | η_{Psi4} |
|-----|-------|-------|--|-------|--------|----------|-----|----------|-----------------------|----------------------|
| (j) | HOMO | I_5 | -6.00, -5.50 | 12785 | 67516 | 3262.404 | 9 | -5.51096 | -6.01995 | Err. |
| (k) | LUMO | I_5 | 1.00, 1.50 | 12785 | 67516 | 6.355 | 9 | 1.49046 | 1.53046 | Err. |
| (l) | GAP | I_1 | 4.50, 5.00 | 18325 | 108328 | 618.418 | 17 | 4.98681 | 4.86001 | 5.13423 |

significantly increases in Phase 2. Instance I_5 had the highest number of solved formulations, likely because it was designed to resemble molecules in the QM9 dataset, while instances with more complex structures (e.g., I_2 and I_3) showed lower success rates.

To further assess the quality of our inferred chemical graphs, we used two free and open-source quantum chemistry software PySCF [37, 38] and Psi4 [36] to compute the property values using DFT at the B3LYP/6-31G(2df,p) level and compare them against the predicted values obtained from our constructed prediction functions.

We summarize some selected results about MILP formulations in Tables 5 and 6 for the model 2L-GNN₁₆ and 2L-GNN₃₂, respectively. The following notations are used:

- No.: numbering of the MILP;

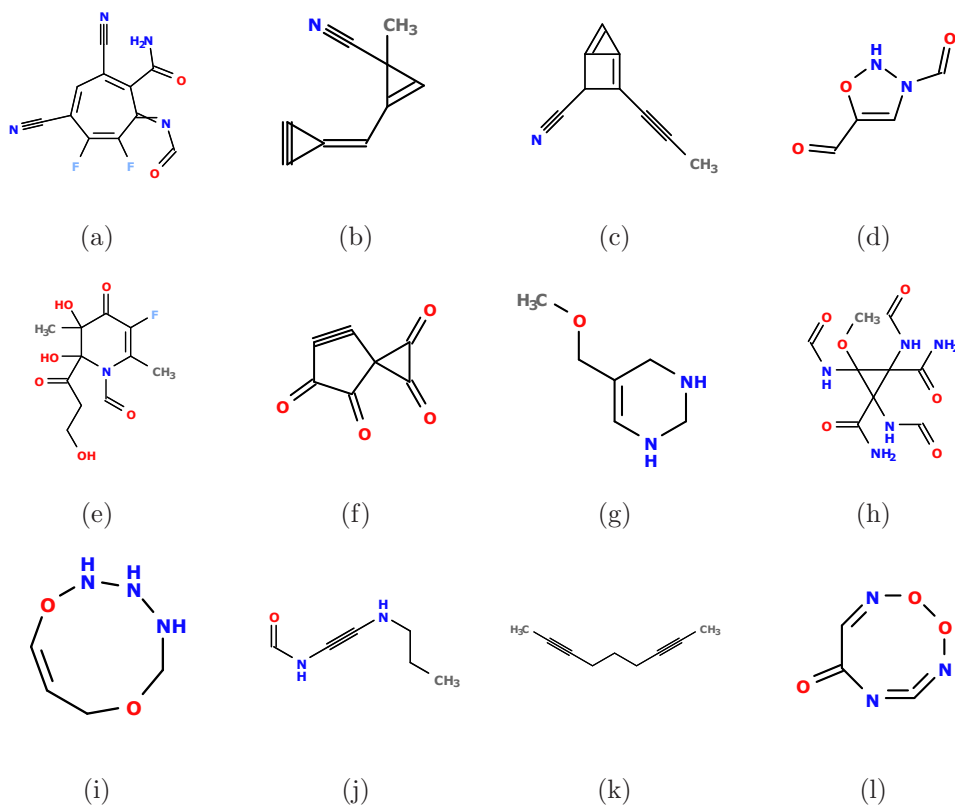


Figure 7: Illustrations of the inferred chemical graphs. (a)-(l) correspond to the first column No. in Tables 5 and 6, respectively.

- π : the property;
- inst.: instance;
- $\underline{y}^*, \overline{y}^*$: range $[\underline{y}^*, \overline{y}^*]$ (in eV) of target value of the chemical graph to be inferred;
- #v: the number of variables in the MILP formulation;
- #c: the number of constraints in the MILP formulation;
- I-time: the time (in seconds) to solve the MILP by CPLEX 12.10;
- n : the number of non-hydrogen atoms in the inferred chemical graph;
- η : the predicted property value by our constructed prediction function;
- η_{PySCF} : the predicted property value by the software PySCF [37, 38]; and
- η_{Psi4} : the predicted property value by the software Psi4 [36] (Err. indicates that an error occurred during the computation).

The inferred molecules contained up to 20 non-hydrogen atoms, demonstrating the practical applicability of our approach. We notice that the predicted values obtained from our prediction function sometimes differ significantly from those computed by PySCF and Psi4 (e.g., the chemical graphs (d), (e) and (j)). We can also see that the differences between the values computed

by PySCF and Psi4 are big, pointing out the instability of DFT methods. In certain cases, Psi4 calculations failed due to chemically unstable structures, indicating potential limitations in the MILP-generated molecular graphs. The issue of unstable generated structures is common in molecular inference studies and highlights the need to incorporate chemical knowledge [9]. Nevertheless, the inferred chemical graphs were of rather good quality, demonstrating the potential of our proposed framework. Figure 7 provides graphical representations of the inferred chemical graphs. The results of our experiments indicate that **mol-infer-GNN** successfully integrates GNN-based learning with MILP-driven molecular inference.

5 Concluding Remarks

In this study, we proposed **mol-infer-GNN**, a novel inverse QSAR/QSPR framework that integrates GNNs into the existing **mol-infer** approach. A key contribution of our work is the successful formulation of the inverse problem of GNN within the 2L-model of **mol-infer** as an MILP formulation. This enables the combination of the deep learning-based molecular property prediction with the rigorous inference capabilities of MILP. The use of the 2L-model plays a crucial role in our framework, as it significantly broadens the class of chemical graphs that can be effectively inferred compared with previous studies. By leveraging GNNs, our framework allows to use the chemical graphs directly, eliminating the need for handcrafted feature vectors while enhancing prediction accuracy. We validated our approach through computational experiments on the QM9 dataset. The results demonstrated that our proposed simple GNN model, **2L-GNN**, can effectively predict molecular properties using only 2D graphical information, which is necessary for the inverse problem to be formulated as MILP formulations at present. Our experiments also indicated that the framework can infer chemical graphs with up to 20 non-hydrogen atoms, highlighting its potential applications in cheminformatics and molecular design.

However, several challenges remain. The computational cost of solving MILP formulations remains high, particularly as the complexity of the target molecular graphs and GNN architectures increases. Future research should focus more on optimizing the inverse problem formulations, using heuristics to solve MILP formulations, and exploring alternative graph learning architectures. Discrepancies between predicted and software-computed property values suggest that further improvements are needed in both GNN training and MILP constraint formulations. Enhancing the graph representation learning and incorporating additional chemical constraints could mitigate these issues. Additionally, trying to incorporate 3D information about molecules is also desired since they can significantly improve prediction accuracy and enhance the overall effectiveness of the framework. These are left as future works. We believe with further refinements and a more integrated hybrid approach, our framework has the potential to significantly advance computational molecular design and inverse QSAR/QSPR research.

Acknowledgement

This work is partially supported by JSPS KAKENHI Grant Numbers JP22H00532 and JP22KJ1979.

References

- [1] Annotations from HSDB (on pubchem). <https://pubchem.ncbi.nlm.nih.gov/source/11933>. Accessed on May 16th, 2025.
- [2] N. A. Azam, R. Chiewvanichakorn, F. Zhang, A. Shurbevski, H. Nagamochi, and T. Akutsu. A novel method for the inverse QSAR/QSPR based on artificial neural networks and mixed integer linear programming with guaranteed admissibility. In *Proceedings of the 13th International Joint Conference on Biomedical Engineering Systems and Technologies - BIOINFORMATICS*, pages 101–108. INSTICC, SciTePress, 2020.
- [3] N. A. Azam, J. Zhu, K. Haraguchi, L. Zhao, H. Nagamochi, and T. Akutsu. Molecular design based on artificial neural networks, integer programming and grid neighbor search. In *2021 IEEE International Conference on Bioinformatics and Biomedicine (BIBM)*, pages 360–363. IEEE, 2021.
- [4] N. A. Azam, J. Zhu, Y. Sun, Y. Shi, A. Shurbevski, L. Zhao, H. Nagamochi, and T. Akutsu. A novel method for inference of acyclic chemical compounds with bounded branch-height based on artificial neural networks and integer programming. *Algorithms for Molecular Biology*, 16:1–39, 2021.
- [5] A. Bojchevski, O. Shchur, D. Zügner, and S. Günnemann. NetGAN: Generating graphs via random walks. In J. Dy and A. Krause, editors, *Proceedings of the 35th International Conference on Machine Learning*, volume 80 of *Proceedings of Machine Learning Research*, pages 610–619. PMLR, 10–15 Jul 2018.
- [6] W. Bort, D. Mazitov, D. Horvath, F. Bonachera, A. Lin, G. Marcou, I. Baskin, T. Madzhidov, and A. Varnek. Inverse QSAR: Reversing descriptor-driven prediction pipeline using attention-based conditional variational autoencoder. *Journal of Chemical Information and Modeling*, 62(22):5471–5484, 11 2022.
- [7] H. Cai, H. Zhang, D. Zhao, J. Wu, and L. Wang. FP-GNN: a versatile deep learning architecture for enhanced molecular property prediction. *Briefings in Bioinformatics*, 23(6):bbac408, 09 2022.
- [8] N. D. Cao and T. Kipf. MolGAN: An implicit generative model for small molecular graphs. arXiv:1805.11973, 2022.
- [9] Y. Cheng, Y. Gong, Y. Liu, B. Song, and Q. Zou. Molecular design in drug discovery: a comprehensive review of deep generative models. *Briefings in Bioinformatics*, 22(6):bbab344, 08 2021.
- [10] A. Cherkasov, E. N. Muratov, D. Fourches, A. Varnek, I. I. Baskin, M. Cronin, J. Dearden, P. Gramatica, Y. C. Martin, R. Todeschini, et al. QSAR modeling: where have you been? where are you going to? *Journal of Medicinal Chemistry*, 57(12):4977–5010, 2014.
- [11] D. Duvenaud, D. Maclaurin, J. Aguilera-Iparraguirre, R. Gómez-Bombarelli, T. Hirzel, A. Aspuru-Guzik, and R. P. Adams. Convolutional networks on graphs for learning molecular fingerprints. In *Proceedings of the 29th International Conference on Neural Information Processing Systems - Volume 2*, NIPS’15, pages 2224–2232, Cambridge, MA, USA, 2015. MIT Press.

- [12] M. Fey and J. E. Lenssen. Fast graph representation learning with PyTorch Geometric. In *ICLR Workshop on Representation Learning on Graphs and Manifolds*, 2019.
- [13] J. Gasteiger, S. Giri, J. T. Margraf, and S. Günnemann. Fast and uncertainty-aware directional message passing for non-equilibrium molecules. arXiv:2011.14115, 2022.
- [14] J. Gilmer, S. S. Schoenholz, P. F. Riley, O. Vinyals, and G. E. Dahl. Neural message passing for quantum chemistry. In D. Precup and Y. W. Teh, editors, *Proceedings of the 34th International Conference on Machine Learning*, volume 70 of *Proceedings of Machine Learning Research*, pages 1263–1272. PMLR, 06–11 Aug 2017.
- [15] R. Gómez-Bombarelli, J. N. Wei, D. Duvenaud, J. M. Hernández-Lobato, B. Sánchez-Lengeling, D. Sheberla, J. Aguilera-Iparraguirre, T. D. Hirzel, R. P. Adams, and A. Aspuru-Guzik. Automatic chemical design using a data-driven continuous representation of molecules. *ACS Central Science*, 4(2):268–276, 2018.
- [16] R. Ido, N. A. Azam, J. Zhu, H. Nagamochi, and T. Akutsu. A dynamic programming algorithm for generating chemical isomers based on frequency vectors. *Scientific Reports*, 15(1):22214, 2025.
- [17] H. Ikebata, K. Hongo, T. Isomura, R. Maezono, and R. Yoshida. Bayesian molecular design with a chemical language model. *Journal of Computer-aided Molecular Design*, 31:379–391, 2017.
- [18] R. Ito, N. A. Azam, C. Wang, A. Shurbevski, H. Nagamochi, and T. Akutsu. A novel method for the inverse QSAR/QSPR to monocyclic chemical compounds based on artificial neural networks and integer programming. In *Advances in Computer Vision and Computational Biology: Proceedings from IPCV’20, HIMS’20, BIOCOMP’20, and BIOENG’20*, pages 641–655. Springer, 2021.
- [19] H. Kaneko. Molecular descriptors, structure generation, and inverse QSAR/QSPR based on SELFIES. *ACS Omega*, 8(24):21781–21786, 06 2023.
- [20] S. Kim, J. Chen, T. Cheng, A. Gindulyte, J. He, S. He, Q. Li, B. A. Shoemaker, P. A. Thiessen, B. Yu, et al. PubChem 2023 update. *Nucleic Acids Research*, 51(D1):D1373–D1380, 2023.
- [21] T. N. Kipf and M. Welling. Semi-supervised classification with graph convolutional networks. arXiv:1609.02907, 2017.
- [22] M. J. Kusner, B. Paige, and J. M. Hernández-Lobato. Grammar variational autoencoder. In *International Conference on Machine Learning*, pages 1945–1954. PMLR, 2017.
- [23] Y.-C. Lo, S. E. Rensi, W. Torng, and R. B. Altman. Machine learning in chemoinformatics and drug discovery. *Drug Discovery Today*, 23(8):1538–1546, 2018.
- [24] C. Lu, Q. Liu, C. Wang, Z. Huang, P. Lin, and L. He. Molecular property prediction: a multilevel quantum interactions modeling perspective. In *Proceedings of the Thirty-Third AAAI Conference on Artificial Intelligence and Thirty-First Innovative Applications of Artificial Intelligence Conference and Ninth AAAI Symposium on Educational Advances in Artificial Intelligence*, AAAI’19/IAAI’19/EAAI’19. AAAI Press, 2019.

- [25] T. McDonald, C. Tsay, A. M. Schweidtmann, and N. Yorke-Smith. Mixed-integer optimisation of graph neural networks for computer-aided molecular design. *Computers & Chemical Engineering*, 185:108660, 2024.
- [26] A. Micheli. Neural network for graphs: A contextual constructive approach. *IEEE Transactions on Neural Networks*, 20(3):498–511, 2009.
- [27] T. Miyao, H. Kaneko, and K. Funatsu. Inverse QSPR/QSAR analysis for chemical structure generation (from y to x). *Journal of Chemical Information and Modeling*, 56(2):286–299, 2016.
- [28] D. Morgan and R. Jacobs. Opportunities and challenges for machine learning in materials science. *Annual Review of Materials Research*, 50(Volume 50, 2020):71–103, 2020.
- [29] R. Ramakrishnan, P. O. Dral, M. Rupp, and O. A. Von Lilienfeld. Quantum chemistry structures and properties of 134 kilo molecules. *Scientific data*, 1(1):1–7, 2014.
- [30] C. Rupakheti, A. Virshup, W. Yang, and D. N. Beratan. Strategy to discover diverse optimal molecules in the small molecule universe. *Journal of Chemical Information and Modeling*, 55(3):529–537, 2015.
- [31] K. T. Schütt, F. Arbabzadah, S. Chmiela, K. R. Müller, and A. Tkatchenko. Quantum-chemical insights from deep tensor neural networks. *Nature Communications*, 8(1):13890, 2017.
- [32] C. Shi, M. Xu, Z. Zhu, W. Zhang, M. Zhang, and J. Tang. GraphAF: a flow-based autoregressive model for molecular graph generation. arXiv:2001.09382, 2020.
- [33] Y. Shi, J. Zhu, N. A. Azam, K. Haraguchi, L. Zhao, H. Nagamochi, and T. Akutsu. An inverse QSAR method based on a two-layered model and integer programming. *International Journal of Molecular Sciences*, 22(6):2847, 2021.
- [34] Y. Shino and H. Kaneko. Improving molecular design with direct inverse analysis of QSAR/QSPR model. *Molecular Informatics*, 44(1):e202400227, 2025.
- [35] M. I. Skvortsova, I. I. Baskin, O. L. Slovokhotova, V. A. Palyulin, and N. S. Zefirov. Inverse problem in QSAR/QSPR studies for the case of topological indexes characterizing molecular shape (kier indices). *Journal of Chemical Information and Computer Sciences*, 33(4):630–634, 1993.
- [36] D. G. A. Smith, L. A. Burns, A. C. Simmonett, R. M. Parrish, M. C. Schieber, R. Galvelis, P. Kraus, H. Kruse, R. Di Remigio, A. Alenaizan, A. M. James, S. Lehtola, J. P. Misiewicz, M. Scheurer, R. A. Shaw, J. B. Schriber, Y. Xie, Z. L. Glick, D. A. Sirianni, J. S. O’Brien, J. M. Waldrop, A. Kumar, E. G. Hohenstein, B. P. Pritchard, B. R. Brooks, I. Schaefer, Henry F., A. Y. Sokolov, K. Patkowski, I. DePrince, A. Eugene, U. Bozkaya, R. A. King, F. A. Evangelista, J. M. Turney, T. D. Crawford, and C. D. Sherrill. PSI4 1.4: Open-source software for high-throughput quantum chemistry. *The Journal of Chemical Physics*, 152(18):184108, 05 2020.
- [37] Q. Sun, T. C. Berkelbach, N. S. Blunt, G. H. Booth, S. Guo, Z. Li, J. Liu, J. D. McClain, E. R. Sayfutyarova, S. Sharma, S. Wouters, and G. K.-L. Chan. PySCF: the python-based simulations of chemistry framework. *WIREs Computational Molecular Science*, 8(1):e1340, 2018.

- [38] Q. Sun, X. Zhang, S. Banerjee, P. Bao, M. Barbry, N. S. Blunt, N. A. Bogdanov, G. H. Booth, J. Chen, Z.-H. Cui, J. J. Eriksen, Y. Gao, S. Guo, J. Hermann, M. R. Hermes, K. Koh, P. Koval, S. Lehtola, Z. Li, J. Liu, N. Mardirossian, J. D. McClain, M. Motta, B. Mussard, H. Q. Pham, A. Pulkin, W. Purwanto, P. J. Robinson, E. Ronca, E. R. Sayfutyarova, M. Scheurer, H. F. Schurkus, J. E. T. Smith, C. Sun, S.-N. Sun, S. Upadhyay, L. K. Wagner, X. Wang, A. White, J. D. Whitfield, M. J. Williamson, S. Wouters, J. Yang, J. M. Yu, T. Zhu, T. C. Berkelbach, S. Sharma, A. Y. Sokolov, and G. K.-L. Chan. Recent developments in the PySCF program package. *The Journal of Chemical Physics*, 153(2):024109, 07 2020.
- [39] K. Tanaka, J. Zhu, N. A. Azam, K. Haraguchi, L. Zhao, H. Nagamochi, and T. Akutsu. An inverse QSAR method based on decision tree and integer programming. In *Intelligent Computing Theories and Application: 17th International Conference, ICIC 2021, Shenzhen, China, August 12–15, 2021, Proceedings, Part II*, pages 628–644. Springer, 2021.
- [40] I. V. Tetko and O. Engkvist. From big data to artificial intelligence: chemoinformatics meets new challenges. *Journal of Cheminformatics*, 12:1–3, 2020.
- [41] Z. Wu, S. Pan, F. Chen, G. Long, C. Zhang, and P. S. Yu. A comprehensive survey on graph neural networks. *IEEE Transactions on Neural Networks and Learning Systems*, 32(1):4–24, 2021.
- [42] Z. Wu, B. Ramsundar, E. N. Feinberg, J. Gomes, C. Geniesse, A. S. Pappu, K. Leswing, and V. Pande. MoleculeNet: a benchmark for molecular machine learning. *Chemical Science*, 9(2):513–530, 2018.
- [43] K. Xu, W. Hu, J. Leskovec, and S. Jegelka. How powerful are graph neural networks? In *International Conference on Learning Representations*, 2019.
- [44] F. Zhang, J. Zhu, R. Chiewvanichakorn, A. Shurbevski, H. Nagamochi, and T. Akutsu. A new approach to the design of acyclic chemical compounds using skeleton trees and integer linear programming. *Applied Intelligence*, 52(15):17058–17072, 2022.
- [45] S. Zhang, J. S. Campos, C. Feldmann, F. Sandfort, M. Mathea, and R. Misener. Augmenting optimization-based molecular design with graph neural networks. *Computers & Chemical Engineering*, 186:108684, 2024.
- [46] S. Zhang, Y. Liu, and L. Xie. A universal framework for accurate and efficient geometric deep learning of molecular systems. *Scientific Reports*, 13(1):19171, 2023.
- [47] J. Zhu. *Novel Methods for Chemical Compound Inference Based on Machine Learning and Mixed Integer Linear Programming*. PhD thesis, Kyoto University, 9 2023.
- [48] J. Zhu, N. A. Azam, S. Cao, R. Ido, K. Haraguchi, L. Zhao, H. Nagamochi, and T. Akutsu. Quadratic descriptors and reduction methods in a two-layered model for compound inference. *Frontiers in Genetics*, 15:1483490, 2025.
- [49] J. Zhu, N. A. Azam, K. Haraguchi, L. Zhao, H. Nagamochi, and T. Akutsu. An inverse QSAR method based on linear regression and integer programming. *Frontiers in Bioscience-Landmark*, 27(6):188, 2022.

- [50] J. Zhu, N. A. Azam, K. Haraguchi, L. Zhao, H. Nagamochi, and T. Akutsu. Molecular design based on integer programming and splitting data sets by hyperplanes. *IEEE/ACM Transactions on Computational Biology and Bioinformatics*, 21(5):1529–1541, 2024.
- [51] J. Zhu, K. Haraguchi, H. Nagamochi, and T. Akutsu. Adjustive linear regression and its application to the inverse QSAR. In *Proceedings of the 15th International Joint Conference on Biomedical Engineering Systems and Technologies - BIOINFORMATICS*, pages 144–151. INSTICC, SciTePress, 2022.
- [52] J. Zhu, C. Wang, A. Shurbevski, H. Nagamochi, and T. Akutsu. A novel method for inference of chemical compounds of cycle index two with desired properties based on artificial neural networks and integer programming. *Algorithms*, 13(5):124, 2020.

Appendix

A Specifying Target Chemical Graphs

In this section, we review the way of specifying target chemical graphs in the two-layered model introduced by Zhu et al. [49], with some modifications for this work.

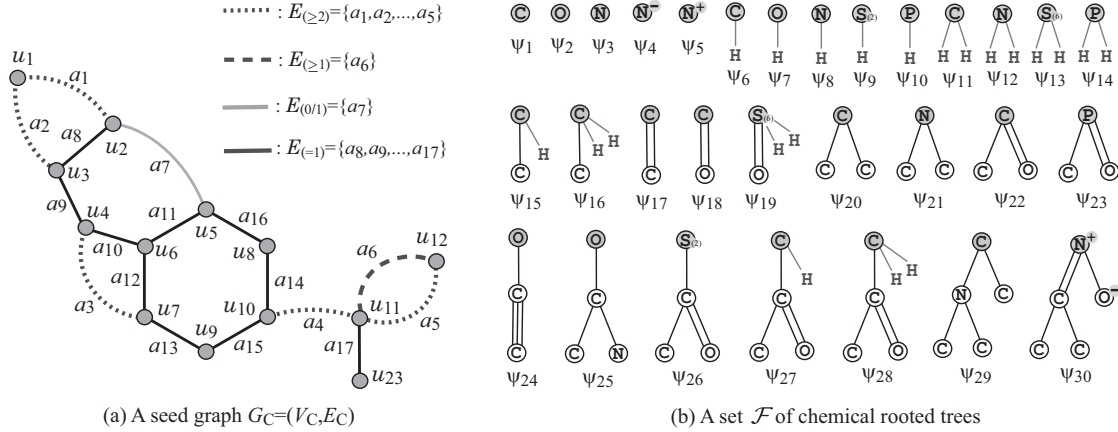


Figure 8: (a) An illustration of a seed graph G_C with $r(G_C) = 5$ where the vertices in V_C are depicted with gray circles, the edges in $E_{(\geq 2)}$ are depicted with dotted lines, the edges in $E_{(\geq 1)}$ are depicted with dashed lines, the edges in $E_{(0/1)}$ are depicted with gray bold lines and the edges in $E_{(=1)}$ are depicted with black solid lines; (b) A set $\mathcal{F} = \{\psi_1, \psi_2, \dots, \psi_{30}\} \subseteq \mathcal{F}(D_\pi)$ of 30 chemical rooted trees $\psi_i, i \in [1, 30]$, where the root of each tree is depicted with a gray circle, where the hydrogens attached to non-root vertices are omitted in the figure.

Given a prediction function η and a target value $y^* \in \mathbb{R}$, we call a chemical graph \mathbb{C}^* such that $\eta(\mathbb{C}^*) = y^*$ a *target chemical graph*. This section presents a set of rules for specifying topological substructure of a target chemical graph in a flexible way in Phase 2.

We first describe how to reduce a chemical graph $\mathbb{C} = (H, \alpha, \beta)$ into an abstract form based on which our specification rules will be defined. To illustrate the reduction process, we use the chemical graph $\mathbb{C} = (H, \alpha, \beta)$ such that $\langle \mathbb{C} \rangle$ is given in Figure 2.

R1 Removal of all ρ -fringe-trees: The interior $H^{\text{int}} = (V^{\text{int}}(\mathbb{C}), E^{\text{int}}(\mathbb{C}))$ of \mathbb{C} is obtained by removing the non-root vertices of each ρ -fringe-trees $\mathbb{C}[u] \in \mathcal{T}(\mathbb{C}), u \in V^{\text{int}}(\mathbb{C})$. Figure 9 illustrates the interior H^{int} of chemical graph \mathbb{C} with $\rho = 2$ in Figure 2.

R2 Removal of some leaf paths: We call a u, v -path Q in H^{int} a *leaf path* if vertex v is a leaf-vertex of H^{int} and the degree of each internal vertex of Q in H^{int} is 2, where we regard that Q is rooted at vertex u . A connected subgraph S of the interior H^{int} of \mathbb{C} is called a *cyclical-base* if S is obtained from H by removing the vertices in $V(Q_u) \setminus \{u\}, u \in X$ for a subset X of interior-vertices and a set $\{Q_u \mid u \in X\}$ of leaf u, v -paths Q_u such that no two paths Q_u and $Q_{u'}$ share a vertex. Figure 10(a) illustrates a cyclical-base $S = H^{\text{int}} - \bigcup_{u \in X} (V(Q_u) \setminus \{u\})$ of the interior H^{int} for a set $\{Q_{u_5} = (u_5, u_{24}), Q_{u_{18}} = (u_{18}, u_{25}, u_{26}, u_{27}), Q_{u_{22}} = (u_{22}, u_{28})\}$ of leaf paths in Figure 9.

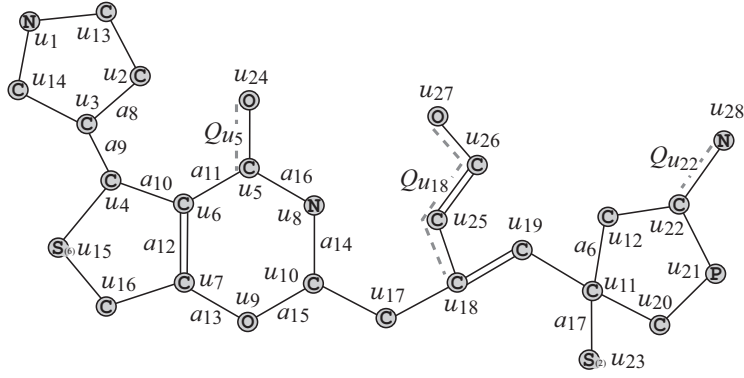


Figure 9: The interior H^{int} of chemical graph \mathbb{C} with $\langle \mathbb{C} \rangle$ in Figure 2 for $\rho = 2$.

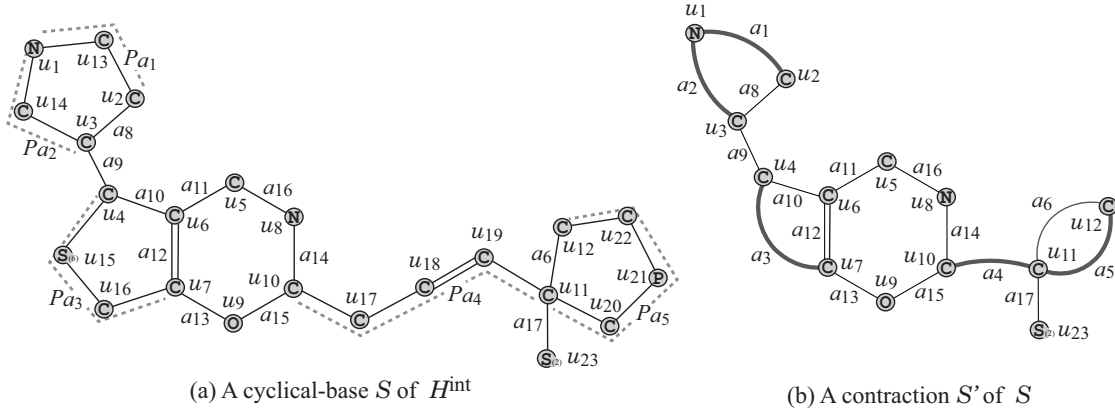


Figure 10: (a) A cyclical-base $S = H^{\text{int}} - \bigcup_{u \in \{u_5, u_{18}, u_{22}\}} (V(Q_u) \setminus \{u\})$ of the interior H^{int} in Figure 9; (b) A contraction S' of S for a pure path set $\mathcal{P} = \{P_{a_1}, P_{a_2}, \dots, P_{a_5}\}$ in (a), where a new edge obtained by contracting a pure path is depicted with a thick line.

R3 Contraction of some pure paths: A path in S is called *pure* if each internal vertex of the path is of degree 2. Choose a set \mathcal{P} of several pure paths in S so that no two paths share vertices except for their end-vertices. A graph S' is called a *contraction* of a graph S (with respect to \mathcal{P}) if S' is obtained from S by replacing each pure u, v -path with a single edge $a = uv$, where S' may contain multiple edges between the same pair of adjacent vertices. Figure 10(b) illustrates a contraction S' obtained from the chemical graph S by contracting each uv -path $P_a \in \mathcal{P}$ into a new edge $a = uv$, where $a_1 = u_1u_2, a_2 = u_1u_3, a_3 = u_4u_7, a_4 = u_{10}u_{11}$ and $a_5 = u_{11}u_{12}$ and $\mathcal{P} = \{P_{a_1} = (u_1, u_{13}, u_2), P_{a_2} = (u_1, u_{14}, u_3), P_{a_3} = (u_4, u_{15}, u_{16}, u_7), P_{a_4} = (u_{10}, u_{17}, u_{18}, u_{19}, u_{11}), P_{a_5} = (u_{11}, u_{20}, u_{21}, u_{22}, u_{12})\}$ of pure paths in Figure 10(a).

We will define a set of rules so that a chemical graph can be obtained from a graph (called a seed graph in the next section) by applying processes R3 to R1 in a reverse way. We specify topological substructures of a target chemical graph with a tuple $(G_C, \sigma_{\text{int}}, \sigma_{\text{ce}})$ called a *target specification* defined under the set of the following rules.

Seed Graph

A *seed graph* $G_C = (V_C, E_C)$ is defined to be a graph (possibly with multiple edges) such that the edge set E_C consists of four sets $E_{(\geq 2)}$, $E_{(\geq 1)}$, $E_{(0/1)}$ and $E_{(=1)}$, where each of them can be empty. A seed graph plays a role of the most abstract form S' in R3. Figure 8(a) illustrates an example of a seed graph G_C with $r(G_C) = 5$, where $V_C = \{u_1, u_2, \dots, u_{12}, u_{23}\}$, $E_{(\geq 2)} = \{a_1, a_2, \dots, a_5\}$, $E_{(\geq 1)} = \{a_6\}$, $E_{(0/1)} = \{a_7\}$ and $E_{(=1)} = \{a_8, a_9, \dots, a_{16}\}$.

A *subdivision* S of G_C is a graph constructed from a seed graph G_C according to the following rules:

- Each edge $e = uv \in E_{(\geq 2)}$ is replaced with a u, v -path P_e of length at least 2;
- Each edge $e = uv \in E_{(\geq 1)}$ is replaced with a u, v -path P_e of length at least 1 (equivalently e is directly used or replaced with a u, v -path P_e of length at least 2);
- Each edge $e \in E_{(0/1)}$ is either used or discarded, where $E_{(0/1)}$ is required to be chosen as a non-separating edge subset of $E(G_C)$ since otherwise the connectivity of a final chemical graph \mathbb{C} is not guaranteed; $r(\mathbb{C}) = r(G_C) - |E'|$ holds for a subset $E' \subseteq E_{(0/1)}$ of edges discarded in a final chemical graph \mathbb{C} ; and
- Each edge $e \in E_{(=1)}$ is always used directly.

We allow a possible elimination of edges in $E_{(0/1)}$ as an optional rule in constructing a target chemical graph from a seed graph, even though such an operation has not been included in the process R3. A subdivision S plays a role of a cyclical-base in R2. A target chemical graph $\mathbb{C} = (H, \alpha, \beta)$ will contain S as a subgraph of the interior H^{int} of \mathbb{C} .

Interior-specification

A graph H^* that serves as the interior H^{int} of a target chemical graph \mathbb{C} will be constructed as follows. First construct a subdivision S of a seed graph G_C by replacing each edge $e = uu' \in E_{(\geq 2)} \cup E_{(\geq 1)}$ with a pure u, u' -path P_e . Next construct a supergraph H^* of S by attaching a leaf path Q_v at each vertex $v \in V_C$ or at an internal vertex $v \in V(P_e) \setminus \{u, u'\}$ of each pure u, u' -path P_e for some edge $e = uu' \in E_{(\geq 2)} \cup E_{(\geq 1)}$, where possibly $Q_v = (v)$, $E(Q_v) = \emptyset$ (i.e., we do not attach any new edges to v). We introduce the following rules for specifying the size of H^* , the length $|E(P_e)|$ of a pure path P_e , the length $|E(Q_v)|$ of a leaf path Q_v , the number of leaf paths Q_v and a bond-multiplicity of each interior-edge, where we call the set of prescribed constants an *interior-specification* σ_{int} :

- Lower and upper bounds $n_{\text{LB}}^{\text{int}}, n_{\text{UB}}^{\text{int}} \in \mathbb{Z}_+$ on the number of interior-vertices of a target chemical graph \mathbb{C} .
- For each edge $e = uu' \in E_{(\geq 2)} \cup E_{(\geq 1)}$,
 - a lower bound $\ell_{\text{LB}}(e)$ and an upper bound $\ell_{\text{UB}}(e)$ on the length $|E(P_e)|$ of a pure u, u' -path P_e . (For a notational convenience, set $\ell_{\text{LB}}(e) := 0$, $\ell_{\text{UB}}(e) := 1$, $e \in E_{(0/1)}$ and $\ell_{\text{LB}}(e) := 1$, $\ell_{\text{UB}}(e) := 1$, $e \in E_{(=1)}$.)
 - a lower bound $\text{bl}_{\text{LB}}(e)$ and an upper bound $\text{bl}_{\text{UB}}(e)$ on the number of leaf paths Q_v attached at internal vertices v of a pure u, u' -path P_e .
 - a lower bound $\text{ch}_{\text{LB}}(e)$ and an upper bound $\text{ch}_{\text{UB}}(e)$ on the maximum length $|E(Q_v)|$ of a leaf path Q_v attached at an internal vertex $v \in V(P_e) \setminus \{u, u'\}$ of a pure u, u' -path P_e .

Table 7: Example 1 of an interior-specification σ_{int} .

| $n_{\text{LB}}^{\text{int}} = 20$ | $n_{\text{UB}}^{\text{int}} = 28$ | | | | | |
|-----------------------------------|-----------------------------------|-------|-------|-------|-------|-------|
| | a_1 | a_2 | a_3 | a_4 | a_5 | a_6 |
| $\ell_{\text{LB}}(a_i)$ | 2 | 2 | 2 | 3 | 2 | 1 |
| $\ell_{\text{UB}}(a_i)$ | 3 | 4 | 3 | 5 | 4 | 4 |
| $\text{bl}_{\text{LB}}(a_i)$ | 0 | 0 | 0 | 1 | 1 | 0 |
| $\text{bl}_{\text{UB}}(a_i)$ | 1 | 1 | 0 | 2 | 1 | 0 |
| $\text{ch}_{\text{LB}}(a_i)$ | 0 | 1 | 0 | 4 | 3 | 0 |
| $\text{ch}_{\text{UB}}(a_i)$ | 3 | 3 | 1 | 6 | 5 | 2 |

| | | | | | | | | | | | | | |
|------------------------------|-------|-------|-------|-------|-------|-------|-------|-------|-------|----------|----------|----------|----------|
| | u_1 | u_2 | u_3 | u_4 | u_5 | u_6 | u_7 | u_8 | u_9 | u_{10} | u_{11} | u_{12} | u_{23} |
| $\text{bl}_{\text{LB}}(u_i)$ | 0 | 0 | 0 | 0 | 0 | 0 | 0 | 0 | 0 | 0 | 0 | 0 | 0 |
| $\text{bl}_{\text{UB}}(u_i)$ | 1 | 1 | 1 | 1 | 1 | 0 | 0 | 0 | 0 | 0 | 0 | 0 | 0 |
| $\text{ch}_{\text{LB}}(u_i)$ | 0 | 0 | 0 | 0 | 1 | 0 | 0 | 0 | 0 | 0 | 0 | 0 | 0 |
| $\text{ch}_{\text{UB}}(u_i)$ | 1 | 0 | 0 | 0 | 3 | 0 | 1 | 1 | 0 | 1 | 2 | 4 | 1 |

| | | | | | | | | | | | | | | | | | |
|--------------------------------|-------|-------|-------|-------|-------|-------|-------|-------|-------|----------|----------|----------|----------|----------|----------|----------|----------|
| | a_1 | a_2 | a_3 | a_4 | a_5 | a_6 | a_7 | a_8 | a_9 | a_{10} | a_{11} | a_{12} | a_{13} | a_{14} | a_{15} | a_{16} | a_{17} |
| $\text{bd}_{2,\text{LB}}(a_i)$ | 0 | 0 | 0 | 1 | 0 | 0 | 0 | 0 | 0 | 0 | 0 | 1 | 0 | 0 | 0 | 0 | 0 |
| $\text{bd}_{2,\text{UB}}(a_i)$ | 1 | 1 | 0 | 2 | 2 | 0 | 0 | 0 | 0 | 0 | 0 | 1 | 0 | 0 | 0 | 0 | 0 |
| $\text{bd}_{3,\text{LB}}(a_i)$ | 0 | 0 | 0 | 0 | 0 | 0 | 0 | 0 | 0 | 0 | 0 | 0 | 0 | 0 | 0 | 0 | 0 |
| $\text{bd}_{3,\text{UB}}(a_i)$ | 0 | 0 | 0 | 0 | 1 | 0 | 0 | 0 | 0 | 0 | 0 | 0 | 0 | 0 | 0 | 0 | 0 |

- For each vertex $v \in V_C$,

a lower bound $\text{ch}_{\text{LB}}(v)$ and an upper bound $\text{ch}_{\text{UB}}(v)$ on the number of leaf paths Q_v attached to v , where $0 \leq \text{ch}_{\text{LB}}(v) \leq \text{ch}_{\text{UB}}(v) \leq 1$.

a lower bound $\text{ch}_{\text{LB}}(v)$ and an upper bound $\text{ch}_{\text{UB}}(v)$ on the length $|E(Q_v)|$ of a leaf path Q_v attached to v .

- For each edge $e = uu' \in E_C$, a lower bound $\text{bd}_{m,\text{LB}}(e)$ and an upper bound $\text{bd}_{m,\text{UB}}(e)$ on the number of edges with bond-multiplicity $m \in [2, 3]$ in u, u' -path P_e , where we regard P_e , $e \in E_{(0/1)} \cup E_{(=1)}$ as single edge e .

We call a graph H^* that satisfies an interior-specification σ_{int} a σ_{int} -extension of G_C , where the bond-multiplicity of each edge has been determined.

Table 7 shows an example of an interior-specification σ_{int} to the seed graph G_C in Figure 8.

Figure 11 illustrates an example of an σ_{int} -extension H^* of seed graph G_C in Figure 8 under the interior-specification σ_{int} in Table 7.

Chemical-specification

Let H^* be a graph that serves as the interior H^{int} of a target chemical graph \mathbb{C} , where the bond-multiplicity of each edge in H^* has been determined. Finally we introduce a set of rules for constructing a target chemical graph \mathbb{C} from H^* by choosing a chemical element $\mathbf{a} \in \Lambda$ and assigning a ρ -fringe-tree ψ to each interior-vertex $v \in V^{\text{int}}$. We introduce the following rules for specifying the size of \mathbb{C} , a set of chemical rooted trees that are allowed to use as ρ -fringe-trees and lower and upper bounds on the frequency of a chemical element, a chemical symbol, and an edge-configuration, where we call the set of prescribed constants a *chemical specification* σ_{ce} :

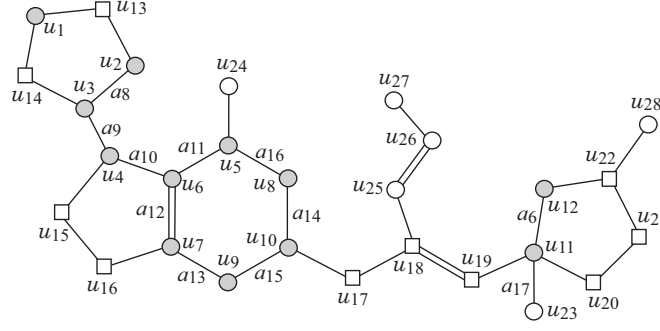


Figure 11: An illustration of a graph H^* that is obtained from the seed graph G_C in Figure 8 under the interior-specification σ_{int} in Table 7, where the vertices newly introduced by pure paths P_{a_i} and leaf paths Q_{v_i} are depicted with white squares and circles, respectively.

- Lower and upper bounds $n_{\text{LB}}, n^* \in \mathbb{Z}_+$ on the number of vertices, where $n_{\text{LB}}^{\text{int}} \leq n_{\text{LB}} \leq n^*$.
- Subsets $\mathcal{F}(v) \subseteq \mathcal{F}(D_\pi), v \in V_C$ and $\mathcal{F}_E \subseteq \mathcal{F}(D_\pi)$ of chemical rooted trees ψ with $\text{ht}(\langle \psi \rangle) \leq \rho$, where we require that every ρ -fringe-tree $\mathbb{C}[v]$ rooted at a vertex $v \in V_C$ (resp., at an internal vertex v not in V_C) in \mathbb{C} belongs to $\mathcal{F}(v)$ (resp., \mathcal{F}_E). Let $\mathcal{F}^* := \mathcal{F}_E \cup \bigcup_{v \in V_C} \mathcal{F}(v)$ and Λ^{ex} denote the set of chemical elements assigned to non-root vertices over all chemical rooted trees in \mathcal{F}^* .
- A subset $\Lambda^{\text{int}} \subseteq \Lambda^{\text{int}}(D_\pi)$, where we require that every chemical element $\alpha(v)$ assigned to an interior-vertex v in \mathbb{C} belongs to Λ^{int} . Let $\Lambda := \Lambda^{\text{int}} \cup \Lambda^{\text{ex}}$ and $\text{na}_a(\mathbb{C})$ (resp., $\text{na}_a^{\text{int}}(\mathbb{C})$ and $\text{na}_a^{\text{ex}}(\mathbb{C})$) denote the number of vertices (resp., interior-vertices and exterior-vertices) v such that $\alpha(v) = a$ in \mathbb{C} .
- A set $\Lambda_{\text{dg}}^{\text{int}} \subseteq \Lambda \times [1, 4]$ of chemical symbols and a set $\Gamma^{\text{int}} \subseteq \Gamma^{\text{int}}(D_\pi)$ of edge-configurations (μ, μ', m) with $\mu \leq \mu'$, where we require that the edge-configuration $\text{ec}(e)$ of an interior-edge e in \mathbb{C} belongs to Γ^{int} . We do not distinguish (μ, μ', m) and (μ', μ, m) .
- Define $\Gamma_{\text{ac}}^{\text{int}}$ to be the set of adjacency-configurations such that $\Gamma_{\text{ac}}^{\text{int}} := \{(\mathbf{a}, \mathbf{b}, m) \mid (\mathbf{a}\mathbf{d}, \mathbf{b}\mathbf{d}', m) \in \Gamma^{\text{int}}\}$. Let $\text{ac}_\nu^{\text{int}}(\mathbb{C}), \nu \in \Gamma_{\text{ac}}^{\text{int}}$ denote the number of interior-edges e such that $\text{ac}(e) = \nu$ in \mathbb{C} .
- Subsets $\Lambda^*(v) \subseteq \{a \in \Lambda^{\text{int}} \mid \text{val}(a) \geq 2\}, v \in V_C$, we require that every chemical element $\alpha(v)$ assigned to a vertex $v \in V_C$ in the seed graph belongs to $\Lambda^*(v)$.
- Lower and upper bound functions $\text{na}_{\text{LB}}, \text{na}_{\text{UB}} : \Lambda \rightarrow [1, n^*]$ and $\text{na}_{\text{LB}}^{\text{int}}, \text{na}_{\text{UB}}^{\text{int}} : \Lambda^{\text{int}} \rightarrow [1, n^*]$ on the number of interior-vertices v such that $\alpha(v) = a$ in \mathbb{C} .
- Lower and upper bound functions $\text{fc}_{\text{LB}}, \text{fc}_{\text{UB}} : \mathcal{F}^* \rightarrow [0, n^*]$ on the number of interior-vertices v such that $\mathbb{C}[v]$ is r-isomorphic to $\psi \in \mathcal{F}^*$ in \mathbb{C} .
- Lower and upper bound functions $\text{ac}_{\text{LB}}^{\text{lf}}, \text{ac}_{\text{UB}}^{\text{lf}} : \Gamma_{\text{ac}}^{\text{lf}} \rightarrow [0, n^*]$ on the number of leaf-edges uv in ac_C with adjacency-configuration ν .

We call a chemical graph \mathbb{C} that satisfies a chemical specification σ_{ce} a $(\sigma_{\text{int}}, \sigma_{\text{ce}})$ -extension of G_C , and denote by $\mathcal{G}(G_C, \sigma_{\text{int}}, \sigma_{\text{ce}})$ the set of all $(\sigma_{\text{int}}, \sigma_{\text{ce}})$ -extensions of G_C .

Table 8 shows an example of a chemical-specification σ_{ce} to the seed graph G_C in Figure 8.

Table 8: Example 2 of a chemical-specification σ_{ce} .

| | | | | | | | | | | | | | | | | | | | | | | | | | | | | | | | | | | | | | | | | | | | | | | |
|--|---|----|---|---|------------------|------------------|------------------|--|----|---|---|------------------|------------------|------------------|------------------|---|-------------------------------------|----|----|---|---|---|---|---|--|---|---|---|---|---|---|-------------------------------------|----|----|---|---|---|---|---|--|----|---|---|---|---|---|
| $n_{\text{LB}} = 30, n^* = 50.$ | | | | | | | | | | | | | | | | | | | | | | | | | | | | | | | | | | | | | | | | | | | | | | |
| branch-parameter: $\rho = 2$ | | | | | | | | | | | | | | | | | | | | | | | | | | | | | | | | | | | | | | | | | | | | | | |
| Each of sets $\mathcal{F}(v), v \in V_C$ and \mathcal{F}_E is set to be the set \mathcal{F} of chemical rooted trees ψ with $\text{ht}(\langle\psi\rangle) \leq \rho = 2$ in Figure 8(b). | | | | | | | | | | | | | | | | | | | | | | | | | | | | | | | | | | | | | | | | | | | | | | |
| $\Lambda = \{\text{H}, \text{C}, \text{N}, \text{O}, \text{S}_{(2)}, \text{S}_{(6)}, \text{P} = \text{P}_{(5)}\}$ | $\Lambda_{\text{dg}}^{\text{int}} = \{\text{C2}, \text{C3}, \text{C4}, \text{N2}, \text{N3}, \text{O2}, \text{S}_{(2)}2, \text{S}_{(6)}3, \text{P4}\}$ | | | | | | | | | | | | | | | | | | | | | | | | | | | | | | | | | | | | | | | | | | | | | |
| $\Gamma_{\text{ac}}^{\text{int}}$ | $\nu_1 = (\text{C}, \text{C}, 1), \nu_2 = (\text{C}, \text{C}, 2), \nu_3 = (\text{C}, \text{N}, 1), \nu_4 = (\text{C}, \text{O}, 1), \nu_5 = (\text{C}, \text{S}_{(2)}, 1), \nu_6 = (\text{C}, \text{S}_{(6)}, 1), \nu_7 = (\text{C}, \text{P}, 1)$ | | | | | | | | | | | | | | | | | | | | | | | | | | | | | | | | | | | | | | | | | | | | | |
| Γ^{int} | $\gamma_1 = (\text{C2}, \text{C2}, 1), \gamma_2 = (\text{C2}, \text{C3}, 1), \gamma_3 = (\text{C2}, \text{C3}, 2), \gamma_4 = (\text{C2}, \text{C4}, 1), \gamma_5 = (\text{C3}, \text{C3}, 1), \gamma_6 = (\text{C3}, \text{C3}, 2),$ $\gamma_7 = (\text{C3}, \text{C4}, 1), \gamma_8 = (\text{C2}, \text{N2}, 1), \gamma_9 = (\text{C3}, \text{N2}, 1), \gamma_{10} = (\text{C3}, \text{O2}, 1), \gamma_{11} = (\text{C2}, \text{C2}, 2), \gamma_{12} = (\text{C2}, \text{O2}, 1),$ $\gamma_{13} = (\text{C3}, \text{N3}, 1), \gamma_{14} = (\text{C4}, \text{S}_{(2)}2, 2), \gamma_{15} = (\text{C2}, \text{S}_{(6)}3, 1), \gamma_{16} = (\text{C3}, \text{S}_{(6)}3, 1), \gamma_{17} = (\text{C2}, \text{P4}, 2),$ $\gamma_{18} = (\text{C3}, \text{P4}, 1)$ | | | | | | | | | | | | | | | | | | | | | | | | | | | | | | | | | | | | | | | | | | | | | |
| $\Lambda^*(u_1) = \Lambda^*(u_8) = \{\text{C}, \text{N}\}, \Lambda^*(u_9) = \{\text{C}, \text{O}\}, \Lambda^*(u) = \{\text{C}\}, u \in V_C \setminus \{u_1, u_8, u_9\}$ | | | | | | | | | | | | | | | | | | | | | | | | | | | | | | | | | | | | | | | | | | | | | | |
| | <table><tr><td></td><td>H</td><td>C</td><td>N</td><td>O</td><td>$\text{S}_{(2)}$</td><td>$\text{S}_{(6)}$</td><td>P</td><td></td><td>C</td><td>N</td><td>O</td><td>$\text{S}_{(2)}$</td><td>$\text{S}_{(6)}$</td><td>P</td></tr><tr><td>$\text{na}_{\text{LB}}(\mathbf{a})$</td><td>40</td><td>27</td><td>1</td><td>1</td><td>0</td><td>0</td><td>0</td><td>$\text{na}_{\text{LB}}^{\text{int}}(\mathbf{a})$</td><td>9</td><td>1</td><td>0</td><td>0</td><td>0</td><td>0</td></tr><tr><td>$\text{na}_{\text{UB}}(\mathbf{a})$</td><td>65</td><td>37</td><td>4</td><td>8</td><td>1</td><td>1</td><td>1</td><td>$\text{na}_{\text{UB}}^{\text{int}}(\mathbf{a})$</td><td>23</td><td>4</td><td>5</td><td>1</td><td>1</td><td>1</td></tr></table> | | H | C | N | O | $\text{S}_{(2)}$ | $\text{S}_{(6)}$ | P | | C | N | O | $\text{S}_{(2)}$ | $\text{S}_{(6)}$ | P | $\text{na}_{\text{LB}}(\mathbf{a})$ | 40 | 27 | 1 | 1 | 0 | 0 | 0 | $\text{na}_{\text{LB}}^{\text{int}}(\mathbf{a})$ | 9 | 1 | 0 | 0 | 0 | 0 | $\text{na}_{\text{UB}}(\mathbf{a})$ | 65 | 37 | 4 | 8 | 1 | 1 | 1 | $\text{na}_{\text{UB}}^{\text{int}}(\mathbf{a})$ | 23 | 4 | 5 | 1 | 1 | 1 |
| | H | C | N | O | $\text{S}_{(2)}$ | $\text{S}_{(6)}$ | P | | C | N | O | $\text{S}_{(2)}$ | $\text{S}_{(6)}$ | P | | | | | | | | | | | | | | | | | | | | | | | | | | | | | | | | |
| $\text{na}_{\text{LB}}(\mathbf{a})$ | 40 | 27 | 1 | 1 | 0 | 0 | 0 | $\text{na}_{\text{LB}}^{\text{int}}(\mathbf{a})$ | 9 | 1 | 0 | 0 | 0 | 0 | | | | | | | | | | | | | | | | | | | | | | | | | | | | | | | | |
| $\text{na}_{\text{UB}}(\mathbf{a})$ | 65 | 37 | 4 | 8 | 1 | 1 | 1 | $\text{na}_{\text{UB}}^{\text{int}}(\mathbf{a})$ | 23 | 4 | 5 | 1 | 1 | 1 | | | | | | | | | | | | | | | | | | | | | | | | | | | | | | | | |
| | $\psi \in \{\psi_i \mid i = 1, 6, 11\} \quad \psi \in \mathcal{F}^* \setminus \{\psi_i \mid i = 1, 6, 11\}$ | | | | | | | | | | | | | | | | | | | | | | | | | | | | | | | | | | | | | | | | | | | | | |
| $\text{fc}_{\text{LB}}(\psi)$ | 1 | | | | | | | 0 | | | | | | | | | | | | | | | | | | | | | | | | | | | | | | | | | | | | | | |
| $\text{fc}_{\text{UB}}(\psi)$ | 10 | | | | | | | 3 | | | | | | | | | | | | | | | | | | | | | | | | | | | | | | | | | | | | | | |
| | $\nu \in \{(\text{C}, \text{C}, 1), (\text{C}, \text{C}, 2)\} \quad \nu \in \Gamma_{\text{ac}}^{\text{lf}} \setminus \{(\text{C}, \text{C}, 1), (\text{C}, \text{C}, 2)\}$ | | | | | | | | | | | | | | | | | | | | | | | | | | | | | | | | | | | | | | | | | | | | | |
| $\text{ac}_{\text{LB}}^{\text{lf}}(\nu)$ | 0 | | | | | | | 0 | | | | | | | | | | | | | | | | | | | | | | | | | | | | | | | | | | | | | | |
| $\text{ac}_{\text{UB}}^{\text{lf}}(\nu)$ | 10 | | | | | | | 8 | | | | | | | | | | | | | | | | | | | | | | | | | | | | | | | | | | | | | | |

Figure 2 illustrates an example \mathbb{C} of a $(\sigma_{\text{int}}, \sigma_{ce})$ -extension of G_C obtained from the σ_{int} -extension H^* in Figure 11 under the chemical-specification σ_{ce} in Table 8. Note that $r(\mathbb{C}) = r(H^*) = r(G_C) - 1 = 4$ holds since the edge in $E_{(0/1)}$ is discarded in H^* .

B Test Instances for Phase 2

We prepared the following instances $I^i, i \in [1, 5]$ for conducting experiments in Phase 2.

- (1) $I_i = (G_C^i, \sigma_{\text{int}}^i, \sigma_{ce}^i), i = 1, 2, 3, 4$: An instance for inferring chemical graphs with rank at most 2. In the four instances $I_i, i = 1, 2, 3, 4$, the following specifications in $(\sigma_{\text{int}}, \sigma_{ce})$ are common.

Set $\Lambda := \Lambda(\pi)$ for a given property $\pi \in \{\text{HOMO}, \text{LUMO}, \text{GAP}\}$, set $\Lambda_{\text{dg}}^{\text{int}}$ to be the set of all possible symbols in $\Lambda \times [1, 4]$ that appear in the data set D_π and set Γ^{int} to be the set of all edge-configurations that appear in the data set D_π . Set $\Lambda^*(v) := \Lambda, v \in V_C$.

The lower bounds $\ell_{LB}, \text{bl}_{LB}, \text{ch}_{LB}, \text{bd}_{2, LB}, \text{bd}_{3, LB}, \text{na}_{LB}, \text{na}_{LB}^{\text{int}}, \text{ns}_{LB}^{\text{int}}, \text{ac}_{LB}^{\text{int}}, \text{ec}_{LB}^{\text{int}}$ and $\text{ac}_{LB}^{\text{lf}}$ are all set to be 0.

The upper bounds $\ell_{UB}, \text{bl}_{UB}, \text{ch}_{UB}, \text{bd}_{2, UB}, \text{bd}_{3, UB}, \text{na}_{UB}, \text{na}_{UB}^{\text{int}}, \text{ns}_{UB}^{\text{int}}, \text{ac}_{UB}^{\text{int}}, \text{ec}_{UB}^{\text{int}}$ and $\text{ac}_{UB}^{\text{lf}}$ are all set to be an upper bound n^* on $n(G^*)$.

For each property π , let $\mathcal{F}(D_\pi)$ denote the set of 2-fringe-trees in the compounds in D_π , and select a subset $\mathcal{F}_\pi^i \subseteq \mathcal{F}(D_\pi)$ with $|\mathcal{F}_\pi^i| = 45 - 5i, i \in [1, 5]$. For each instance I_i , set $\mathcal{F}_E := \mathcal{F}(v) := \mathcal{F}_\pi^i, v \in V_C$ and $\text{fc}_{LB}(\psi) := 0, \text{fc}_{UB}(\psi) := 10, \psi \in \mathcal{F}_\pi^i$.

Instance I_1 is given by the rank-1 seed graph G_C^1 in Figure 6(i) and Instances I_i , $i = 2, 3, 4$ are given by the rank-2 seed graph G_C^i , $i = 2, 3, 4$ in Figure 6(ii)-(iv).

- (i) For the instance I_1 , select as a seed graph the monocyclic graph $G_C^1 = (V_C, E_C = E_{(\geq 2)} \cup E_{(\geq 1)})$ in Figure 6(i), where $V_C = \{u_1, u_2\}$, $E_{(\geq 2)} = \{a_1\}$ and $E_{(\geq 1)} = \{a_2\}$. Set $n_{LB}^{int} := 6$, $n_{UB}^{int} := 8$, $n_{LB} := 15$ and $n^* := 20$.
 - (ii) For the instance I_2 , select as a seed graph the graph $G_C^2 = (V_C, E_C = E_{(\geq 2)} \cup E_{(\geq 1)} \cup E_{(=1)})$ in Figure 6(ii), where $V_C = \{u_1, u_2, u_3, u_4\}$, $E_{(\geq 2)} = \{a_1, a_2\}$, $E_{(\geq 1)} = \{a_3\}$ and $E_{(=1)} = \{a_4, a_5\}$. Set $n_{LB}^{int} := 6$, $n_{UB}^{int} := 12$, $n_{LB} := 10$ and $n^* := 15$.
 - (iii) For the instance I_3 , select as a seed graph the graph $G_C^3 = (V_C, E_C = E_{(\geq 2)} \cup E_{(\geq 1)} \cup E_{(=1)})$ in Figure 6(iii), where $V_C = \{u_1, u_2, u_3, u_4\}$, $E_{(\geq 2)} = \{a_1\}$, $E_{(\geq 1)} = \{a_2, a_3\}$ and $E_{(=1)} = \{a_4, a_5\}$. Set $n_{LB}^{int} := 6$, $n_{UB}^{int} := 12$, $n_{LB} := 10$ and $n^* := 15$.
 - (iv) For the instance I_4 , select as a seed graph the graph $G_C^4 = (V_C, E_C = E_{(\geq 2)} \cup E_{(\geq 1)} \cup E_{(=1)})$ in Figure 6(iv), where $V_C = \{u_1, u_2, u_3, u_4\}$, $E_{(\geq 1)} = \{a_1, a_2, a_3\}$ and $E_{(=1)} = \{a_4, a_5\}$. Set $n_{LB}^{int} := 6$, $n_{UB}^{int} := 12$, $n_{LB} := 10$ and $n^* := 15$.
- (2) $I_5 = (G_C^5, \sigma_{int}^5, \sigma_{ce}^5)$: An instance for inferring chemical graphs resembling the molecules in the QM9 dataset. Below is the specification $(\sigma_{int}^5, \sigma_{ce}^5)$ for I_5 .

Set $\Lambda := \Lambda(\pi)$ for a given property $\pi \in \{\text{HOMO}, \text{LUMO}, \text{GAP}\}$, set Λ_{dg}^{int} to be the set of all possible symbols in $\Lambda \times [1, 4]$ that appear in the data set D_π and set Γ^{int} to be the set of all edge-configurations that appear in the data set D_π . Set $\Lambda^*(v) := \Lambda$, $v \in V_C$.

The lower bounds ℓ_{LB} , bl_{LB} , ch_{LB} , $bd_{2,LB}$, $bd_{3,LB}$, na_{LB} , na_{LB}^{int} , ns_{LB}^{int} , ac_{LB}^{int} , ec_{LB}^{int} and ac_{LB}^{lf} are all set to be 0.

The upper bounds ℓ_{UB} , bl_{UB} , ch_{UB} , $bd_{2,UB}$, $bd_{3,UB}$, na_{UB} , na_{UB}^{int} , ns_{UB}^{int} , ac_{UB}^{int} , ec_{UB}^{int} and ac_{UB}^{lf} are all set to be an upper bound n^* on $n(G^*)$.

For each property π , let $\mathcal{F}(D_\pi)$ denote the set of 2-fringe-trees in the compounds in D_π , and select a subset $\mathcal{F}_\pi^5 \subseteq \mathcal{F}(D_\pi)$ with $|\mathcal{F}_\pi^5| = 50$. For each instance I_i , set $\mathcal{F}_E := \mathcal{F}(v) := \mathcal{F}_\pi^i$, $v \in V_C$ and $fc_{LB}(\psi) := 0$, $fc_{UB}(\psi) := 10$, $\psi \in \mathcal{F}_\pi^i$.

Instance I_5 is given by the seed graph G_C^5 in Figure 6(v).

- (v) For the instance I_5 , select as a seed graph the graph $G_C^5 = (V_C, E_C = E_{(\geq 2)} \cup E_{(0/1)})$ in Figure 6(v), where $V_C = \{u_1, u_2, u_3\}$, $E_{(\geq 2)} = \{a_1, a_2\}$ and $E_{(0/1)} = \{a_3\}$. Set $n_{LB}^{int} := 3$, $n_{UB}^{int} := 9$, $n_{LB} := 3$ and $n^* := 9$.

C All Constraints in an MILP Formulation for Chemical Graphs

We define a standard encoding of a finite set A of elements to be a bijection $\sigma : A \rightarrow [1, |A|]$, where we denote by $[A]$ the set $[1, |A|]$ of integers and by $[e]$ the encoded element $\sigma(e)$. Let ϵ denote *null*, a fictitious chemical element that does not belong to any set of chemical elements, chemical symbols, adjacency-configurations and edge-configurations in the following formulation. Given a finite set A , let A_ϵ denote the set $A \cup \{\epsilon\}$ and define a standard encoding of A_ϵ to be a bijection $\sigma : A \rightarrow [0, |A|]$ such that $\sigma(\epsilon) = 0$, where we denote by $[A_\epsilon]$ the set $[0, |A|]$ of integers and by $[e]$ the encoded element $\sigma(e)$, where $[\epsilon] = 0$.

Let $\sigma = (G_C, \sigma_{\text{int}}, \sigma_{\text{ce}})$ be a target specification, ρ denote the branch-parameter in the specification σ and \mathbb{C} denote a chemical graph in $\mathcal{G}(G_C, \sigma_{\text{int}}, \sigma_{\text{ce}})$.

C.1 Selecting a Cyclical-base

Recall that

$$\begin{aligned} E_{(=1)} &= \{e \in E_C \mid \ell_{\text{LB}}(e) = \ell_{\text{UB}}(e) = 1\}; & E_{(0/1)} &= \{e \in E_C \mid \ell_{\text{LB}}(e) = 0, \ell_{\text{UB}}(e) = 1\}; \\ E_{(\geq 1)} &= \{e \in E_C \mid \ell_{\text{LB}}(e) = 1, \ell_{\text{UB}}(e) \geq 2\}; & E_{(\geq 2)} &= \{e \in E_C \mid \ell_{\text{LB}}(e) \geq 2\}; \end{aligned}$$

- Every edge $a_i \in E_{(=1)}$ is included in $\langle \mathbb{C} \rangle$;
- Each edge $a_i \in E_{(0/1)}$ is included in $\langle \mathbb{C} \rangle$ if necessary;
- For each edge $a_i \in E_{(\geq 2)}$, edge a_i is not included in $\langle \mathbb{C} \rangle$ and instead a path

$$P_i = (v_{\text{tail}(i)}^C, v_{j-1}^T, v_j^T, \dots, v_{j+t}^T, v_{\text{head}(i)}^C)$$

of length at least 2 from vertex $v_{\text{tail}(i)}^C$ to vertex $v_{\text{head}(i)}^C$ visiting some vertices in V_T constructed in $\langle \mathbb{C} \rangle$; and

- For each edge $a_i \in E_{(\geq 1)}$, either edge a_i is directly used in $\langle \mathbb{C} \rangle$ or the above path P_i of length at least 2 is constructed in $\langle \mathbb{C} \rangle$.

Let $t_C \triangleq |V_C|$ and denote V_C by $\{v_i^C \mid i \in [1, t_C]\}$. Regard the seed graph G_C as a digraph such that each edge a_i with end-vertices v_j^C and $v_{j'}^C$ is directed from v_j^C to $v_{j'}^C$ when $j < j'$. For each directed edge $a_i \in E_C$, let $\text{head}(i)$ and $\text{tail}(i)$ denote the head and tail of $e^C(i)$; i.e., $a_i = (v_{\text{tail}(i)}^C, v_{\text{head}(i)}^C)$.

Define

$$k_C \triangleq |E_{(\geq 2)} \cup E_{(\geq 1)}|, \quad \widetilde{k}_C \triangleq |E_{(\geq 2)}|,$$

and denote $E_C = \{a_i \mid i \in [1, m_C]\}$, $E_{(\geq 2)} = \{a_k \mid k \in [1, \widetilde{k}_C]\}$, $E_{(\geq 1)} = \{a_k \mid k \in [\widetilde{k}_C + 1, k_C]\}$, $E_{(0/1)} = \{a_i \mid i \in [k_C + 1, k_C + |E_{(0/1)}|]\}$ and $E_{(=1)} = \{a_i \mid i \in [k_C + |E_{(0/1)}| + 1, m_C]\}$. Let $I_{(=1)}$ denote the set of indices i of edges $a_i \in E_{(=1)}$. Similarly for $I_{(0/1)}$, $I_{(\geq 1)}$ and $I_{(\geq 2)}$.

To control the construction of such a path P_i for each edge $a_k \in E_{(\geq 2)} \cup E_{(\geq 1)}$, we regard the index $k \in [1, k_C]$ of each edge $a_k \in E_{(\geq 2)} \cup E_{(\geq 1)}$ as the “color” of the edge. To introduce necessary linear constraints that can construct such a path P_k properly in our MILP, we assign the color k to the vertices $v_{j-1}^T, v_j^T, \dots, v_{j+t}^T$ in V_T when the above path P_k is used in $\langle \mathbb{C} \rangle$.

For each index $s \in [1, t_C]$, let $I_C(s)$ denote the set of edges $e \in E_C$ incident to vertex v_s^C , and $E_{(=1)}^+(s)$ (resp., $E_{(=1)}^-(s)$) denote the set of edges $a_i \in E_{(=1)}$ such that the tail (resp., head) of a_i is vertex v_s^C . Similarly for $E_{(0/1)}^+(s)$, $E_{(0/1)}^-(s)$, $E_{(\geq 1)}^+(s)$, $E_{(\geq 1)}^-(s)$, $E_{(\geq 2)}^+(s)$ and $E_{(\geq 2)}^-(s)$. Let $I_C(s)$ denote the set of indices i of edges $a_i \in I_C(s)$. Similarly for $I_{(=1)}^+(s)$, $I_{(=1)}^-(s)$, $I_{(0/1)}^+(s)$, $I_{(0/1)}^-(s)$, $I_{(\geq 1)}^+(s)$, $I_{(\geq 1)}^-(s)$, $I_{(\geq 2)}^+(s)$ and $I_{(\geq 2)}^-(s)$. Note that $[1, k_C] = I_{(\geq 2)} \cup I_{(\geq 1)}$ and $[\widetilde{k}_C + 1, m_C] = I_{(\geq 1)} \cup I_{(0/1)} \cup I_{(=1)}$.

constants:

- $t_C = |V_C|$, $\widetilde{k}_C = |E_{(\geq 2)}|$, $k_C = |E_{(\geq 2)} \cup E_{(\geq 1)}|$, $t_T = n_{\text{UB}}^{\text{int}} - |V_C|$, $m_C = |E_C|$. Note that $a_i \in E_C \setminus (E_{(\geq 2)} \cup E_{(\geq 1)})$ holds $i \in [k_C + 1, m_C]$;
- $\ell_{\text{LB}}(k), \ell_{\text{UB}}(k) \in [1, t_T]$, $k \in [1, k_C]$: lower and upper bounds on the length of path P_k ;
- $r_{G_C} \in [1, m_C]$: the rank $r(G_C)$ of seed graph G_C ;

variables:

- $e^C(i) \in [0, 1]$, $i \in [1, m_C]$: $e^C(i)$ represents edge $a_i \in E_C$, $i \in [1, m_C]$ ($e^C(i) = 1$, $i \in I_{(=1)}$; $e^C(i) = 0$, $i \in I_{(\geq 2)}$) ($e^C(i) = 1 \Leftrightarrow$ edge a_i is used in $\langle \mathbb{C} \rangle$);
- $v^T(i) \in [0, 1]$, $i \in [1, t_T]$: $v^T(i) = 1 \Leftrightarrow$ vertex v_i^T is used in $\langle \mathbb{C} \rangle$;
- $e^T(i) \in [0, 1]$, $i \in [1, t_T + 1]$: $e^T(i)$ represents edge $e_i^T = (v_{i-1}^T, v_i^T) \in E_T$, where e_1^T and $e_{t_T+1}^T$ are fictitious edges ($e^T(i) = 1 \Leftrightarrow$ edge e_i^T is used in $\langle \mathbb{C} \rangle$);
- $\chi^T(i) \in [0, k_C]$, $i \in [1, t_T]$: $\chi^T(i)$ represents the color assigned to vertex v_i^T ($\chi^T(i) = k > 0 \Leftrightarrow$ vertex v_i^T is assigned color k ; $\chi^T(i) = 0$ means that vertex v_i^T is not used in $\langle \mathbb{C} \rangle$);
- $\text{clr}^T(k) \in [\ell_{LB}(k) - 1, \ell_{UB}(k) - 1]$, $k \in [1, k_C]$, $\text{clr}^T(0) \in [0, t_T]$: the number of vertices $v_i^T \in V_T$ with color c ;
- $\delta_\chi^T(k) \in [0, 1]$, $k \in [0, k_C]$: $\delta_\chi^T(k) = 1 \Leftrightarrow \chi^T(i) = k$ for some $i \in [1, t_T]$;
- $\chi^T(i, k) \in [0, 1]$, $i \in [1, t_T]$, $k \in [0, k_C]$ ($\chi^T(i, k) = 1 \Leftrightarrow \chi^T(i) = k$);
- $\widetilde{\deg}_C^+(i) \in [0, 4]$, $i \in [1, t_C]$: the out-degree of vertex v_i^C with the used edges e^C in E_C ;
- $\widetilde{\deg}_C^-(i) \in [0, 4]$, $i \in [1, t_C]$: the in-degree of vertex v_i^C with the used edges e^C in E_C ;
- rank: the rank $r(\mathbb{C})$ of a target chemical graph \mathbb{C} ;

constraints:

$$\text{rank} = r_{G_C} - \sum_{i \in I_{(0/1)}} (1 - e^C(i)), \quad (1)$$

$$e^C(i) = 1, \quad i \in I_{(=1)}, \quad (2)$$

$$e^C(i) = 0, \quad \text{clr}^T(i) \geq 1, \quad i \in I_{(\geq 2)}, \quad (3)$$

$$e^C(i) + \text{clr}^T(i) \geq 1, \quad \text{clr}^T(i) \leq t_T \cdot (1 - e^C(i)), \quad i \in I_{(\geq 1)}, \quad (4)$$

$$\sum_{c \in I_{(\geq 1)}^-(i) \cup I_{(0/1)}^-(i) \cup I_{(=1)}^-(i)} e^C(c) = \widetilde{\deg}_C^-(i), \quad \sum_{c \in I_{(\geq 1)}^+(i) \cup I_{(0/1)}^+(i) \cup I_{(=1)}^+(i)} e^C(c) = \widetilde{\deg}_C^+(i), \quad i \in [1, t_C], \quad (5)$$

$$\chi^T(i, 0) = 1 - v^T(i), \quad \sum_{k \in [0, k_C]} \chi^T(i, k) = 1, \quad \sum_{k \in [0, k_C]} k \cdot \chi^T(i, k) = \chi^T(i), \quad i \in [1, t_T], \quad (6)$$

$$\sum_{i \in [1, t_T]} \chi^T(i, k) = \text{clr}^T(k), \quad t_T \cdot \delta_\chi^T(k) \geq \sum_{i \in [1, t_T]} \chi^T(i, k) \geq \delta_\chi^T(k), \quad k \in [0, k_C], \quad (7)$$

$$v^T(i-1) \geq v^T(i), \quad k_C \cdot (v^T(i-1) - e^T(i)) \geq \chi^T(i-1) - \chi^T(i) \geq v^T(i-1) - e^T(i), \quad i \in [2, t_T]. \quad (8)$$

C.2 Constraints for Including Leaf Paths

Let \tilde{t}_C denote the number of vertices $u \in V_C$ such that $\text{bl}_{UB}(u) = 1$ and assume that $V_C = \{u_1, u_2, \dots, u_p\}$ so that

$$\text{bl}_{UB}(u_i) = 1, i \in [1, \tilde{t}_C] \text{ and } \text{bl}_{UB}(u_i) = 0, i \in [\tilde{t}_C + 1, t_C].$$

Define the set of colors for the vertex set $\{u_i \mid i \in [1, \tilde{t}_C]\} \cup V_T$ to be $[1, c_F]$ with

$$c_F \triangleq \tilde{t}_C + t_T = |\{u_i \mid i \in [1, \tilde{t}_C]\} \cup V_T|.$$

Let each vertex v^C_i , $i \in [1, \tilde{t}_C]$ (resp., $v^T_i \in V_T$) correspond to a color $i \in [1, c_F]$ (resp., $i + \tilde{t}_C \in [1, c_F]$). When a path $P = (u, v^F_j, v^F_{j+1}, \dots, v^F_{j+t})$ from a vertex $u \in V_C \cup V_T$ is used in $\langle \mathbb{C} \rangle$, we assign the color $i \in [1, c_F]$ of the vertex u to the vertices $v^F_j, v^F_{j+1}, \dots, v^F_{j+t} \in V_F$.

constants:

- c_F : the maximum number of different colors assigned to the vertices in V_F ;
- n^* : an upper bound on the number $n(\mathbb{C})$ of non-hydrogen atoms in \mathbb{C} ;
- $n_{LB}^{\text{int}}, n_{UB}^{\text{int}} \in [2, n^*]$: lower and upper bounds on the number of interior-vertices in \mathbb{C} ;
- $\text{bl}_{LB}(i) \in [0, 1]$, $i \in [1, \tilde{t}_C]$: a lower bound on the number of leaf ρ -branches in the leaf path rooted at a vertex v^C_i ;
- $\text{bl}_{LB}(k), \text{bl}_{UB}(k) \in [0, \ell_{UB}(k) - 1]$, $k \in [1, k_C] = I_{(\geq 2)} \cup I_{(\geq 1)}$: lower and upper bounds on the number of leaf ρ -branches in the trees rooted at internal vertices of a pure path P_k for an edge $a_k \in E_{(\geq 1)} \cup E_{(\geq 2)}$;

variables:

- $n_G^{\text{int}} \in [n_{LB}^{\text{int}}, n_{UB}^{\text{int}}]$: the number of interior-vertices in \mathbb{C} ;
- $v^F(i) \in [0, 1]$, $i \in [1, t_F]$: $v^F(i) = 1 \Leftrightarrow$ vertex v^F_i is used in \mathbb{C} ;
- $e^F(i) \in [0, 1]$, $i \in [1, t_F + 1]$: $e^F(i)$ represents edge $e^F_i = v^F_{i-1}v^F_i$, where e^F_1 and $e^F_{t_F+1}$ are fictitious edges ($e^F(i) = 1 \Leftrightarrow$ edge e^F_i is used in \mathbb{C});
- $\chi^F(i) \in [0, c_F]$, $i \in [1, t_F]$: $\chi^F(i)$ represents the color assigned to vertex v^F_i ($\chi^F(i) = c \Leftrightarrow$ vertex v^F_i is assigned color c);
- $\text{clr}^F(c) \in [0, t_F]$, $c \in [0, c_F]$: the number of vertices v^F_i with color c ;
- $\delta_\chi^F(c) \in [\text{bl}_{LB}(c), 1]$, $c \in [1, \tilde{t}_C]$: $\delta_\chi^F(c) = 1 \Leftrightarrow \chi^F(i) = c$ for some $i \in [1, t_F]$;
- $\delta_\chi^F(c) \in [0, 1]$, $c \in [\tilde{t}_C + 1, c_F]$: $\delta_\chi^F(c) = 1 \Leftrightarrow \chi^F(i) = c$ for some $i \in [1, t_F]$;
- $\chi^F(i, c) \in [0, 1]$, $i \in [1, t_F]$, $c \in [0, c_F]$: $\chi^F(i, c) = 1 \Leftrightarrow \chi^F(i) = c$;
- $\text{bl}(k, i) \in [0, 1]$, $k \in [1, k_C] = I_{(\geq 2)} \cup I_{(\geq 1)}$, $i \in [1, t_T]$: $\text{bl}(k, i) = 1 \Leftrightarrow$ path P_k contains vertex v^T_i as an internal vertex and the ρ -fringe-tree rooted at v^T_i contains a leaf ρ -branch;

constraints:

$$\chi^F(i, 0) = 1 - v^F(i), \quad \sum_{c \in [0, c_F]} \chi^F(i, c) = 1, \quad \sum_{c \in [0, c_F]} c \cdot \chi^F(i, c) = \chi^F(i), \quad i \in [1, t_F], \quad (9)$$

$$\sum_{i \in [1, t_F]} \chi^F(i, c) = \text{clr}^F(c), \quad t_F \cdot \delta_\chi^F(c) \geq \sum_{i \in [1, t_F]} \chi^F(i, c) \geq \delta_\chi^F(c), \quad c \in [0, c_F], \quad (10)$$

$$e^F(1) = e^F(t_F + 1) = 0, \quad (11)$$

$$v^F(i-1) \geq v^F(i), \\ c_F \cdot (v^F(i-1) - e^F(i)) \geq \chi^F(i-1) - \chi^F(i) \geq v^F(i-1) - e^F(i), \quad i \in [2, t_F], \quad (12)$$

$$\text{bl}(k, i) \geq \delta_\chi^F(\tilde{t}_C + i) + \chi^T(i, k) - 1, \quad k \in [1, k_C], i \in [1, t_T], \quad (13)$$

$$\sum_{k \in [1, k_C], i \in [1, t_T]} \text{bl}(k, i) \leq \sum_{i \in [1, t_T]} \delta_\chi^F(\tilde{t}_C + i), \quad (14)$$

$$\text{bl}_{\text{LB}}(k) \leq \sum_{i \in [1, t_T]} \text{bl}(k, i) \leq \text{bl}_{\text{UB}}(k), \quad k \in [1, k_C], \quad (15)$$

$$t_C + \sum_{i \in [1, t_T]} v^T(i) + \sum_{i \in [1, t_F]} v^F(i) = n_G^{\text{int}}. \quad (16)$$

C.3 Constraints for Including Fringe-trees

Recall that $\mathcal{F}(D_\pi)$ denotes the set of chemical rooted trees ψ r-isomorphic to a chemical rooted tree in $\mathcal{T}(\mathbb{C})$ over all chemical graphs $\mathbb{C} \in D_\pi$, where possibly a chemical rooted tree $\psi \in \mathcal{F}(D_\pi)$ consists of a single chemical element $\mathbf{a} \in \Lambda \setminus \{\mathbf{H}\}$.

To express the condition that the ρ -fringe-tree is chosen from a rooted tree C_i , T_i or F_i , we introduce the following set of variables and constraints.

constants:

- n_{LB} : a lower bound on the number $n(\mathbb{C})$ of non-hydrogen atoms in \mathbb{C} , where $n_{\text{LB}}, n^* \geq n_{\text{LB}}^{\text{int}}$;
- $\text{ch}_{\text{LB}}(i), \text{ch}_{\text{UB}}(i) \in [0, n^*]$, $i \in [1, t_T]$: lower and upper bounds on $\text{ht}(\langle T_i \rangle)$ of the tree T_i rooted at a vertex v_i^C ;
- $\text{ch}_{\text{LB}}(k), \text{ch}_{\text{UB}}(k) \in [0, n^*]$, $k \in [1, k_C] = I_{(\geq 2)} \cup I_{(\geq 1)}$: lower and upper bounds on the maximum height $\text{ht}(\langle T \rangle)$ of the tree $T \in \mathcal{F}(P_k)$ rooted at an internal vertex of a path P_k for an edge $a_k \in E_{(\geq 1)} \cup E_{(\geq 2)}$;
- Prepare a coding of the set $\mathcal{F}(D_\pi)$ and let $[\psi]$ denote the coded integer of an element ψ in $\mathcal{F}(D_\pi)$;

- Sets $\mathcal{F}(v) \subseteq \mathcal{F}(D_\pi)$, $v \in V_C$ and $\mathcal{F}_E \subseteq \mathcal{F}(D_\pi)$ of chemical rooted trees T with $\text{ht}(T) \in [1, \rho]$;
- Define $\mathcal{F}^* := \bigcup_{v \in V_C} \mathcal{F}(v) \cup \mathcal{F}_E$, $\mathcal{F}_i^C := \mathcal{F}(v_i^C)$, $i \in [1, t_C]$, $\mathcal{F}_i^T := \mathcal{F}_E$, $i \in [1, t_T]$ and $\mathcal{F}_i^F := \mathcal{F}_E$, $i \in [1, t_F]$;
- $\text{fc}_{\text{LB}}(\psi), \text{fc}_{\text{UB}}(\psi) \in [0, n^*]$, $\psi \in \mathcal{F}^*$: lower and upper bound functions on the number of interior-vertices v such that $\mathbb{C}[v]$ is r-isomorphic to ψ in \mathbb{C} ;
- $\mathcal{F}_i^X[p]$, $p \in [1, \rho]$, $X \in \{C, T, F\}$: the set of chemical rooted trees $T \in \mathcal{F}_i^X$ with $\text{ht}(\langle T \rangle) = p$;
- $n_{\overline{\mathbb{H}}}([\psi]) \in [0, 3^\rho]$, $\psi \in \mathcal{F}^*$: the number $n(\langle \psi \rangle)$ of non-root hydrogen vertices in a chemical rooted tree ψ ;
- $\text{ht}_{\overline{\mathbb{H}}}([\psi]) \in [0, \rho]$, $\psi \in \mathcal{F}^*$: the height $\text{ht}(\langle \psi \rangle)$ of the hydrogen-suppressed chemical rooted tree $\langle \psi \rangle$;
- $\text{deg}_{\overline{\mathbb{H}}}([\psi]) \in [0, 3]$, $\psi \in \mathcal{F}^*$: the number $\text{deg}_r(\langle \psi \rangle)$ of non-hydrogen children of the root r of a chemical rooted tree ψ ;
- $\text{deg}_r^{\text{hyd}}([\psi]) \in [0, 3]$, $\psi \in \mathcal{F}^*$: the number $\text{deg}_r(\psi) - \text{deg}_r(\langle \psi \rangle)$ of hydrogen children of the root r of a chemical rooted tree ψ ;
- $v_{\text{ion}}(\psi) \in [-3, +3]$, $\psi \in \mathcal{F}^*$: the ion-valence of the root in ψ ;
- $\text{ac}_{\nu}^{\text{lf}}(\psi)$, $\nu \in \Gamma_{\text{ac}}^{\text{lf}}$: the frequency of leaf-edges with adjacency-configuration ν in ψ ;
- $\text{ac}_{\text{LB}}^{\text{lf}}, \text{ac}_{\text{UB}}^{\text{lf}} : \Gamma_{\text{ac}}^{\text{lf}} \rightarrow [0, n^*]$: lower and upper bound functions on the number of leaf-edges uv in $\text{ac}_{\mathbb{C}}$ with adjacency-configuration ν ;

variables:

- $n_G \in [n_{\text{LB}}, n^*]$: the number $n(\mathbb{C})$ of non-hydrogen atoms in \mathbb{C} ;
- $v^X(i) \in [0, 1]$, $i \in [1, t_X]$, $X \in \{T, F\}$: $v^X(i) = 1 \Leftrightarrow$ vertex v_i^X is used in \mathbb{C} ;
- $\delta_{\text{fr}}^X(i, [\psi]) \in [0, 1]$, $i \in [1, t_X]$, $\psi \in \mathcal{F}_i^X$, $X \in \{C, T, F\}$: $\delta_{\text{fr}}^X(i, [\psi]) = 1 \Leftrightarrow \psi$ is the ρ -fringe-tree rooted at vertex v_i^X in \mathbb{C} ;
- $\text{fc}([\psi]) \in [\text{fc}_{\text{LB}}(\psi), \text{fc}_{\text{UB}}(\psi)]$, $\psi \in \mathcal{F}^*$: the number of interior-vertices v such that $\mathbb{C}[v]$ is r-isomorphic to ψ in \mathbb{C} ;
- $\text{ac}^{\text{lf}}([\nu]) \in [\text{ac}_{\text{LB}}^{\text{lf}}(\nu), \text{ac}_{\text{UB}}^{\text{lf}}(\nu)]$, $\nu \in \Gamma_{\text{ac}}^{\text{lf}}$: the number of leaf-edge with adjacency-configuration ν in \mathbb{C} ;
- $\text{deg}_X^{\text{ex}}(i) \in [0, 3]$, $i \in [1, t_X]$, $X \in \{C, T, F\}$: the number of non-hydrogen children of the root of the ρ -fringe-tree rooted at vertex v_i^X in \mathbb{C} ;
- $\text{hyddeg}^X(i) \in [0, 4]$, $i \in [1, t_X]$, $X \in \{C, T, F\}$: the number of hydrogen atoms adjacent to vertex v_i^X (i.e., $\text{hyddeg}(v_i^X)$) in $\mathbb{C} = (H, \alpha, \beta)$;
- $\text{eledeg}_X(i) \in [-3, +3]$, $i \in [1, t_X]$, $X \in \{C, T, F\}$: the ion-valence $v_{\text{ion}}(\psi)$ of vertex v_i^X (i.e., $\text{eledeg}_X(i) = v_{\text{ion}}(\psi)$ for the ρ -fringe-tree ψ rooted at v_i^X) in $\mathbb{C} = (H, \alpha, \beta)$;
- $h^X(i) \in [0, \rho]$, $i \in [1, t_X]$, $X \in \{C, T, F\}$: the height $\text{ht}(\langle T \rangle)$ of the hydrogen-suppressed chemical rooted tree $\langle T \rangle$ of the ρ -fringe-tree T rooted at vertex v_i^X in \mathbb{C} ;

- $\sigma(k, i) \in [0, 1]$, $k \in [1, k_C] = I_{(\geq 2)} \cup I_{(\geq 1)}$, $i \in [1, t_T]$: $\sigma(k, i) = 1 \Leftrightarrow$ the ρ -fringe-tree T_v rooted at vertex $v = v_i^T$ with color k has the largest height $\text{ht}(\langle \mathcal{T}_v \rangle)$ among such trees $T_v, v \in V_T$;

constraints:

$$\begin{aligned} \sum_{\psi \in \mathcal{F}_i^C} \delta_{\text{fr}}^C(i, [\psi]) &= 1, & i \in [1, t_C], \\ \sum_{\psi \in \mathcal{F}_i^X} \delta_{\text{fr}}^X(i, [\psi]) &= v^X(i), & i \in [1, t_X], X \in \{T, F\}, \end{aligned} \quad (17)$$

$$\begin{aligned} \sum_{\psi \in \mathcal{F}_i^X} \deg_{\text{fr}}^{\bar{H}}([\psi]) \cdot \delta_{\text{fr}}^X(i, [\psi]) &= \deg_X^{\text{ex}}(i), \\ \sum_{\psi \in \mathcal{F}_i^X} \deg_{\text{fr}}^{\text{hyd}}([\psi]) \cdot \delta_{\text{fr}}^X(i, [\psi]) &= \text{hydeg}^X(i), \\ \sum_{\psi \in \mathcal{F}_i^X} v_{\text{ion}}([\psi]) \cdot \delta_{\text{fr}}^X(i, [\psi]) &= \text{eledeg}_X(i), & i \in [1, t_X], X \in \{C, T, F\}, \end{aligned} \quad (18)$$

$$\sum_{\psi \in \mathcal{F}_i^F[\rho]} \delta_{\text{fr}}^F(i, [\psi]) \geq v^F(i) - e^F(i + 1), \quad i \in [1, t_F] \ (e^F(t_F + 1) = 0), \quad (19)$$

$$\sum_{\psi \in \mathcal{F}_i^X} \text{ht}_{\bar{H}}([\psi]) \cdot \delta_{\text{fr}}^X(i, [\psi]) = h^X(i), \quad i \in [1, t_X], X \in \{C, T, F\}, \quad (20)$$

$$\sum_{\substack{\psi \in \mathcal{F}_i^X \\ i \in [1, t_X], X \in \{C, T, F\}}} n_{\bar{H}}([\psi]) \cdot \delta_{\text{fr}}^X(i, [\psi]) + \sum_{i \in [1, t_X], X \in \{T, F\}} v^X(i) + t_C = n_G, \quad (21)$$

$$\sum_{i \in [1, t_X], X \in \{C, T, F\}} \delta_{\text{fr}}^X(i, [\psi]) = \text{fc}([\psi]), \quad \psi \in \mathcal{F}^*, \quad (22)$$

$$\sum_{\psi \in \mathcal{F}_i^X, i \in [1, t_X], X \in \{C, T, F\}} \text{ac}_{\nu}^{\text{lf}}(\psi) \cdot \delta_{\text{fr}}^X(i, [\psi]) = \text{ac}^{\text{lf}}([\nu]), \quad \nu \in \Gamma_{\text{ac}}^{\text{lf}}, \quad (23)$$

$$\begin{aligned} h^C(i) &\geq \text{ch}_{\text{LB}}(i) - n^* \cdot \delta_{\chi}^F(i), \quad \text{clr}^F(i) + \rho \geq \text{ch}_{\text{LB}}(i), \\ h^C(i) &\leq \text{ch}_{\text{UB}}(i), \quad \text{clr}^F(i) + \rho \leq \text{ch}_{\text{UB}}(i) + n^* \cdot (1 - \delta_{\chi}^F(i)), & i \in [1, \tilde{t}_C], \end{aligned} \quad (24)$$

$$\text{ch}_{\text{LB}}(i) \leq h^C(i) \leq \text{ch}_{\text{UB}}(i), \quad i \in [\tilde{t}_C + 1, t_C], \quad (25)$$

$$\begin{aligned} h^T(i) &\leq \text{ch}_{\text{UB}}(k) + n^* \cdot (\delta_{\chi}^F(\tilde{t}_C + i) + 1 - \chi^T(i, k)), \\ \text{clr}^F(\tilde{t}_C + i) + \rho &\leq \text{ch}_{\text{UB}}(k) + n^* \cdot (2 - \delta_{\chi}^F(\tilde{t}_C + i) - \chi^T(i, k)), & k \in [1, k_C], i \in [1, t_T], \end{aligned} \quad (26)$$

$$\sum_{i \in [1, t_T]} \sigma(k, i) = \delta_\chi^T(k), \quad k \in [1, k_C], \quad (27)$$

$$\begin{aligned} \chi^T(i, k) &\geq \sigma(k, i), \\ h^T(i) &\geq \text{ch}_{\text{LB}}(k) - n^* \cdot (\delta_\chi^F(\tilde{t}_C + i) + 1 - \sigma(k, i)), \\ \text{clr}^F(\tilde{t}_C + i) + \rho &\geq \text{ch}_{\text{LB}}(k) - n^* \cdot (2 - \delta_\chi^F(\tilde{t}_C + i) - \sigma(k, i)), \quad k \in [1, k_C], i \in [1, t_T]. \end{aligned} \quad (28)$$

C.4 Descriptor for the Number of Specified Degree

We include constraints to compute descriptors for degrees in \mathbb{C} .

variables:

- $\deg^X(i) \in [0, 4]$, $i \in [1, t_X]$, $X \in \{C, T, F\}$: the number of non-hydrogen atoms adjacent to vertex $v = v^X_i$ (i.e., $\deg_{\langle \mathbb{C} \rangle}(v) = \deg_H(v) - \text{hyddeg}_{\mathbb{C}}(v)$) in $\mathbb{C} = (H, \alpha, \beta)$;
- $\deg_{\text{CT}}(i) \in [0, 4]$, $i \in [1, t_C]$: the number of edges from vertex v^C_i to vertices v^T_j , $j \in [1, t_T]$;
- $\deg_{\text{TC}}(i) \in [0, 4]$, $i \in [1, t_C]$: the number of edges from vertices v^T_j , $j \in [1, t_T]$ to vertex v^C_i ;
- $\delta_{\text{dg}}^C(i, d) \in [0, 1]$, $i \in [1, t_C]$, $d \in [1, 4]$, $\delta_{\text{dg}}^X(i, d) \in [0, 1]$, $i \in [1, t_X]$, $d \in [0, 4]$, $X \in \{T, F\}$: $\delta_{\text{dg}}^X(i, d) = 1 \Leftrightarrow \deg^X(i) + \text{hyddeg}^X(i) = d$;
- $\text{dg}(d) \in [\text{dg}_{\text{LB}}(d), \text{dg}_{\text{UB}}(d)]$, $d \in [1, 4]$: the number of interior-vertices v with $\deg_H(v^X_i) = d$ in $\mathbb{C} = (H, \alpha, \beta)$;
- $\deg_C^{\text{int}}(i) \in [1, 4]$, $i \in [1, t_C]$, $\deg_X^{\text{int}}(i) \in [0, 4]$, $i \in [1, t_X]$, $X \in \{T, F\}$: the interior-degree $\deg_{H^{\text{int}}}(v^X_i)$ in the interior $H^{\text{int}} = (V^{\text{int}}(\mathbb{C}), E^{\text{int}}(\mathbb{C}))$ of \mathbb{C} ; i.e., the number of interior-edges incident to vertex v^X_i ;
- $\delta_{\text{dg}, C}^{\text{int}}(i, d) \in [0, 1]$, $i \in [1, t_C]$, $d \in [1, 4]$, $\delta_{\text{dg}, X}^{\text{int}}(i, d) \in [0, 1]$, $i \in [1, t_X]$, $d \in [0, 4]$, $X \in \{T, F\}$: $\delta_{\text{dg}, X}^{\text{int}}(i, d) = 1 \Leftrightarrow \deg_X^{\text{int}}(i) = d$;
- $\text{dg}^{\text{int}}(d) \in [\text{dg}_{\text{LB}}(d), \text{dg}_{\text{UB}}(d)]$, $d \in [1, 4]$: the number of interior-vertices v with the interior-degree $\deg_{H^{\text{int}}}(v) = d$ in the interior $H^{\text{int}} = (V^{\text{int}}(\mathbb{C}), E^{\text{int}}(\mathbb{C}))$ of $\mathbb{C} = (H, \alpha, \beta)$.

constraints:

$$\sum_{k \in I_{(\geq 2)}^+(i) \cup I_{(\geq 1)}^+(i)} \delta_\chi^T(k) = \deg_{\text{CT}}(i), \quad \sum_{k \in I_{(\geq 2)}^-(i) \cup I_{(\geq 1)}^-(i)} \delta_\chi^T(k) = \deg_{\text{TC}}(i), \quad i \in [1, t_C], \quad (29)$$

$$\widetilde{\deg_C^-}(i) + \widetilde{\deg_C^+}(i) + \deg_{\text{CT}}(i) + \deg_{\text{TC}}(i) + \delta_\chi^F(i) = \deg_C^{\text{int}}(i), \quad i \in [1, \tilde{t}_C], \quad (30)$$

$$\widetilde{\deg_C^-}(i) + \widetilde{\deg_C^+}(i) + \deg_{\text{CT}}(i) + \deg_{\text{TC}}(i) = \deg_C^{\text{int}}(i), \quad i \in [\tilde{t}_C + 1, t_C], \quad (31)$$

$$\deg_C^{\text{int}}(i) + \deg_C^{\text{ex}}(i) = \deg^C(i), \quad i \in [1, t_C], \quad (32)$$

$$\sum_{\psi \in \mathcal{F}_i^C[\rho]} \delta_{\text{fr}}^C(i, [\psi]) \geq 2 - \deg_C^{\text{int}}(i) \quad i \in [1, t_C], \quad (33)$$

$$\begin{aligned} 2v^T(i) + \delta_\chi^F(\tilde{t}_C + i) &= \deg_T^{\text{int}}(i), \\ \deg_T^{\text{int}}(i) + \deg_T^{\text{ex}}(i) &= \deg^T(i), \quad i \in [1, t_T] \ (e^T(1) = e^T(t_T + 1) = 0), \end{aligned} \quad (34)$$

$$\begin{aligned} v^F(i) + e^F(i + 1) &= \deg_F^{\text{int}}(i), \\ \deg_F^{\text{int}}(i) + \deg_F^{\text{ex}}(i) &= \deg^F(i), \quad i \in [1, t_F] \ (e^F(1) = e^F(t_F + 1) = 0), \end{aligned} \quad (35)$$

$$\begin{aligned} \sum_{d \in [0, 4]} \delta_{\text{dg}}^X(i, d) &= 1, \quad \sum_{d \in [1, 4]} d \cdot \delta_{\text{dg}}^X(i, d) = \deg^X(i) + \text{hyddg}^X(i), \\ \sum_{d \in [0, 4]} \delta_{\text{dg}, X}^{\text{int}}(i, d) &= 1, \quad \sum_{d \in [1, 4]} d \cdot \delta_{\text{dg}, X}^{\text{int}}(i, d) = \deg_X^{\text{int}}(i), \quad i \in [1, t_X], X \in \{T, C, F\}, \end{aligned} \quad (36)$$

$$\begin{aligned} \sum_{i \in [1, t_C]} \delta_{\text{dg}}^C(i, d) + \sum_{i \in [1, t_T]} \delta_{\text{dg}}^T(i, d) + \sum_{i \in [1, t_F]} \delta_{\text{dg}}^F(i, d) &= \text{dg}(d), \\ \sum_{i \in [1, t_C]} \delta_{\text{dg}, C}^{\text{int}}(i, d) + \sum_{i \in [1, t_T]} \delta_{\text{dg}, T}^{\text{int}}(i, d) + \sum_{i \in [1, t_F]} \delta_{\text{dg}, F}^{\text{int}}(i, d) &= \text{dg}^{\text{int}}(d), \quad d \in [1, 4]. \end{aligned} \quad (37)$$

C.5 Assigning Multiplicity

We prepare an integer variable $\beta(e)$ for each edge e in the scheme graph SG to denote the bond-multiplicity of e in a selected graph H and include necessary constraints for the variables to satisfy in H .

constants:

- $\beta_r([\psi])$: the sum $\beta_\psi(r)$ of bond-multiplicities of edges incident to the root r of a chemical rooted tree $\psi \in \mathcal{F}^*$;

variables:

- $\beta^X(i) \in [0, 3]$, $i \in [2, t_X]$, $X \in \{T, F\}$: the bond-multiplicity of edge e^X_i in \mathbb{C} ;
- $\beta^C(i) \in [0, 3]$, $i \in [\tilde{k}_C + 1, m_C] = I_{(\geq 1)} \cup I_{(0/1)} \cup I_{(=1)}$: the bond-multiplicity of edge $a_i \in E_{(\geq 1)} \cup E_{(0/1)} \cup E_{(=1)}$ in \mathbb{C} ;
- $\beta^{\text{CT}}(k), \beta^{\text{TC}}(k) \in [0, 3]$, $k \in [1, k_C] = I_{(\geq 2)} \cup I_{(\geq 1)}$: the bond-multiplicity of the first (resp., last) edge of the pure path P_k in \mathbb{C} ;
- $\beta^{*F}(c) \in [0, 3]$, $c \in [1, c_F = \tilde{t}_C + t_T]$: the bond-multiplicity of the first edge of the leaf path Q_c rooted at vertex v^C_c , $c \leq \tilde{t}_C$ or $v^T_{c-\tilde{t}_C}$, $c > \tilde{t}_C$ in \mathbb{C} ;

- $\beta_{\text{ex}}^X(i) \in [0, 4], i \in [1, t_X], X \in \{C, T, F\}$: the sum $\beta_{\mathbb{C}[v]}(v)$ of bond-multiplicities of edges in the ρ -fringe-tree $\mathbb{C}[v]$ rooted at interior-vertex $v = v^X_i$;
- $\delta_\beta^X(i, m) \in [0, 1], i \in [2, t_X], m \in [0, 3], X \in \{T, F\}$: $\delta_\beta^X(i, m) = 1 \Leftrightarrow \beta^X(i) = m$;
- $\delta_\beta^C(i, m) \in [0, 1], i \in [\widetilde{k_C}, m_C] = I_{(\geq 1)} \cup I_{(0/1)} \cup I_{(=1)}, m \in [0, 3]$: $\delta_\beta^C(i, m) = 1 \Leftrightarrow \beta^C(i) = m$;
- $\delta_\beta^{CT}(k, m), \delta_\beta^{TC}(k, m) \in [0, 1], k \in [1, k_C] = I_{(\geq 2)} \cup I_{(\geq 1)}, m \in [0, 3]$: $\delta_\beta^{CT}(k, m) = 1$ (resp., $\delta_\beta^{TC}(k, m) = 1$) $\Leftrightarrow \beta^{CT}(k) = m$ (resp., $\beta^{TC}(k) = m$);
- $\delta_\beta^{*F}(c, m) \in [0, 1], c \in [1, c_F], m \in [0, 3], X \in \{C, T\}$: $\delta_\beta^{*F}(c, m) = 1 \Leftrightarrow \beta^{*F}(c) = m$;
- $\text{bd}^{\text{int}}(m) \in [0, 2n_{\text{UB}}^{\text{int}}], m \in [1, 3]$: the number of interior-edges with bond-multiplicity m in \mathbb{C} ;
- $\text{bd}_X(m) \in [0, 2n_{\text{UB}}^{\text{int}}], X \in \{C, T, CT, TC\}, \text{bd}_X(m) \in [0, 2n_{\text{UB}}^{\text{int}}], X \in \{F, CF, TF\}, m \in [1, 3]$: the number of interior-edges $e \in E_X$ with bond-multiplicity m in \mathbb{C} ;

constraints:

$$e^C(i) \leq \beta^C(i) \leq 3e^C(i), i \in [\widetilde{k_C} + 1, m_C] = I_{(\geq 1)} \cup I_{(0/1)} \cup I_{(=1)}, \quad (38)$$

$$e^X(i) \leq \beta^X(i) \leq 3e^X(i), \quad i \in [2, t_X], X \in \{T, F\}, \quad (39)$$

$$\delta_\chi^T(k) \leq \beta^{CT}(k) \leq 3\delta_\chi^T(k), \quad \delta_\chi^T(k) \leq \beta^{TC}(k) \leq 3\delta_\chi^T(k), \quad k \in [1, k_C], \quad (40)$$

$$\delta_\chi^F(c) \leq \beta^{*F}(c) \leq 3\delta_\chi^F(c), \quad c \in [1, c_F], \quad (41)$$

$$\sum_{m \in [0, 3]} \delta_\beta^X(i, m) = 1, \quad \sum_{m \in [0, 3]} m \cdot \delta_\beta^X(i, m) = \beta^X(i), \quad i \in [2, t_X], X \in \{T, F\}, \quad (42)$$

$$\sum_{m \in [0, 3]} \delta_\beta^C(i, m) = 1, \quad \sum_{m \in [0, 3]} m \cdot \delta_\beta^C(i, m) = \beta^C(i), \quad i \in [\widetilde{k_C} + 1, m_C], \quad (43)$$

$$\begin{aligned} \sum_{m \in [0, 3]} \delta_\beta^{CT}(k, m) &= 1, & \sum_{m \in [0, 3]} m \cdot \delta_\beta^{CT}(k, m) &= \beta^{CT}(k), & k \in [1, k_C], \\ \sum_{m \in [0, 3]} \delta_\beta^{TC}(k, m) &= 1, & \sum_{m \in [0, 3]} m \cdot \delta_\beta^{TC}(k, m) &= \beta^{TC}(k), & k \in [1, k_C], \\ \sum_{m \in [0, 3]} \delta_\beta^{*F}(c, m) &= 1, & \sum_{m \in [0, 3]} m \cdot \delta_\beta^{*F}(c, m) &= \beta^{*F}(c), & c \in [1, c_F], \end{aligned} \quad (44)$$

$$\sum_{\psi \in \mathcal{F}_i^X} \beta_r([\psi]) \cdot \delta_{\text{fr}}^X(i, [\psi]) = \beta_{\text{ex}}^X(i), \quad i \in [1, t_X], X \in \{C, T, F\}, \quad (45)$$

$$\begin{aligned}
\sum_{i \in [\widetilde{k_C}+1, m_C]} \delta_\beta^C(i, m) &= \text{bd}_C(m), & \sum_{i \in [2, t_T]} \delta_\beta^T(i, m) &= \text{bd}_T(m), \\
\sum_{k \in [1, k_C]} \delta_\beta^{CT}(k, m) &= \text{bd}_{CT}(m), & \sum_{k \in [1, k_C]} \delta_\beta^{TC}(k, m) &= \text{bd}_{TC}(m), \\
\sum_{i \in [2, t_F]} \delta_\beta^F(i, m) &= \text{bd}_F(m), & \sum_{c \in [1, \widetilde{t_C}]} \delta_\beta^{*F}(c, m) &= \text{bd}_{CF}(m), \\
& & \sum_{c \in [\widetilde{t_C}+1, c_F]} \delta_\beta^{*F}(c, m) &= \text{bd}_{TF}(m), \\
\text{bd}_C(m) + \text{bd}_T(m) + \text{bd}_F(m) + \text{bd}_{CT}(m) + \text{bd}_{TC}(m) + \text{bd}_{TF}(m) + \text{bd}_{CF}(m) &= \text{bd}^{\text{int}}(m), \\
& & m \in [1, 3]. & (46)
\end{aligned}$$

C.6 Assigning Chemical Elements and Valence Condition

We include constraints so that each vertex v in a selected graph H satisfies the valence condition; i.e., $\beta_C(v) = \text{val}(\alpha(v)) + \text{eledeg}_C(v)$, where $\text{eledeg}_C(v) = v_{\text{ion}}(\psi)$ for the ρ -fringe-tree $\mathbb{C}[v]$ r-isomorphic to ψ . With these constraints, a chemical graph $\mathbb{C} = (H, \alpha, \beta)$ on a selected subgraph H will be constructed.

constants:

- Subsets $\Lambda^{\text{int}} \subseteq \Lambda \setminus \{\text{H}\}$, $\Lambda^{\text{ex}} \subseteq \Lambda$ of chemical elements, where we denote by $[\mathbf{e}]$ (resp., $[\mathbf{e}]^{\text{int}}$ and $[\mathbf{e}]^{\text{ex}}$) of a standard encoding of an element \mathbf{e} in the set Λ (resp., Λ^{int} and Λ^{ex});
- A valence function: $\text{val} : \Lambda \rightarrow [1, 6]$;
- A function $\text{mass}^* : \Lambda \rightarrow \mathbb{Z}$ (we let $\text{mass}(\mathbf{a})$ denote the observed mass of a chemical element $\mathbf{a} \in \Lambda$, and define $\text{mass}^*(\mathbf{a}) \triangleq \lfloor 10 \cdot \text{mass}(\mathbf{a}) \rfloor$);
- Subsets $\Lambda^*(i) \subseteq \Lambda^{\text{int}}$, $i \in [1, t_C]$;
- $\text{na}_{\text{LB}}(\mathbf{a}), \text{na}_{\text{UB}}(\mathbf{a}) \in [0, n^*]$, $\mathbf{a} \in \Lambda$: lower and upper bounds on the number of vertices v with $\alpha(v) = \mathbf{a}$;
- $\text{na}_{\text{LB}}^{\text{int}}(\mathbf{a}), \text{na}_{\text{UB}}^{\text{int}}(\mathbf{a}) \in [0, n^*]$, $\mathbf{a} \in \Lambda^{\text{int}}$: lower and upper bounds on the number of interior-vertices v with $\alpha(v) = \mathbf{a}$;
- $\alpha_r([\psi]) \in [\Lambda^{\text{ex}}]$, $\in \mathcal{F}^*$: the chemical element $\alpha(r)$ of the root r of ψ ;
- $\text{na}_{\mathbf{a}}^{\text{ex}}([\psi]) \in [0, n^*]$, $\mathbf{a} \in \Lambda^{\text{ex}}$, $\psi \in \mathcal{F}^*$: the frequency of chemical element \mathbf{a} in the set of non-rooted vertices in ψ , where possibly $\mathbf{a} = \text{H}$;
- M : an upper bound for the average $\overline{\text{ms}}(\mathbb{C})$ of mass^* over all atoms in \mathbb{C} ;

variables:

- $\beta^{\text{CT}}(i), \beta^{\text{TC}}(i) \in [0, 3]$, $i \in [1, t_T]$: the bond-multiplicity of edge $e^{\text{CT}}_{j,i}$ (resp., $e^{\text{TC}}_{j,i}$) if one exists;
- $\beta^{\text{CF}}(i), \beta^{\text{TF}}(i) \in [0, 3]$, $i \in [1, t_F]$: the bond-multiplicity of $e^{\text{CF}}_{j,i}$ (resp., $e^{\text{TF}}_{j,i}$) if one exists;

- $\alpha^X(i) \in [\Lambda_\epsilon^{\text{int}}], \delta_\alpha^X(i, [\mathbf{a}]^{\text{int}}) \in [0, 1], \mathbf{a} \in \Lambda_\epsilon^{\text{int}}, i \in [1, t_X], X \in \{C, T, F\}$: $\alpha^X(i) = [\mathbf{a}]^{\text{int}} \geq 1$ (resp., $\alpha^X(i) = 0$) $\Leftrightarrow \delta_\alpha^X(i, [\mathbf{a}]^{\text{int}}) = 1$ (resp., $\delta_\alpha^X(i, 0) = 0$) $\Leftrightarrow \alpha(v^X_i) = \mathbf{a} \in \Lambda$ (resp., vertex v^X_i is not used in \mathbb{C});
- $\delta_\alpha^X(i, [\mathbf{a}]^{\text{int}}) \in [0, 1], i \in [1, t_X], \mathbf{a} \in \Lambda^{\text{int}}, X \in \{C, T, F\}$: $\delta_\alpha^X(i, [\mathbf{a}]^{\text{t}}) = 1 \Leftrightarrow \alpha(v^X_i) = \mathbf{a}$;
- $\text{Mass} \in \mathbb{Z}_+$: $\sum_{v \in V(H)} \text{mass}^*(\alpha(v))$;
- $\overline{\text{ms}} \in \mathbb{R}_+$: $\sum_{v \in V(H)} \text{mass}^*(\alpha(v))/|V(H)|$;
- $\delta_{\text{atm}}(i) \in [0, 1], i \in [n_{\text{LB}} + n_{\text{LB}}(\mathbf{H}), n^* + n_{\text{UB}}(\mathbf{H})]$: $\delta_{\text{atm}}(i) = 1 \Leftrightarrow |V(H)| = i$;
- $n_{\mathbf{a}}([\mathbf{a}]) \in [n_{\text{LB}}(\mathbf{a}), n_{\text{UB}}(\mathbf{a})], \mathbf{a} \in \Lambda$: the number of vertices $v \in V(H)$ with $\alpha(v) = \mathbf{a}$, where possibly $\mathbf{a} = \mathbf{H}$;
- $n_{\mathbf{a}}^{\text{int}}([\mathbf{a}]^{\text{int}}) \in [n_{\text{LB}}^{\text{int}}(\mathbf{a}), n_{\text{UB}}^{\text{int}}(\mathbf{a})], \mathbf{a} \in \Lambda, X \in \{C, T, F\}$: the number of interior-vertices $v \in V(\mathbb{C})$ with $\alpha(v) = \mathbf{a}$;
- $n_{\mathbf{a}}^{\text{ex}}([\mathbf{a}]^{\text{ex}}), n_{\mathbf{a}}^{\text{ex}}([\mathbf{a}]^{\text{ex}}) \in [0, n_{\text{UB}}(\mathbf{a})], \mathbf{a} \in \Lambda, X \in \{C, T, F\}$: the number of exterior-vertices rooted at vertices $v \in V_X$ and the number of exterior-vertices v such that $\alpha(v) = \mathbf{a}$;

constraints:

$$\begin{aligned}
 \beta^{\text{CT}}(k) - 3(e^{\text{T}}(i) - \chi^{\text{T}}(i, k) + 1) &\leq \beta^{\text{CT}}(i) \leq \beta^{\text{CT}}(k) + 3(e^{\text{T}}(i) - \chi^{\text{T}}(i, k) + 1), i \in [1, t_{\text{T}}], \\
 \beta^{\text{TC}}(k) - 3(e^{\text{T}}(i+1) - \chi^{\text{T}}(i, k) + 1) &\leq \beta^{\text{TC}}(i) \leq \beta^{\text{TC}}(k) + 3(e^{\text{T}}(i+1) - \chi^{\text{T}}(i, k) + 1), i \in [1, t_{\text{T}}], \\
 &k \in [1, k_{\text{C}}],
 \end{aligned} \tag{47}$$

$$\begin{aligned}
 \beta^{*\text{F}}(c) - 3(e^{\text{F}}(i) - \chi^{\text{F}}(i, c) + 1) &\leq \beta^{\text{CF}}(i) \leq \beta^{*\text{F}}(c) + 3(e^{\text{F}}(i) - \chi^{\text{F}}(i, c) + 1), i \in [1, t_{\text{F}}], \quad c \in [1, \tilde{t}_{\text{C}}], \\
 \beta^{*\text{F}}(c) - 3(e^{\text{F}}(i) - \chi^{\text{F}}(i, c) + 1) &\leq \beta^{\text{TF}}(i) \leq \beta^{*\text{F}}(c) + 3(e^{\text{F}}(i) - \chi^{\text{F}}(i, c) + 1), i \in [1, t_{\text{F}}], \quad c \in [\tilde{t}_{\text{C}} + 1, c_{\text{F}}],
 \end{aligned} \tag{48}$$

$$\begin{aligned}
 \sum_{\mathbf{a} \in \Lambda^{\text{int}}} \delta_\alpha^{\text{C}}(i, [\mathbf{a}]^{\text{int}}) &= 1, \quad \sum_{\mathbf{a} \in \Lambda^{\text{int}}} [\mathbf{a}]^{\text{int}} \cdot \delta_\alpha^{\text{X}}(i, [\mathbf{a}]^{\text{int}}) = \alpha^{\text{C}}(i), \quad i \in [1, t_{\text{C}}], \\
 \sum_{\mathbf{a} \in \Lambda^{\text{int}}} \delta_\alpha^{\text{X}}(i, [\mathbf{a}]^{\text{int}}) &= v^{\text{X}}(i), \quad \sum_{\mathbf{a} \in \Lambda^{\text{int}}} [\mathbf{a}]^{\text{int}} \cdot \delta_\alpha^{\text{X}}(i, [\mathbf{a}]^{\text{int}}) = \alpha^{\text{X}}(i), \quad i \in [1, t_{\text{X}}], X \in \{T, F\},
 \end{aligned} \tag{49}$$

$$\sum_{\psi \in \mathcal{F}_i^{\text{X}}} \alpha_{\text{r}}([\psi]) \cdot \delta_{\text{fr}}^{\text{X}}(i, [\psi]) = \alpha^{\text{X}}(i), \quad i \in [1, t_{\text{X}}], X \in \{C, T, F\}, \tag{50}$$

$$\begin{aligned}
 \sum_{j \in I_{\text{C}}(i)} \beta^{\text{C}}(j) + \sum_{k \in I_{(\geq 2)}^+(i) \cup I_{(\geq 1)}^+(i)} \beta^{\text{CT}}(k) + \sum_{k \in I_{(\geq 2)}^-(i) \cup I_{(\geq 1)}^-(i)} \beta^{\text{TC}}(k) \\
 + \beta^{*\text{F}}(i) + \beta_{\text{ex}}^{\text{C}}(i) - \text{eledeg}_{\text{C}}(i) = \sum_{\mathbf{a} \in \Lambda^{\text{int}}} \text{val}(\mathbf{a}) \delta_\alpha^{\text{C}}(i, [\mathbf{a}]^{\text{int}}), \quad i \in [1, \tilde{t}_{\text{C}}],
 \end{aligned} \tag{51}$$

$$\begin{aligned}
& \sum_{j \in I_C(i)} \beta^C(j) + \sum_{k \in I_{(\geq 2)}^+(i) \cup I_{(\geq 1)}^+(i)} \beta^{CT}(k) + \sum_{k \in I_{(\geq 2)}^-(i) \cup I_{(\geq 1)}^-(i)} \beta^{TC}(k) \\
& + \beta_{\text{ex}}^C(i) - \text{eledeg}_C(i) = \sum_{\mathbf{a} \in \Lambda^{\text{int}}} \text{val}(\mathbf{a}) \delta_{\alpha}^C(i, [\mathbf{a}]^{\text{int}}), \quad i \in [\tilde{t}_C + 1, t_C], \quad (52)
\end{aligned}$$

$$\begin{aligned}
& \beta^T(i) + \beta^T(i+1) + \beta_{\text{ex}}^T(i) + \beta^{CT}(i) + \beta^{TC}(i) \\
& + \beta^{*F}(\tilde{t}_C + i) - \text{eledeg}_T(i) = \sum_{\mathbf{a} \in \Lambda^{\text{int}}} \text{val}(\mathbf{a}) \delta_{\alpha}^T(i, [\mathbf{a}]^{\text{int}}), \\
& i \in [1, t_T] \quad (\beta^T(1) = \beta^T(t_T + 1) = 0), \quad (53)
\end{aligned}$$

$$\begin{aligned}
& \beta^F(i) + \beta^F(i+1) + \beta^{CF}(i) + \beta^{TF}(i) \\
& + \beta_{\text{ex}}^F(i) - \text{eledeg}_F(i) = \sum_{\mathbf{a} \in \Lambda^{\text{int}}} \text{val}(\mathbf{a}) \delta_{\alpha}^F(i, [\mathbf{a}]^{\text{int}}), \\
& i \in [1, t_F] \quad (\beta^F(1) = \beta^F(t_F + 1) = 0), \quad (54)
\end{aligned}$$

$$\sum_{i \in [1, t_X]} \delta_{\alpha}^X(i, [\mathbf{a}]^{\text{int}}) = \text{na}_X([\mathbf{a}]^{\text{int}}), \quad \mathbf{a} \in \Lambda^{\text{int}}, X \in \{C, T, F\}, \quad (55)$$

$$\sum_{\psi \in \mathcal{F}_i^X, i \in [1, t_X]} \text{na}_{\mathbf{a}}^{\text{ex}}([\psi]) \cdot \delta_{\text{fr}}^X(i, [\psi]) = \text{na}_X^{\text{ex}}([\mathbf{a}]^{\text{ex}}), \quad \mathbf{a} \in \Lambda^{\text{ex}}, X \in \{C, T, F\}, \quad (56)$$

$$\begin{aligned}
& \text{na}_C([\mathbf{a}]^{\text{int}}) + \text{na}_T([\mathbf{a}]^{\text{int}}) + \text{na}_F([\mathbf{a}]^{\text{int}}) = \text{na}^{\text{int}}([\mathbf{a}]^{\text{int}}), \quad \mathbf{a} \in \Lambda^{\text{int}}, \\
& \sum_{X \in \{C, T, F\}} \text{na}_X^{\text{ex}}([\mathbf{a}]^{\text{ex}}) = \text{na}^{\text{ex}}([\mathbf{a}]^{\text{ex}}), \quad \mathbf{a} \in \Lambda^{\text{ex}}, \\
& \text{na}^{\text{int}}([\mathbf{a}]^{\text{int}}) + \text{na}^{\text{ex}}([\mathbf{a}]^{\text{ex}}) = \text{na}([\mathbf{a}]), \quad \mathbf{a} \in \Lambda^{\text{int}} \cap \Lambda^{\text{ex}}, \\
& \text{na}^{\text{int}}([\mathbf{a}]^{\text{int}}) = \text{na}([\mathbf{a}]), \quad \mathbf{a} \in \Lambda^{\text{int}} \setminus \Lambda^{\text{ex}}, \\
& \text{na}^{\text{ex}}([\mathbf{a}]^{\text{ex}}) = \text{na}([\mathbf{a}]), \quad \mathbf{a} \in \Lambda^{\text{ex}} \setminus \Lambda^{\text{int}}, \quad (57)
\end{aligned}$$

$$\sum_{\mathbf{a} \in \Lambda^*(i)} \delta_{\alpha}^C(i, [\mathbf{a}]^{\text{int}}) = 1, \quad i \in [1, t_C], \quad (58)$$

$$\sum_{\mathbf{a} \in \Lambda} \text{mass}^*(\mathbf{a}) \cdot \text{na}([\mathbf{a}]) = \text{Mass}, \quad (59)$$

$$\sum_{i \in [n_{\text{LB}} + \text{na}_{\text{LB}}(\mathbf{H}), n^* + \text{na}_{\text{UB}}(\mathbf{H})]} \delta_{\text{atm}}(i) = 1, \quad (60)$$

$$\sum_{i \in [n_{\text{LB}} + \text{na}_{\text{LB}}(\mathbf{H}), n^* + \text{na}_{\text{UB}}(\mathbf{H})]} i \cdot \delta_{\text{atm}}(i) = n_G + \text{na}^{\text{ex}}([\mathbf{H}]^{\text{ex}}), \quad (61)$$

$$\text{Mass}/i - M \cdot (1 - \delta_{\text{atm}}(i)) \leq \overline{\text{ms}} \leq \text{Mass}/i + M \cdot (1 - \delta_{\text{atm}}(i)), \quad i \in [n_{\text{LB}} + \text{na}_{\text{LB}}(\mathbf{H}), n^* + \text{na}_{\text{UB}}(\mathbf{H})]. \quad (62)$$

C.7 Constraints for Bounds on the Number of Bonds

We include constraints for specification of lower and upper bounds bd_{LB} and bd_{UB} .

constants:

- $\text{bd}_{m,\text{LB}}(i), \text{bd}_{m,\text{UB}}(i) \in [0, n_{\text{UB}}^{\text{int}}], i \in [1, m_C], m \in [2, 3]$: lower and upper bounds on the number of edges $e \in E(P_i)$ with bond-multiplicity $\beta(e) = m$ in the pure path P_i for edge $e_i \in E_C$;

variables :

- $\text{bd}_T(k, i, m) \in [0, 1], k \in [1, k_C], i \in [2, t_T], m \in [2, 3]$: $\text{bd}_T(k, i, m) = 1 \Leftrightarrow$ the pure path P_k for edge $e_k \in E_C$ contains edge e_i^T with $\beta(e_i^T) = m$;

constraints:

$$\text{bd}_{m,\text{LB}}(i) \leq \delta_\beta^C(i, m) \leq \text{bd}_{m,\text{UB}}(i), i \in I_{(=1)} \cup I_{(0/1)}, m \in [2, 3], \quad (63)$$

$$\text{bd}_T(k, i, m) \geq \delta_\beta^T(i, m) + \chi^T(i, k) - 1, \quad k \in [1, k_C], i \in [2, t_T], m \in [2, 3], \quad (64)$$

$$\sum_{j \in [2, t_T]} \delta_\beta^T(j, m) \geq \sum_{k \in [1, k_C], i \in [2, t_T]} \text{bd}_T(k, i, m), \quad m \in [2, 3], \quad (65)$$

$$\begin{aligned} \text{bd}_{m,\text{LB}}(k) &\leq \sum_{i \in [2, t_T]} \text{bd}_T(k, i, m) + \delta_\beta^{\text{CT}}(k, m) + \delta_\beta^{\text{TC}}(k, m) \leq \text{bd}_{m,\text{UB}}(k), \\ k &\in [1, k_C], m \in [2, 3]. \end{aligned} \quad (66)$$

C.8 Constraints for 2L-GNN

Recall that the node feature vector $\theta_v^{(0)}$ for each interior-vertex $v = v_i^X, i \in [1, t_X], X \in \{C, T, F\}$ consists of the following $K_{\text{node}} = 15$ entries, where a ρ -fringe-tree ψ is encoded into a $K_{\mathcal{F}} (= 8)$ -dimension real vector.

- $\delta_\alpha^X(i, [\mathbf{C}]^{\text{int}}) \in [0, 1], i \in [1, t_X], X \in \{C, T, F\}$;
- $\delta_\alpha^X(i, [\mathbf{0}]^{\text{int}}) \in [0, 1], i \in [1, t_X], X \in \{C, T, F\}$;
- $\delta_\alpha^X(i, [\mathbf{N}]^{\text{int}}) \in [0, 1], i \in [1, t_X], X \in \{C, T, F\}$;
- $\text{dg}_X(i) + \text{hyddeg}^X(i), i \in [1, t_X], X \in \{C, T, F\}$;
- $\sum_{\mathbf{a} \in \Lambda^{\text{int}}} \text{val}(\mathbf{a}) \delta_\alpha^X(i, [\mathbf{a}]^{\text{int}}) + \text{eledeg}_X(i), i \in [1, t_X], X \in \{C, T, F\}$;
- $\text{hyddeg}^X(i), i \in [1, t_X], X \in \{C, T, F\}$;
- $\text{eledeg}_X(i), i \in [1, t_X], X \in \{C, T, F\}$;
- $\theta_\psi(\cdot, [\psi]) \in \mathbb{R}^{K_{\mathcal{F}}}$: the encoded feature vector of the ρ -fringe-tree ψ .

constants:

$\kappa = 0.1$, the parameter used for the LeakyReLU activation function;

Let $I_a^+(i) \triangleq I_{(\geq 1)}^+(i) \cup I_{(0/1)}^+(i) \cup I_{(=1)}^+(i)$ and $I_a^-(i) \triangleq I_{(\geq 1)}^-(i) \cup I_{(0/1)}^-(i) \cup I_{(=1)}^-(i)$;

Let $I_b^+(i) \triangleq I_{(\geq 2)}^+(i) \cup I_{(\geq 1)}^+(i)$ and $I_b^-(i) \triangleq I_{(\geq 2)}^-(i) \cup I_{(\geq 1)}^-(i)$;

Let $N_a^+(i)$ denote the set of indices i of the tails v_j^C of edges in $(v_j^C, v_i^C) \in E_{(\geq 1)} \cup E_{(0/1)} \cup E_{(=1)}$ and $N_a^-(i)$ denote the set of indices i of the heads v_j^C of edges $(v_i^C, v_j^C) \in E_{(\geq 1)} \cup E_{(0/1)} \cup E_{(=1)}$;

$K_{\text{node}}, K_{\text{hid}}, L, K_{\text{C}} \in \mathbb{Z}_+$;

$w_0(i, j) \in \mathbb{R}, i \in [1, K_{\text{node}}], j \in [1, K_{\text{hid}}], \ell \in [1, L - 1]$;

$w_\ell(i, j) \in \mathbb{R}, i, j \in [1, K_{\text{hid}}], \ell \in [1, L - 1]$;

$w_{\text{C}}(i, j) \in \mathbb{R}, i \in [1, K_{\text{hid}}], j \in [1, K_{\text{C}}]$;

$\text{bias}(z; \ell) \in \mathbb{R}, z \in [1, K_{\text{hid}}], \ell \in [0, L - 1]$;

$M_\ell \in \mathbb{R}_+, \ell \in [0, L]$: An upper bound on the maximum value $\theta_{\max}(z, \ell)$ of entry z in the ℓ -th layer over all training data D_π .

variables:

(In order to improve the readability, we will sometimes use $\theta(v, z)$ instead of $\theta_v(z)$.)

$\theta_{\text{C}}(p) \in \mathbb{R}, p \in [1, K_{\text{C}}]$: the p -th entry of a representation vector $\theta_{\text{C}} \in \mathbb{R}^{K_{\text{C}}}$; $\tau_{\text{C}}(p) \in \mathbb{R}, \delta_{\text{C}}^\tau(p) \in \{0, 1\}, p \in [1, K_{\text{C}}]$;

$\theta^{\text{C}}(0; z; \ell) \in \mathbb{R}, i \in [1, t_{\text{C}}], z \in [1, K_{\text{node}}]$: the z -th entry of vector $\theta_v^{(\ell)}$ of vertex $v = v_i^{\text{C}}$ in the 0-th layer;

$\theta^{\text{T}}(0; z; \ell) \in \mathbb{R}, i \in [0, t_{\text{T}} + 1], z \in [1, K_{\text{node}}]$: the z -th entry of vector $\theta_v^{(\ell)}$ of vertex $v = v_i^{\text{T}}$ in the 0-th layer, where v_i^{T} may be not used in a target chemical graph;

$\theta^{\text{F}}(0; z; \ell) \in \mathbb{R}, i \in [0, t_{\text{F}} + 1], z \in [1, K_{\text{node}}]$: the z -th entry of vector $\theta_v^{(\ell)}$ of vertex $v = v_i^{\text{F}}$ in the 0-th layer, where v_i^{F} may be not used in a target chemical graph;

$\theta^{\text{C}}(i; z; \ell) \in \mathbb{R}, i \in [1, t_{\text{C}}], z \in [1, K_{\text{hid}}], \ell \in [1, L]$: the z -th entry of vector $\theta_v^{(\ell)}$ of vertex $v = v_i^{\text{C}}$ in the ℓ -th layer; $\tau^{\text{C}}(i; z; \ell) \in \mathbb{R}, \delta_{\text{C}}^\tau(i; z; \ell) \in \{0, 1\}, i \in [1, t_{\text{C}}], z \in [1, K_{\text{hid}}], \ell \in [1, L]$;

$\theta^{\text{T}}(i; z; \ell) \in \mathbb{R}, i \in [0, t_{\text{T}} + 1], z \in [1, K_{\text{hid}}], \ell \in [1, L]$: the z -th entry of vector $\theta_v^{(\ell)}$ of vertex $v = v_i^{\text{T}}$ in the ℓ -th layer, where v_i^{T} may be not used in a target chemical graph; $\tau^{\text{T}}(i; z; \ell) \in \mathbb{R}, \delta_{\text{T}}^\tau(i; z; \ell) \in \{0, 1\}, i \in [0, t_{\text{T}} + 1], z \in [1, K_{\text{hid}}], \ell \in [1, L]$;

$\theta^{\text{F}}(i; z; \ell) \in \mathbb{R}, i \in [0, t_{\text{F}} + 1], z \in [1, K_{\text{hid}}], \ell \in [1, L]$: the z -th entry of vector $\theta_v^{(\ell)}$ of vertex $v = v_i^{\text{F}}$ in the ℓ -th layer, where v_i^{F} may be not used in a target chemical graph; $\tau^{\text{F}}(i; z; \ell) \in \mathbb{R}, \delta_{\text{F}}^\tau(i; z; \ell) \in \{0, 1\}, i \in [0, t_{\text{F}} + 1], z \in [1, K_{\text{hid}}], \ell \in [1, L]$;

$\theta_{\text{C}}^{\text{C}}(k; z; \ell), \theta_{\text{C}}^{\text{T}}(k; z; \ell) \in \mathbb{R}, k \in [\widetilde{k_{\text{C}}} + 1, m_{\text{C}}], z \in [1, K_{\text{hid}}], \ell \in [0, L - 1]$: the z -th entry of vector $\theta_v^{(\ell)}$ of the head and tail v of edge $a_k \in E_{(\geq 1)} \cup E_{(0/1)} \cup E_{(=1)}$, where $a_k \in E_{(\geq 1)} \cup E_{(0/1)}$ may be not used in a target chemical graph;

$\theta_{\text{C}}^{\text{T}}(i; z; \ell), \theta_{\text{C}}^{\text{F}}(i; z; \ell) \in \mathbb{R}, i \in [1, t_{\text{T}} + 1], z \in [1, K_{\text{hid}}], \ell \in [0, L - 1]$: the value to $\sum_{z' \in [1, K_{\text{node}}]} w_\ell(z', z) \theta^{(\ell)}(v_i^{\text{T}}, z')$ for edge $e = e_i^{\text{T}}$ (resp., edge $e = e_{i+1}^{\text{T}}$), where such an edge $e \in E_{\text{T}}$ may be not used in a target chemical graph;

$\theta_{\text{C}}^{\text{F}}(i; z; \ell), \theta_{\text{C}}^{\text{T}}(i; z; \ell) \in \mathbb{R}, i \in [1, t_{\text{F}} + 1], z \in [1, K_{\text{hid}}], \ell \in [0, L - 1]$: the value to $\sum_{z' \in [1, K_{\text{node}}]} w_\ell(z', z) \theta^{(\ell)}(v_i^{\text{F}}, z')$ for edge $e = e_i^{\text{F}}$ (resp., edge $e = e_{i+1}^{\text{F}}$), where such an edge $e \in E_{\text{F}}$ may be not used in a target chemical graph;

$\theta_{\text{T}}^{\text{CT}}(k; z; \ell), \theta_{\text{T}}^{\text{TC}}(k; z; \ell) \in \mathbb{R}, k \in [1, k_{\text{C}}], z \in [1, K_{\text{hid}}], \ell \in [0, L - 1]$: the value to $\sum_{z' \in [1, K_{\text{node}}]} w_\ell(z', z) \theta^{(\ell)}(v, z')$ for the edge $(u = v_j^{\text{C}}, v = v_i^{\text{T}}) \in E_{\text{CT}}$ (resp., $(v = v_i^{\text{T}}, u = v_j^{\text{C}}) \in E_{\text{TC}}$ and $(v = v_i^{\text{T}}, u = v_j^{\text{F}}) \in E_{\text{TF}}$), where such an edge uv may be not used in a target chemical graph;

$\theta_{\text{C}}^{\text{CT}}(i; z; \ell), \theta_{\text{C}}^{\text{TC}}(i; z; \ell), \theta_{\text{F}}^{\text{TF}}(i; z; \ell) \in \mathbb{R}, i \in [1, t_{\text{T}}], z \in [1, K_{\text{hid}}], \ell \in [0, L - 1]$: the value to $\sum_{z' \in [1, K_{\text{node}}]} w_\ell(z', z) \theta^{(\ell)}(u, z')$ for the edge $(u = v_j^{\text{C}}, v = v_i^{\text{T}}) \in E_{\text{CT}}$ (resp., $(v = v_i^{\text{T}}, u = v_j^{\text{C}}) \in$

E_{TC} and $(v = v^{\text{T}}_i, u = v^{\text{F}}_j) \in E_{\text{TF}}$), where such an edge uv may be not used in a target chemical graph;

$\theta_{\text{F}}^{\text{CF}}(c; z; \ell) \in \mathbb{R}, c \in [1, \tilde{t}_{\text{C}}], z \in [1, K_{\text{hid}}], \ell \in [0, L - 1]$: the value to $\sum_{z' \in [1, K_{\text{node}}]} w_{\ell}(z', z) \theta^{(\ell)}(u, z')$ for the edge $(v = v^{\text{C}}_c, u = v^{\text{F}}_i) \in E_{\text{CF}}$, where such an edge uv may be not used in a target chemical graph;

$\theta_{\text{C}}^{\text{CF}}(i; z; \ell), \theta_{\text{T}}^{\text{TF}}(i; z; \ell) \in \mathbb{R}, i \in [1, t_{\text{F}}], z \in [1, K_{\text{hid}}], \ell \in [0, L - 1]$: the value to $\sum_{z' \in [1, K_{\text{node}}]} w_{\ell}(z', z) \theta^{(\ell)}(u, z')$ for the edge $(u = v^{\text{C}}_j, v = v^{\text{F}}_i) \in E_{\text{CF}}$ (resp., $(v = v^{\text{T}}_j, u = v^{\text{F}}_i) \in E_{\text{TF}}$), where such an edge uv may be not used in a target chemical graph;

constraints:

Initializing vectors $\theta^{(0)}(v)$:

$$\begin{aligned}
\theta^{\text{X}}(i; 1; 0) &= \delta_{\alpha}^{\text{X}}(i; [\text{C}]^{\text{int}}), \\
\theta^{\text{X}}(i; 2; 0) &= \delta_{\alpha}^{\text{X}}(i; [\text{O}]^{\text{int}}), \\
\theta^{\text{X}}(i; 3; 0) &= \delta_{\alpha}^{\text{X}}(i; [\text{N}]^{\text{int}}), \\
\theta^{\text{X}}(i; 4; 0) &= \text{dg}_{\text{X}}(i) + \text{hyddeg}^{\text{X}}(i), \\
\theta^{\text{X}}(i; 5; 0) &= \sum_{\mathbf{a} \in \Lambda^{\text{int}}} \text{val}(\mathbf{a}) \delta_{\alpha}^{\text{X}}(i, [\mathbf{a}]^{\text{int}}) + \text{eledeg}_{\text{X}}(i), \\
\theta^{\text{X}}(i; 6; 0) &= \text{hyddeg}^{\text{X}}(i), \\
\theta^{\text{X}}(i; 7; 0) &= \text{eledeg}_{\text{X}}(i), & i \in [1, t_{\text{X}}], \text{X} \in \{\text{C}, \text{T}, \text{F}\} \\
\theta^{\text{X}}(i; j; 0) &= \sum_{\psi \in \mathcal{F}_i^{\text{X}}} \delta_{\text{fr}}^{\text{X}}(i, [\psi]) \theta_{\psi}(j - 7; [\psi]) & i \in [1, t_{\text{X}}], j \in [8, K_{\text{node}}], \text{X} \in \{\text{C}, \text{T}, \text{F}\} \quad (67)
\end{aligned}$$

We denote the function h such that $h(\ell) := K_{\text{node}}$ when $\ell = 0$ and $h(\ell) := K_{\text{hid}}$ otherwise in order to simplify the formulations.

Calculating the $(\ell + 1)$ -th vector from the ℓ -th vecctor:

$$\begin{aligned}
-M_{\ell+1} &\leq \sum_{z' \in [1, h(\ell)]} w_{\ell}(z', z) \theta^{\text{C}}(i; z'; \ell) + \sum_{k \in I_a^-(i)} \theta_{-}^{\text{C}}(k; z; \ell) + \sum_{k \in I_a^+(i)} \theta_{+}^{\text{C}}(k; z; \ell) \\
&+ \sum_{k \in I_b^+(i)} \theta_{\text{T}}^{\text{CT}}(k; z; \ell) + \sum_{k \in I_b^-(i)} \theta_{\text{T}}^{\text{TC}}(k; z; \ell) + \theta_{\text{F}}^{\text{CF}}(i; z; \ell) + \text{bias}(z; \ell) = \tau^{\text{C}}(i; z; \ell + 1) \leq M_{\ell+1}, \\
-M_{\ell+1} \delta_{\text{C}}^{\tau}(i; z; \ell + 1) &\leq \theta^{\text{C}}(i; z; \ell + 1) - \kappa \tau^{\text{C}}(i; z; \ell + 1) \leq M_{\ell+1} \delta_{\text{C}}^{\tau}(i; z; \ell + 1), \\
-M_{\ell+1} (1 - \delta_{\text{C}}^{\tau}(i; z; \ell + 1)) &\leq \theta^{\text{C}}(i; z; \ell + 1) - \tau^{\text{C}}(i; z; \ell + 1) \leq M_{\ell+1} (1 - \delta_{\text{C}}^{\tau}(i; z; \ell + 1)), \\
-M_{\ell+1} \delta_{\text{C}}^{\tau}(i; z; \ell + 1) &\leq \tau^{\text{C}}(i; z; \ell + 1) \leq M_{\ell+1} (1 - \delta_{\text{C}}^{\tau}(i; z; \ell + 1)), \\
&z \in [1, K_{\text{hid}}], \ell \in [0, L - 1], i \in [1, \tilde{t}_{\text{C}}], \quad (68)
\end{aligned}$$

$$\begin{aligned}
-M_{\ell+1} &\leq \sum_{z' \in [1, h(\ell)]} w_\ell(z', z) \theta^C(i; z'; \ell) + \sum_{k \in I_a^-(i)} \theta_-^C(k; z; \ell) + \sum_{k \in I_a^+(i)} \theta_+^C(k; z; \ell) \\
&+ \sum_{k \in I_b^+(i)} \theta_{\text{T}}^{\text{CT}}(k; z; \ell) + \sum_{k \in I_b^-(i)} \theta_{\text{T}}^{\text{TC}}(k; z; \ell) + \text{bias}(z; \ell) = \tau^C(i; z; \ell + 1) \leq M_{\ell+1} \\
-M_{\ell+1} \delta_{\text{C}}^T(i; z; \ell + 1) &\leq \theta^C(i; z; \ell + 1) - \kappa \tau^C(i; z; \ell + 1) \leq M_{\ell+1} \delta_{\text{C}}^T(i; z; \ell + 1), \\
-M_{\ell+1} (1 - \delta_{\text{C}}^T(i; z; \ell + 1)) &\leq \theta^C(i; z; \ell + 1) - \tau^C(i; z; \ell + 1) \leq M_{\ell+1} (1 - \delta_{\text{C}}^T(i; z; \ell + 1)), \\
-M_{\ell+1} \delta_{\text{C}}^T(i; z; \ell + 1) &\leq \tau^C(i; z; \ell + 1) \leq M_{\ell+1} (1 - \delta_{\text{C}}^T(i; z; \ell + 1)), \\
&z \in [1, K_{\text{hid}}], \ell \in [0, L - 1], i \in [\tilde{t}_{\text{C}} + 1, t_{\text{C}}], \quad (69)
\end{aligned}$$

$$\begin{aligned}
-M_{\ell+1} \cdot (1 - v^{\text{T}}(i)) &\leq \tau^{\text{T}}(i; z; \ell + 1) - \left(\sum_{z' \in [1, h(\ell)]} w_\ell(z', z) \theta^{\text{T}}(i; z'; \ell) + \theta_-^{\text{T}}(i; z; \ell) + \theta_+^{\text{T}}(i; z; \ell) \right. \\
&\quad \left. + \theta_{\text{C}}^{\text{CT}}(i; z; \ell) + \theta_{\text{C}}^{\text{TC}}(i; z; \ell) + \theta_{\text{F}}^{\text{TF}}(i; z; \ell) + \text{bias}(z; \ell) \right) \leq M_{\ell+1} \cdot (1 - v^{\text{T}}(i)), \\
-M_{\ell+1} \cdot v^{\text{T}}(i) &\leq \theta^{\text{T}}(i; z; \ell + 1) \leq M_{\ell+1} \cdot v^{\text{T}}(i), \\
-M_{\ell+1} \delta_{\text{T}}^T(i; z; \ell + 1) &\leq \theta^{\text{T}}(i; z; \ell + 1) - \kappa \tau^{\text{T}}(i; z; \ell + 1) \leq M_{\ell+1} \delta_{\text{T}}^T(i; z; \ell + 1), \\
-M_{\ell+1} (1 - \delta_{\text{T}}^T(i; z; \ell + 1)) &\leq \theta^{\text{T}}(i; z; \ell + 1) - \tau^{\text{T}}(i; z; \ell + 1) \leq M_{\ell+1} (1 - \delta_{\text{T}}^T(i; z; \ell + 1)), \\
-M_{\ell+1} \delta_{\text{T}}^T(i; z; \ell + 1) &\leq \tau^{\text{T}}(i; z; \ell + 1) \leq M_{\ell+1} (1 - \delta_{\text{T}}^T(i; z; \ell + 1)), \\
&\theta^{\text{T}}(0; z; \ell) = \theta^{\text{T}}(t_{\text{T}} + 1; z; \ell) = 0, \\
&z \in [1, K_{\text{hid}}], \ell \in [0, L - 1], i \in [1, t_{\text{T}}], \quad (70)
\end{aligned}$$

$$\begin{aligned}
-M_{\ell+1} \cdot (1 - v^{\text{F}}(i)) &\leq \tau^{\text{F}}(i; z; \ell + 1) - \left(\sum_{z' \in [1, h(\ell)]} w_\ell(z', z) \theta^{\text{F}}(i; z'; \ell) + \theta_-^{\text{F}}(i; z; \ell) + \theta_+^{\text{F}}(i; z; \ell) \right. \\
&\quad \left. + \theta_{\text{C}}^{\text{CF}}(i; z; \ell) + \theta_{\text{T}}^{\text{TF}}(i; z; \ell) + \text{bias}(z; \ell) \right) \leq M_{\ell+1} \cdot (1 - v^{\text{F}}(i)), \\
-M_{\ell+1} \cdot v^{\text{F}}(i) &\leq \theta^{\text{F}}(i; z; \ell + 1) \leq M_{\ell+1} \cdot v^{\text{F}}(i), \\
-M_{\ell+1} \delta_{\text{F}}^T(i; z; \ell + 1) &\leq \theta^{\text{F}}(i; z; \ell + 1) - \kappa \tau^{\text{F}}(i; z; \ell + 1) \leq M_{\ell+1} \delta_{\text{F}}^T(i; z; \ell + 1), \\
-M_{\ell+1} (1 - \delta_{\text{F}}^T(i; z; \ell + 1)) &\leq \theta^{\text{F}}(i; z; \ell + 1) - \tau^{\text{F}}(i; z; \ell + 1) \leq M_{\ell+1} (1 - \delta_{\text{F}}^T(i; z; \ell + 1)), \\
-M_{\ell+1} \delta_{\text{F}}^T(i; z; \ell + 1) &\leq \tau^{\text{F}}(i; z; \ell + 1) \leq M_{\ell+1} (1 - \delta_{\text{F}}^T(i; z; \ell + 1)), \\
&\theta^{\text{F}}(0; z; \ell) = \theta^{\text{F}}(t_{\text{F}} + 1; z; \ell) = 0, \\
&z \in [1, K_{\text{hid}}], \ell \in [0, L - 1], i \in [1, t_{\text{F}}], \quad (71)
\end{aligned}$$

Preparing associated variables: /* The values for $\theta^{\text{C}}(i; z; \ell)$, $\theta^{\text{T}}(i; z; \ell)$ and $\theta^{\text{F}}(i; z; \ell)$ determine the values for $\theta_-^{\text{C}}(k; z; \ell)$, $\theta_+^{\text{C}}(k; z; \ell)$, $\theta_-^{\text{T}}(k; z; \ell)$, $\theta_+^{\text{T}}(k; z; \ell)$, $\theta_-^{\text{F}}(k; z; \ell)$, $\theta_+^{\text{F}}(k; z; \ell)$, $\theta_{\text{T}}^{\text{CT}}(k; z; \ell)$, $\theta_{\text{T}}^{\text{TC}}(k; z; \ell)$, $\theta_{\text{C}}^{\text{CT}}(k; z; \ell)$, $\theta_{\text{C}}^{\text{TC}}(k; z; \ell)$, $\theta_{\text{F}}^{\text{TF}}(k; z; \ell)$, $\theta_{\text{F}}^{\text{CF}}(k; z; \ell)$, $\theta_{\text{C}}^{\text{CF}}(k; z; \ell)$ and $\theta_{\text{T}}^{\text{TF}}(k; z; \ell)$ by the following. */

$$\begin{aligned}
\sum_{z' \in [1, h(\ell)]} w_\ell(z', z) \theta^C(\text{tail}(k); z'; \ell) &= \theta_-^C(k; z; \ell), \\
\sum_{z' \in [1, h(\ell)]} w_\ell(z', z) \theta^C(\text{head}(k); z'; \ell) &= \theta_+^C(k; z; \ell), \\
-M_\ell \cdot e^C(k) &\leq \theta_-^C(k; z; \ell) \leq M_\ell \cdot e^C(k), \\
-M_\ell \cdot e^C(k) &\leq \theta_+^C(k; z; \ell) \leq M_\ell \cdot e^C(k), \\
k &\in [\widetilde{k}_C + 1, m_C], z \in [1, K_{\text{hid}}], \ell \in [0, L - 1],
\end{aligned} \tag{72}$$

$$\begin{aligned}
\sum_{z' \in [1, h(\ell)]} w_\ell(z', z) \theta^T(i - 1; z'; \ell) &= \theta_-^T(i; z; \ell), i \in [2, t_T], \\
\sum_{z' \in [1, h(\ell)]} w_\ell(z', z) \theta^T(i + 1; z'; \ell) &= \theta_+^T(i; z; \ell), i \in [1, t_T - 1], \\
-M_\ell \cdot e^T(i) &\leq \theta_-^T(i; z; \ell) \leq M_\ell \cdot e^T(i), \\
-M_\ell \cdot e^T(i + 1) &\leq \theta_+^T(i; z; \ell) \leq M_\ell \cdot e^T(i + 1), i \in [1, t_T], \\
z &\in [1, K_{\text{hid}}], \ell \in [0, L - 1],
\end{aligned} \tag{73}$$

$$\begin{aligned}
\sum_{z' \in [1, h(\ell)]} w_\ell(z', z) \theta^F(i - 1; z'; \ell) &= \theta_-^F(i; z; \ell), i \in [2, t_F], \\
\sum_{z' \in [1, h(\ell)]} w_\ell(z', z) \theta^F(i + 1; z'; \ell) &= \theta_+^F(i; z; \ell), i \in [1, t_F - 1], \\
-M_\ell \cdot e^F(i) &\leq \theta_-^F(i; z; \ell) \leq M_\ell \cdot e^F(i), \\
-M_\ell \cdot e^F(i + 1) &\leq \theta_+^F(i; z; \ell) \leq M_\ell \cdot e^F(i + 1), i \in [1, t_F], \\
z &\in [1, K_{\text{hid}}], \ell \in [0, L - 1],
\end{aligned} \tag{74}$$

$$\begin{aligned}
\sum_{z' \in [1, h(\ell)]} w_\ell(z', z) \theta^T(i; z'; \ell) - M_\ell \cdot (1 - \chi^T(i, k) + e^T(i)) &\leq \theta_T^{\text{CT}}(k; z; \ell) \\
\leq \sum_{z' \in [1, h(\ell)]} w_\ell(z', z) \theta^T(i; z'; \ell) + M_\ell \cdot (1 - \chi^T(i, k) + e^T(i)), &i \in [1, t_T], \\
\sum_{z' \in [1, h(\ell)]} w_\ell(z', z) \theta^T(i; z'; \ell) - M_\ell \cdot (1 - \chi^T(i, k) + e^T(i + 1)) &\leq \theta_T^{\text{TC}}(k; z; \ell) \\
\leq \sum_{z' \in [1, h(\ell)]} w_\ell(z', z) \theta^T(i; z'; \ell) + M_\ell \cdot (1 - \chi^T(i, k) + e^T(i + 1)), &i \in [1, t_T], \\
-M_\ell \cdot \delta_\chi^T(k) &\leq \theta_T^{\text{CT}}(k; z; \ell) \leq M_\ell \cdot \delta_\chi^T(k), \\
-M_\ell \cdot \delta_\chi^T(k) &\leq \theta_T^{\text{TC}}(k; z; \ell) \leq M_\ell \cdot \delta_\chi^T(k), \\
k &\in [1, k_C], z \in [1, K_{\text{hid}}], \ell \in [0, L - 1],
\end{aligned} \tag{75}$$

$$\begin{aligned}
& \sum_{z' \in [1, h(\ell)]} w_\ell(z', z) \theta^C(\text{tail}(k); z'; \ell) - M_\ell \cdot (1 - \chi^T(i, k) + e^T(i)) \leq \theta_C^{CT}(i; z; \ell) \\
& \leq \sum_{z' \in [1, h(\ell)]} w_\ell(z', z) \theta^C(\text{tail}(k); z'; \ell) + M_\ell \cdot (1 - \chi^T(i, k) + e^T(i)), k \in [1, k_C], \\
& \sum_{z' \in [1, h(\ell)]} w_\ell(z', z) \theta^C(\text{head}(k); z'; \ell) - M_\ell \cdot (1 - \chi^T(i, k) + e^T(i+1)) \leq \theta_C^{TC}(i; z; \ell) \\
& \leq \sum_{z' \in [1, h(\ell)]} w_\ell(z', z) \theta^C(\text{head}(k); z'; \ell) + M_\ell \cdot (1 - \chi^T(i, k) + e^T(i+1)), k \in [1, k_C], \\
& -M_\ell \cdot (1 - e^T(i)) \leq \theta_C^{CT}(i; z; \ell) \leq M_\ell \cdot (1 - e^T(i)), \\
& -M_\ell \cdot v^T(i) \leq \theta_C^{CT}(i; z; \ell) \leq M_\ell \cdot v^T(i), \\
& -M_\ell \cdot (1 - e^T(i+1)) \leq \theta_C^{TC}(i; z; \ell) \leq M_\ell \cdot (1 - e^T(i+1)), \\
& -M_\ell \cdot v^T(i) \leq \theta_C^{TC}(i; z; \ell) \leq M_\ell \cdot v^T(i), \\
& i \in [1, t_T], z \in [1, K_{\text{hid}}], \ell \in [0, L-1], \tag{76}
\end{aligned}$$

$$\begin{aligned}
& \sum_{z' \in [1, h(\ell)]} w_\ell(z', z) \theta^F(i; z'; \ell) - M_\ell \cdot (1 - \chi^F(i, c) + e^F(i)) \leq \theta_F^{CF}(c; z; \ell) \\
& \leq \sum_{z' \in [1, h(\ell)]} w_\ell(z', z) \theta^F(i; z'; \ell) + M_\ell \cdot (1 - \chi^F(i, c) + e^F(i)), i \in [1, t_F], \\
& -M_\ell \cdot \chi^F(c) \leq \theta_F^{CF}(c; z; \ell) \leq M_\ell \cdot \chi^F(c), \\
& c \in [1, \tilde{t}_C], z \in [1, K_{\text{hid}}], \ell \in [0, L-1], \tag{77}
\end{aligned}$$

$$\begin{aligned}
& \sum_{z' \in [1, h(\ell)]} w_\ell(z', z) \theta^C(c; z'; \ell) - M_\ell \cdot (1 - \chi^F(i, c) + e^F(i)) \leq \theta_C^{CF}(i; z; \ell) \\
& \leq \sum_{z' \in [1, h(\ell)]} w_\ell(z', z) \theta^C(c; z'; \ell) + M_\ell \cdot (1 - \chi^F(i, c) + e^F(i)), c \in [1, \tilde{t}_C], \\
& -M_\ell \cdot \sum_{c \in [1, \tilde{t}_C]} \chi^F(i, c) \leq \theta_C^{CF}(i; z; \ell) \leq M_\ell \cdot \sum_{c \in [1, \tilde{t}_C]} \chi^F(i, c), \\
& -M_\ell \cdot (1 - e^F(i)) \leq \theta_C^{CF}(i; z; \ell) \leq M_\ell \cdot (1 - e^F(i)), \\
& i \in [1, t_F], z \in [1, K_{\text{hid}}], \ell \in [0, L-1], \tag{78}
\end{aligned}$$

$$\begin{aligned}
& \sum_{z' \in [1, h(\ell)]} w_\ell(z', z) \theta^F(j; z'; \ell) - M_\ell \cdot (1 - \chi^F(j, \tilde{t}_C + i) + e^F(j)) \leq \theta_F^{TF}(i; z; \ell) \\
& \leq \sum_{z' \in [1, h(\ell)]} w_\ell(z', z) \theta^F(j; z'; \ell) + M_\ell \cdot (1 - \chi^F(j, \tilde{t}_C + i) + e^F(j)), j \in [1, t_F], \\
& -M_\ell \cdot \chi^F(\tilde{t}_C + i) \leq \theta_F^{TF}(i; z; \ell) \leq M_\ell \cdot \chi^F(\tilde{t}_C + i), \\
& i \in [1, t_T], z \in [1, K_{\text{hid}}], \ell \in [0, L-1], \tag{79}
\end{aligned}$$

$$\begin{aligned}
& \sum_{z' \in [1, h(\ell)]} w_\ell(z', z) \theta^T(j; z'; \ell) - M_\ell \cdot (1 - \chi^F(i, \tilde{t}_C + j) + e^F(i)) \leq \theta_T^{\text{TF}}(i; z; \ell) \\
& \leq \sum_{z' \in [1, h(\ell)]} w_\ell(z', z) \theta^T(j; z'; \ell) + M_\ell \cdot (1 - \chi^F(i, \tilde{t}_C + j) + e^F(i)), j \in [1, t_T], \\
& \quad -M_\ell \cdot \sum_{j \in [1, t_T]} \chi^F(i, \tilde{t}_C + j) \leq \theta_T^{\text{TF}}(i; z; \ell) \leq M_\ell \cdot \sum_{j \in [1, t_T]} \chi^F(i, \tilde{t}_C + j), \\
& \quad -M_\ell \cdot (1 - e^F(i)) \leq \theta_T^{\text{TF}}(i; z; \ell) \leq M_\ell \cdot (1 - e^F(i)), \\
& \quad i \in [1, t_F], z \in [1, K_{\text{hid}}], \ell \in [0, L - 1], \tag{80}
\end{aligned}$$

$$\begin{aligned}
& \sum_{i \in [1, t_X], X \in \{C, T, F\}} \sum_{z \in [1, K_{\text{hid}}]} w_C(z, p) \theta^X(i; z; L) = \tau_{\text{ftr}}(p), \\
& \quad -M_L \delta_{\text{ftr}}^\tau(p) \leq \theta_C(p) - \kappa \tau_{\text{ftr}}(p) \leq M_L \delta_{\text{ftr}}^\tau(p), \\
& \quad -M_L (1 - \delta_{\text{ftr}}^\tau(p)) \leq \theta_C(p) - \tau_{\text{ftr}}(p) \leq M_L (1 - \delta_{\text{ftr}}^\tau(p)), \\
& \quad -M_L \delta_{\text{ftr}}^\tau(p) \leq \tau_{\text{ftr}}(p) \leq M_L (1 - \delta_{\text{ftr}}^\tau(p)), \quad p \in [1, K_C], \tag{81}
\end{aligned}$$